ISTANBUL TECHNICAL UNIVERSITY ★ GRADUATE SCHOOL

DETAILED DESIGN OF A LONG ENDURACE SMALL UNMANNED AERIAL VEHICLE

M.Sc. THESIS

Şems İkbal YÜZGEÇ

Department of Aeronautical and Astronautical Engineering

Aeronautical and Astronautical Engineering Programme

JUNE 2024

ISTANBUL TECHNICAL UNIVERSITY ★ GRADUATE SCHOOL

DETAILED DESIGN OF A LONG ENDURACE SMALL UNMANNED AERIAL VEHICLE

M.Sc. THESIS

Şems İkbal YÜZGEÇ
(511201186)

Department of Aeronautical and Astronautical Engineering

Aeronautical and Astronautical Engineering Programme

Thesis Advisor: Asst. Prof. Hayri ACAR

JUNE 2024

ISTANBUL TEKNİK ÜNİVERSİTESİ ★ LİSANSÜSTÜ EĞİTİM ENSTİTÜSÜ

YÜKSEK SEYİR SÜRESİNE SAHİP KÜÇÜK BİR İNSANSIZ HAVA ARACININ DETAY TASARIMI

YÜKSEK LİSANS TEZİ

Şems İkbal YÜZGEÇ
(511201186)

Uçak ve Uzay Mühendisliği Ana Bilim Dalı
Uçak ve Uzay Mühendisliği Programı

Tez Danışmanı: Dr. Öğr. Üyesi Hayri ACAR

HAZİRAN 2024

Şems İkbal Yüzgeç, a M.Sc. student of İTU Graduate School student ID 511201186 successfully defended the thesis/dissertation entitled "DETAILED DESIGN OF A LONG ENDURACE SMALL UNMANNED AERIAL VEHICLE", which he prepared after fulfilling the requirements specified in the associated legislations, before the jury whose signatures are below.

Thesis Advisor :	**Asst. Prof. Hayri ACAR** İstanbul Technical University	....
Jury Members :	**Prof. Dr. N. L. Okşan ÇETİNER YILDIRIM** Istanbul Technical University	....
	Asst. Prof. Onur SON Gebze Technical University	....

Date of Submission : 23 May 2024
Date of Defense : 13 June 2024

To my family,

FOREWORD

This study consists of presenting the outputs obtained during the development of a small long-endurance unmanned aerial vehicle system within the scope of a master's thesis.

Since unmanned aerial system design is a multidisciplinary field covering aerodynamics, structure, cost, communication, navigation, electronics, propulsion, etc., this study focuses on specific parts due to the difficulty of covering all of them.

Although most of the effort was spent on the preliminary design of the aircraft, the systems and physical conditions of the take-off and recovery phases are discussed too. Since the recovery system mentioned in the study is a little-known system, it is aimed to increase interest in this and similar systems by emphasizing the advantages of this system.

In addition, the development cost, fixed cost and variable costs of the project are revealed and it is shown how much the UAV system mentioned in the study will cost to the investor or institution that wants to realize this project.

I would like to thank my advisor Hayri Acar for giving me the opportunity to work in this field. I am grateful for his patience and contionus support.

Special thanks to my father for his moral support. When things went wrong his guidance helped me to overcome many obstacles.

I would like to thank my colleague and cousin Cafer Nazım Yüzgeç for his help, many usefull disscussions, and suggestions.

Furthermore, I would like to express my gratitude to my uncle, who is my guide and whom I am proud to be his colleague, for all the efforts he has made throughout my life and even before.

Thanks to my undergraduate advisor Kemal Bülent Yüceil, who is unfurtunately not among us anymore, for his all effort and support.

Many thanks also to memebers of my jury committee for spending time on evaluating my thesis, and for providing useful comments and suggestions.

June 2024 Şems İkbal Yüzgeç

TABLE OF CONTENTS

Page

ABBREVIATIONS

AR	: Aspect Ratio
ATC	: Air Traffic Control
AV	: Air Vehicle
BLOS	: Beyond Line of Sight
CFD	: Computational Fluid Dynamics
CG	: Center of Gravity
EASA	: European Union Aviation Safety Agency
EO/IR	: Electro-Optical/Infrared
FAA	: Federal Aviation Administration
FEA	: Finite Element Analysis
GCS	: Ground Control Station
GPS	: Global Positioning System
HALE	: High-Altitude Long-Endurance
IEEE	: Institute of Electrical and Electronics Engineers
IFR	: Instrument Flight Rules
IMU	: Inertial Measurement Unit
ISR	: Intelligence, Surveillance, Reconnaissance
L/D	: Lift-to-Drag Ratio
LIDAR	: Light Detection and Ranging
LOS	: Line of Sight
LRS	: Launch and Recovery Systems
MALE	: Medium-Altitude Long-Endurance
MTOW	: Maximum Takeoff Weight
PPL	: Private Pilot License
RF	: Radio Frequency
RPA	: Remotely Piloted Aircraft
RPM	: Revolutions Per Minute
SAR	: Search and Rescue
SATCOM	: Satellite Communication
STOL	: Short Take-Off and Landing

sUAS : smal Unmanned Aircraft System
sUAV : small Unmanned Aerial Vehicle
UAS : Unmanned Aircraft System
UAV : Unmanned Aerial Vehicle
UAVC : Unmanned Aerial Vehicle Camera
VFR : Visual Flight Rules
VTOL : Vertical Take-Off and Landing

SYMBOLS

(L/D)max	**:** Maximum lift to drag ratio
$\mathbf{C_{m_0}}$	: Profile zero angle moment coefficient
$\mathbf{C_{L_R}}$	: Take-off rotation lift coefficient
$\mathbf{C_{L_{TO}}}$	: Take-off lift coefficient
$\mathbf{C_{L_c}}$	: Cruise lift coefficient
$\mathbf{C_{L_{max}}}$	: Maximum lift coefficient
$\mathbf{C_{M_\alpha}}$	: Moment curve coefficient
$\mathbf{C_{d_{min}}}$	: Profile minimum drag coefficient
$\mathbf{C_{l_{max}}}$	: Profile maximum lift coefficient
$\mathbf{C_{l_\alpha}}$	: Profile lift curve coefficient
$\mathbf{C_{l_0}}$	: Profile zero-angle lift coefficient
$\boldsymbol{C_{D_{TO}}}$	: Take off drag coefficient
$\boldsymbol{C_{D0_{HDL}}}$	: Zero lift high drag coefficient
$\boldsymbol{C_{D0_{TO}}}$	: Zero lift take off drag coefficient
$\mathbf{C_L}$	: Lift Coefficient
$\mathbf{C_d}$	: Profile drag coefficient
$\mathbf{C_d}$	: Profile drag coefficient
$\mathbf{C_d}$	: Profile drag coefficient
$\mathbf{C_l}$	: Profile lift coefficient
$\mathbf{C_m}$	: Profile moment coefficient
$\boldsymbol{C_{D0}}$	: Zero lift drag coefficient
$\boldsymbol{c_{w_h}}$	: Chord corresponding to tail span
$\boldsymbol{t_{w_h}}$	: Profile thickness corresponding to tail span
$\boldsymbol{t_{MGC}}$	: Maximum profile thickness at MGC
$\boldsymbol{t_r}$	: Maximum profile thickness at root
$\boldsymbol{t_t}$	: Maximum profile thickness at tip
$\boldsymbol{x_{LE}}$	: Chordwise position of wing root LE from airplane nose
$\boldsymbol{x_{MGC}}$	: Chordwise position of MGC from wing root LE

$x_{0.25MGC}$: Chordwise position of quarter MGC from wing root LE
y_{MGC} : Spanwise position of LE of MGC from wing root LE
$\Delta C_{L_{flap}}$: Flap down lift coefficient
Λ_{LE} : Sweep angle of leading-edge line
Λ_{TE} : Sweep angle of trailing-edge line
$\Lambda_{0.25}$: Sweep angle of quarter chord line
$\Lambda_{0.5}$: Sweep angle of half chord line
$\alpha_{l=0}$: Profile zero lift angle of attack
α_{stall} : Profile stall angle of attack
δ_e : Elevator deflection angle
a.c. or ac : Aerodynamic center
b : Span
c or MGC : Mean geometric (aerodynamic) chord
C or SFC_c : Specific fuel consumptions at cruise
c.g. or cg : Center of gravitiyLanding weight
C_D : Drag Coefficient
CLa : Lift curve slope
CLO : Zero-lift coefficient
C_M : Moment Coefficient
c_r : Root chord
c_t : Tip chord
E : Endurance
e : Oswald efficiency
h : Generic index for horizontal tail
h_c : Cruise altitude
h_{loi} : Loiter altitude
h_{max} : Maximum altitude
h_{sc} : Service ceiling
h_{TO} : Take-Off Altitude
h_{turn} : Sustain turn altitude
i : Generic index for summations
Lf : Fuselage length
L_h : Distance between wing quarter-chord and horizontal tail quarter-chord
l_{r2t} : Distance between wing root LE and tip LE

n	: Efficiency factor
n	: Total number of components or elements in a summation
n_f	: Fuselage height coefficient
Nult	: Ultimate load factor
P	: Power
P_{TO}	: Power Take-Off
R	**:** Range
ROC_c	**:** Rate of climb at service ceiling
ROC_{max}	**:** Maximum rate of climb
S	: Wing area
S_e	: Elevator area
SFC_{loiter}	**:** Specific fuel consumptions at loiter
S_h	: Horizontal area
S_r	: Rudder area
S_v	: Vertical area
v	: Generic index for vertical tail
V	: Tail volume coefficient
V_c	**:** Cruise speed
V_{Emax}	**:** Speed for maximum endurance
V_{loi}	**:** Loiter speed
V_{max}	**:** Maximum altitude
V_s	**:** Stall speed
V_{TO}	**:** Take-Off Speed
V_{turn}	**:** Sustain turn speed
W	: Weight
W_{ai}	: Air induction system weight
W_{boom}	: Booms weight
W_c	: Crew weight
W_E	: Empty weight
W_e	: Engine weight
W_f	: Fuel weight
wf	: Fuselage width
W_{feq}	: Fixed equipment weight
W_{fs}	: Fuel system weight
W_{fus}	: Fuselage weight

$W_{landing}$: Landing weight

$W_{landing}$: Landing weight

W_p : Propulsion system weight

W_{PL} : Payload weight

W_{prop} : Propeller weight

W_{pwr} : Installed engine weight

W_{tfo} : Trapped fuel oil weight

W_{TO} : Take-off weight

x : Chordwise position

x_{cg} : Position of center of gravity

X_{LE} : Position of leading edge

y : Spanwise position

η_{prop} : Propeller efficiency

η_{propTO} : Propeller efficiency at take-off

l : Tail arm

Λ : Sweep angle

α : Angle of attack

λ : Taper ratio

LIST OF TABLES

Page

LIST OF FIGURES

DETAILED DESIGN OF A LONG ENDURACE SMALL UNMANNED AERIAL VEHICLE

SUMMARY

Unmanned Aerial Vehicles (UAVs) are finding applications in various fields both in our country and around the world, driven by steadily increasing demand. The applications of UAVs span diverse sectors, including agriculture, surveillance, environmental monitoring, disaster response, and delivery services. In agriculture, UAVs equipped with multispectral cameras contribute to precision farming by providing real-time data for crop health assessment. In surveillance and security, UAVs play a pivotal role in monitoring large areas and critical infrastructure. Moreover, UAVs have proven invaluable in disaster response scenarios, offering rapid and efficient aerial assessments of affected areas.

Hence, this study presents an overview of our ongoing study focused on the design and development of a small Unmanned Aerial Vehicle (UAV) tailored for low altitude, long endurance Intelligence, Surveillance, Reconnaissance (ISR) missions. The project aims to address current gaps in UAV technology in Turkey for efficient and sustainable ISR operations.

One of the key features of the UAV design is its independence from traditional runways for takeoff and landing. It integrates a catapult-assisted takeoff system, which allows for rapid deployment from confined spaces. For recovery, the UAV is designed to be captured using a hook system. This capability significantly enhances the UAV's operational flexibility, allowing it to be deployed and retrieved in diverse environments, including remote or rugged terrains and also on ship decks.

Although the main effort of the study focuses on the design of the UAV platform, requirements for launch and recovery are determined, and the load created in these phases is calculated to determine the structural requirements of the airframe.

Since the recovery system mentioned in the study is a little-known system, it is aimed to increase interest in this and similar systems by emphasizing the advantages of this system.

In addition, the development cost, fixed cost and variable costs of the project are revealed and it is shown how much the UAV system mentioned in the study will cost to the investor or institution that wants to realize this project.

YÜKSEK SEYİR SÜRESİNE SAHİP KÜÇÜK BİR İNSANSIZ HAVA ARACININ DETAY TASARIMI

ÖZET

İnsansız hava araçları basitçe düşünülenin aksine içinden mürettebat çıkarılmış ve yerine bilgisayar sistemi yerleştirilmiş bir uçak olmaktan ziyade bir sistemler bütünüdür. Uçak (Platform) bu sistemin ana öğesi alsa da sistemin yalnızca bir parçasıdır. Sistemin diğer parçaları basitçe şu şekilde sıralanabilir, faydalı yük, sistem operatörlerini barındıran bir kontrol istasyonu, kontrol girdilerini hava aracına ileten ve araçtan geri bildirim almayı münkün kılan iletişim sistemi, uçak kalkış ve iniş sistemileri, destek alt sistemleri, nakliye alt sistemi, vb.

Bu çalışmanın amacı en kısa ifadesiyle yüksek seyir süresine sahip küçük bir insansız hava sisteminin gereksinim kümsesi göz önüne alınarak bu gereksinimleri karşılayacak tasarım çözümünün ortaya konmasıdır.

Çalışmada ana gayret uçak alt sisteminin tasarımına verilmiş olsa da iniş kalkış sistemlerinin tasarımı ve bu tasarımların uçak üzerindeki etkilerine de yer verilmiştir. Ayrıca projenin geliştirme ve üretim maaliyetleri analiz edilerek birim satış fiyatı elde edilmiştir.

Çalışmaya ilk olarak systemin gereksinim kümesi tanımlanarak başlanmıştır. Bu gereksinimleri karşılayacak görev çerçevesi ve safhaları ve dahi hangi safhanın önem arz ettiği ortaya konmuştur. Sonrasında gereksinimleri karşılayacak şekilde uygun görülen iniş ve kalkış sistemi belirlenmiştir. Iniş-kalkış sistemi uçağın kavramsal tasarımını etkileceyecek ek gereksinimler türettiğinden bunları da göz önüne alarak uçağın tahrik tipi ve tahrik teçhizatının uçak üzerindeki konumu belirlenmiştir. Tahrik teçhizatının konumunun olası faydalı yük konumlarının seçim kümesini daralttığı göz önüne alınarak faydalı yük konumu belirlenmiştir. Kanadın gövde üzerindeki konumu, yaklaşık geometrik biçimi; gereksinimler ve benzer insansız hava sistemleri göz önüne alınarak tespit edilmiştir. Kuyruk tespiti de kanat tespitinde izlenen yola uyularak yapılmıştır. Uçağın kavramsal tasarım süreci yukarıda bahsedilenler ışığında sonlandırılıp ortaya çıkan kavramsal tasarımın 3-görünüşü kabaca resmedilmiştir. Bu aşamadan sonra uçağın ön dizayn aşamasına başlanmıştır.

Ön dizayn aşaması ilk ağırlık tahmini ile başlamaktadır. İlk ağırlık tahmini için gerekli ön değerler uçağın gereksinim kümesi, görev çerçevesi ve benzer uçak verilerinden gelmektedir. İlk ağırlık tahmini sonrası uçağın kalkış ağırlığı, boş ağırlığı ve yakıt ağırlığı elde edilmiştir.

Sonrasında uçağın gereksinimlerini karşılayacak performans girdilerinin meydana getirdiği "kısıt şeması" çizdirilmiş ve tasarım noktası tespit edilmiştir. Bu şema ile elde edilen kanat yüklemesi ve güç yüklemesi oranları ve bir önceki kısımda hesaplanan kalkış ağırlığı yardımıyla uçağın kanat alanı ve güç gereksinimi hesaplanmıştır.

İlerleyen kısımlarda uçağın alt parçalarına dair tasarımlara başlanmıştır. Öncelikle kanat sonrasında kuyruk boyutlandırılmıştır. Kanat ve kuyruk için uygun kanat profili adayları belirlenip bu adaylar arasında bir karşılaştırma yapılarak uygun profil

belirlenmiştir. Geometrilerin belirlenmesinde benzer uçak verilerinden faydalanarak insansız hava sisteminin performans ve görev kriterlerini karşılamasına dikkat edilmiştir.

Gövde boyutlandırmasında kritik olan alt sistemlerin boyutlarını belirlemek esas teşkil ettiğinden öncelikle tahrik sistemi için motor ve faydalı yük seçimi yapılmıştır. Gövde dört ana kısma ayrılmak suretiyle boyutlandırılmıştır: faydalı yük modülü, aviyonik modülü, yakıt modülü, ve motor bloğu. Bu şekilde ana komponentlerin boyutlandırması tamamlanmış olup sonraki safha olan ağırlık analizi safhasına geçilmiştir.

Ağırlık analizi için uçağın ağırlık kalemlerinin tespit edilmesi gereklidir. Bu iki şekilde yapılmıştır. İlki benzer uçakların ağırlık kesirleri kullanılmak suretiyle parçaların ağırlıkları tahmin edilmiştir. İkinci olarak da her parça için oluşturulmuş istatistiki verilere dayanan denkem kümeleri kullanılarak ağırlık tahmini yapılmıştır. Bu iki yöntem beraber ele alınarak uçağın ağırlık kalemleri elde edilmiştir.

Bu aşamadan sonra kütle merkezinin tespitine girişilmiştir. Bunun için öncelikle her bir parçanın ağırlık merkezinin tayin edilmesi gerekir. Bu işlem için uçakların tipik kütle merkezi verilerinden yardım alınmıştır. Uçağın farklı yükleme durumları göz önünde bulundurularak uçağın kütle merkezinin gezinti zarfı çizdirilmiştir. Bu zarfın uçak tipi için ön görülen sınırlar içerisinde olmasını sağlayacak şekilde uçak sistemlerinin konumları ile oynanmıştır. Sonrasında uçağın eylemsizlik momenti bileşenleri elde edilmiştir. Ağırlık merkezi konumundan tatmin olunaraktan uçağın denge ve kontrol analizlerine geçilmiştir.

Bu çalışmada Denge ve kontrol analizleri sadece boylamsal denge için gerçekleştirilmiştir. Boylamsal denge için gereken aerodinamik hesaplamalar ilerleyen kısımlarda gerçekleştirilmiştir.

Uçağın aerodinamik karakterine dair hesaplamlar 4 kısımda gerçekleştirmiştir. Bunlar, Taşıma Analizi (Lift Analysis), Sürükleme Analizi (Drag Analysis), Yunuslama Momenti Analizi (Pitching Moment Analysis), ve Türevler (Derivatives). Bu kısımlardaki aerodinamik hesaplamalar ve modeler ihitiyaç halinde daha da genişletilip detaylandırılabilir fakat güncel şekli çalışmanın ihtiyaçlarını görmektedir. Bu kısımın tamamlanmasıyla beraber Ön Dizayn aşaması tamamlanmş kabul edilir ve tezin sonraki kısımlarına geçilir.

İnsansız hava sisteminin kalkış safhası mancınık yardımıyla gerçekleştirilecektir. Sistemin gereksinimleri, uçağın boyutu ve kalkış hızı isteri göz önüne alınarak uygun bir fırlatma sistemi (mancınık) seçilmiştir. Sonrasında mancınığın boyutları da göz önüne alınarak kalkış seneryoları ve kalkış performansı analiz edilmiştir. Uçağın fırlatmadan sonra irtifa kaybetmemesi şart koşularak asgari kalkış hızı hesaplanmıştır. İleriki kısımlarda bu kalkış hızı göz önüne alınarak uçağa kalkış esnasında uygulanacak kuvvetler hesaplanmıştır.

Geri dönüş safhası insansız hava sistemini diğer insansız hava sistemlerinden ayırıan en büyük farklılıktır. Dikey Kablolu Yakalama Sistemi (Vertical Rope Arresting System) adı verilen bir sistem yardımıyla geri dönüş safhasının gerçekleştirilmesi sağlanacaktır. Bu systemin yakalama esnasında uçağa uygulayacağı ve uçağın da yakalama sistemine uygulayacağı yükün belirlenmesi elzemdir. Bu tez kapsamında geri dönüş safhasını konu alan bir modelleme çalışması yapılmamıştır fakat benzer çalışmalar göz önüne alınarak ve bunların sonuçları yorumlanarak çıktılar elde edilmiştir. Bu çıktılar kısaca, yakalama sonrası uçağın kütle merkezinin durgun haldeki kablo ekseni etrafında izledği yörüngenin azami yarıçapı ve yakalama esnasında uçağa 3 eksende etki eden kuvvetlerin G, yerçekimi ivmesinin katı cinsinden ifadesinin elde edilmesidir. Bunlar ışığında uçağa etki eden geri dönüş yükleri elde edilmiş olup ayrıca yakalama sistemi için de önemli olan tasarım kriterleri vurgulanmıştır.

Uçağa inişte kalkışta ve uçarken etkiyecek yükler en basit şekliyle listelenmiştir. İniş yükleri yukarıda bahsedildiği şekliyle elde edilmiştir. Kalkış yükleri ise fırlatıcı boyutları ve asgari kalkış hızı göz önüne alınırak sabit ivmeli hareket denklermleri yardımıyla hesaplanmıştır. Uçuş yükleri ise v-N diagramı çizdirilerek elde edilmiştir. Bu yüklere göz önüne alınarak uçağın ön yapısal boyutlandırmasına başlanılabilir fakat bu tez kabsamında içeriği daha da fazla şişirmemek için yapısal boyutlandırma ve yapısal tasarım kısımlarına değinilmemiştir.

Son olarak projenin maaliyet analizi gerçekleştirilmiştir. Bu analizler sonucunda projenin geliştirme maaliyeti, değişken maaliyet, asgari satış fiyatı gibi değerler elde edilmek suretiyle bu tarz bir projeye başlamak isteyen kurum ve ya yatırımcıya öngörü sağlanmıştır.

1. INTRODUCTION

The rapid evolution of technology has fostered significant advancements in the field of unmanned aerial vehicles (UAVs), broadening their application spectrum to include agriculture, surveillance, environmental monitoring, disaster response, and delivery services. Particularly, Small Unmanned Aircraft Systems (sUAS) represent an important segment that creates niche applications in both military and civilian sectors due to their unique operational advantages. As demand for precise, reliable and discrete surveillance capabilities grows, small UAVs have emerged as important tools for a wide range of applications, from environmental monitoring to advanced military reconnaissance missions.

The importance of UAVs extends beyond their immediate operational capabilities to include their potential in long-endurance missions. Long endurance is critical for continuous data collection and prolonged surveillance missions, necessitating UAVs that can operate over extended periods without the need for frequent returns to base for refueling or maintenance. However, designing UAVs that can meet these requirements poses significant challenges, primarily related to optimizing aerodynamic efficiency, enhancing payload capacity, and ensuring robustness in diverse environmental conditions.

current technological advancements have made significant strides in improving UAV endurance, yet there remain inherent limitations in the existing designs that impact their practical usability in long-endurance roles. These challenges are often related to the trade-offs between the UAV's weight, its aerodynamic properties, and the capacity to carry various payloads. Furthermore, the operational dynamics of deploying and recovering UAVs in varying terrains and conditions present additional complexity, requiring innovative solutions to ensure reliability and safety.

The need for improved design solutions is evident in the context of increasing reliance on UAVs for critical tasks that require uninterrupted operation over extended periods. This is where this thesis aims to contribute by exploring advanced design frameworks that integrate novel materials, optimized aerodynamic configurations, and enhanced power management systems to extend the operational capabilities of small UAVs.

1.1 Purpose of Thesis

The primary objective of this thesis is to conceptualize, design, and evaluate a small UAV that can efficiently perform low altitude, long endurance ISR missions. This involves a comprehensive study that extends from the initial design phase to the load analysis and performance assessment of the UAV. The UAV, named "HavaKaşifi," aims to fulfill specific operational needs such as the ability to be deployed from various terrains including ship decks and rugged landscapes, carry diverse payloads, and achieve extended flight durations.

By focusing on a catapult-assisted takeoff and vertical arresting cable-based recovery system, the thesis proposes a design that not only meets the operational requirements but also enhances flexibility and adaptability in diverse mission scenarios. Furthermore, the study aims to contribute to the UAV technological advancements in Turkey, proposing a design that is cheap, efficient and sustainable for ISR operations. Specifically, this research aims to:

- To design a UAV system capable of carrying a payload of 3.5 kg for up to 20 hours of continuous flight.
- To improve aerodynamic efficiency to reduce energy consumption during flight.
- Using lightweight, high-strength materials to improve structural integrity and flight duration.
- Identify the requirements for a reliable and versatile system for launching and recovering the UAV under different environmental conditions and design the platform to meet these requirements.
- Determine the project cost and the minimum selling price of the system

1.2 Literature Review

A comprehensive review of the existing literature forms the basis of this thesis. The review covers studies on UAV design, focusing specifically on small UAVs used for

ISR missions. It includes analysis of current technologies in UAV design, propulsion systems, material selection and aerodynamics. Special attention is paid to current designs that include features such as long durability and versatility in takeoff and landing capabilities.

The literature review also covers regulatory frameworks governing UAV operations, which are crucial in shaping design parameters. This thesis examines previous research and existing UAV models and produces solutions by considering the gaps in current UAV technology, especially in the context of Turkey's needs in ISR applications.

1.2.1 Significance of sUAV

Unmanned Aerial Vehicles (UAVs), broadly classified into various categories based on size, range, and capabilities, have fundamentally transformed modern aerial operations. Within this broad spectrum, Small Unmanned Aircraft Systems (sUAS) like the Insitu ScanEagle represent a significant segment that has carved out niche applications in both military and civilian sectors due to their unique operational advantages. As the demand for precise, reliable, and discrete surveillance capabilities increases, small UAVs have emerged as pivotal tools for a wide range of applications, from environmental monitoring to advanced military reconnaissance missions.

The Insitu ScanEagle, a small, long-endurance UAV developed by Boeing subsidiary Insitu Inc., is particularly noteworthy. Launched initially for maritime fish-spotting, the ScanEagle quickly adapted to broader roles due to its compact size, ease of deployment, and impressive endurance capabilities. Unlike larger UAVs that require significant infrastructure and logistical support, the ScanEagle operates from a catapult launcher and is recovered via a patented "SkyHook" recovery system, allowing it to be deployed from virtually anywhere, including confined spaces on land or at sea. This versatility is coupled with its ability to fly at altitudes up to 19,500 feet while providing real-time video feeds for hours, making it an ideal choice for tasks requiring stealth and extended surveillance.

1.3 Structure of Report

The structure of this thesis is meticulously organized to provide a clear and logical progression of the research conducted. The report is set up as follows:

- Chapter 2 discusses the model assumptions critical for the design and analysis of the UAV.
- Chapter 3 provides a detailed overview of the theoretical frameworks applied to the UAV's geometry and aerodynamic characteristics.
- Chapter 4 discusses launch and recovery system requirements and load analysis of them.
- Chapter 5 elaborates on the forces applied to the UAV during operation, in launch and recovery.
- Chapter 6 focus on the cost items of the UAS.
- Chapter 7 presents further studies and recommendations.

2. CONCEPTUAL DESIGN

2.1 Introduction

In this section brief conceptual design of the aircraft is presented.

2.2 Project Name

The UAV system as named as “HavaKaşifi”. “Hava” means air and “Kaşif” means explorer. Thus, HavaKaşifi is a name compatible by mission and purpose of the UAV. Also, short form of HavaKaşifi is “HAVK” resemble the English word “Hawk”. A bird observes its target at higher altitude.

2.3 Requirements

2.3.1 Design requirements

The features that should be included in HavaKaşifi are as follows in their most general form.

1. Must be able to safely perform Intelligence, Surveillance and Reconnaissance (ISR) mission day and night.
2. Must be able to take off and land in all types of terrain (forest, tundra, desert, etc.) and on the ship deck.
3. Must be able to fly for 20 hours with a payload of 3.5 kg.
4. Must be able to perform operations within a 100 km radius.
5. Maximum take-off weight should not exceed 20 kg.
6. It should be able to be used with different payload types.
7. It should have a modular design.

2.4 Mission Profile

The mission profile is crucial for aircraft since fuel weight of aircrafts directly related by it. Mission profile is determined according to requirements presented at chapter 2.3. In reconnaissance missions most important segment of mission is loiter unlike to transport aircraft which cruise phase is the most important. Mission profile of HavaKaşifi is represented simply in Figure 2.3. Here every number show starting and finishing point of segment. For example, “2” donates the beginning of climb and 3 is the end of climb. Also, it can be easily seen that the mission profile includes 9 segments. Each segment and their starting ending denote are listed in Table 2.1.

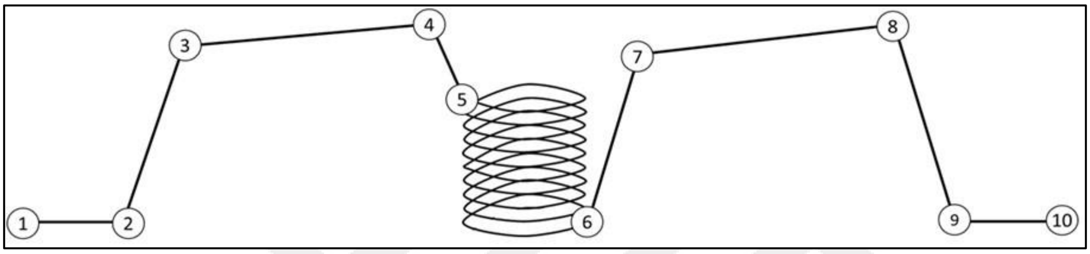

Figure 2.1 : Mission profile model.

Table 2.1 : Mission profile.

No	Path	Mission Segment	Constraint
1	1-2	Taxi and take-off	
2	2-3	Climb	
3	3-4	Cruise	100 km range
4	4-5	Descent	
5	5-6	Loiter	20 hours
6	6-7	Return Climb	
7	7-8	Return Cruise	100 km range
8	8-9	Return Descent	
9	9-10	Approach and landing	

2.5 Configuration Layout

2.5.1 Launch and Recovery

Configuration of UAV system is highly dependent on launch and recovery options. In this study catapult launch is selected as a launch concept whereas catching hook as a recovery concept to meet requirement 2. These selections automatically cancel landing gear needs.

2.5.2 Engine selection

Given the specific requirements of the UAV, characterized by a 20 kg MTOW, and 20-hour endurance with a 3.5 kg payload. The selection of a piston engine is substantiated as the optimal choice. This is primarily due to the superior energy density of fuel which facilitates sustained long-duration flights [1]. In contrast, electric motors, despite their advantages in weight reduction, efficiency, and environmental impact, are limited by the current state of battery technology [2][3]. This limitation is a critical factor, as the existing battery capacities are inadequate to support the required 20-hour endurance without adversely affecting the UAV's payload capacity and operational efficiency [4]. Therefore, the piston engine, with its higher energy density, emerges as the more suitable power plant for this UAV configuration, ensuring extended flight duration while maintaining the necessary payload capabilities.

Pusher configuration is selected since safety concern (Propeller can hit the arresting cable in recovery).

2.5.3 Wing and Tail

Tail configuration is determined considering engine position and controllability thus inverse-U tail with a boom attachment is selected; whereas, wing positioning is determined as high since it gives neutral stability to an aircraft.

2.5.4 Summary of configuration layout

Consequently, HavaKaşifi system configuration summary is given in Table 2.2 and it represented in Figure 2.2.

Table 2.2 : Configuration summary

Parameter	Configuration	Comment
Wing position	High	Stability
Tail	Inverse U	Controllability
Landing gear	None	Endurance
Engine Type	Piston	Endurance
Engine Position	Pusher	Safety
Launch	Catapult	Mission requirement
Recovery	Catching hook	Mission requirement

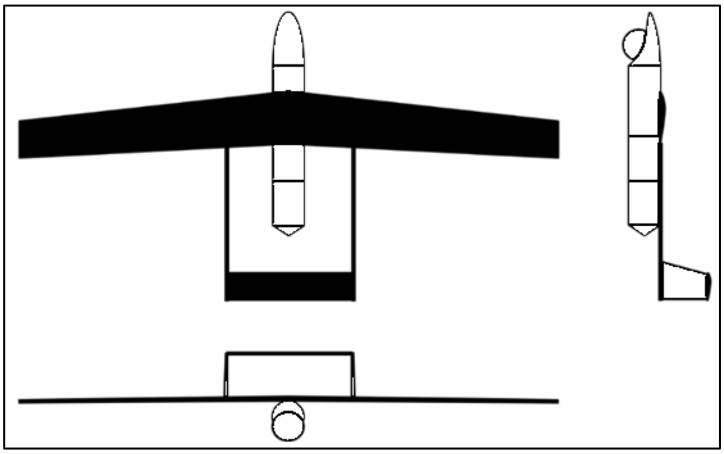

Figure 2.2 : Configuration layout

3. PRELAMINARY DESIGN

3.1 Introduction

In this chapter preliminary design of HavaKaşifi is presented. Preliminary design required preliminary inputs. Some of these inputs come from requirements (endurance, range etc.) whereas most of it should be estimated using formulas based on statistical data or/and estimations based on similar aircrafts data. Similar aircraft list can be found Table 3.1. Initial speed, altitude rate of climb and geometrical inputs like aspect ratio (AR) are estimated based on these aircraft data [5]. Performance and aerodynamic inputs are taken from [6].

Preliminary design inputs for these chapter can be found in following tables.

Table 3.1 : Similar aircrafts list.[5]

No	UAV	No	UAV
1	ACS	17	Border Eagle Mk 2
2	AL-20	18	Explorer
3	AR3 Net Ray	19	Nishan TJ-1000
4	AR3 Net Ray Maritime Radar	20	Tornado
5	PD 1	21	Vision Mk I
6	Penguin B	22	Filmcam
7	Penguin C	23	Yarara
8	ScanEagle	24	VAPOR 55
9	ScanEagle 2	25	Eagle Plus VTOL
10	Skyzer 450	26	Black Eagle 50
11	UAS20	27	CSV 40
12	Shahbaz	28	STREAM
13	SPEAR	29	Penguin BE Electric
14	LUNA	30	UVH 120E
15	Eurotech Vermin	31	Avartek AT-04
16	ALBA	32	BRUS H

Table 3.2 : Initial speed inputs.[5]

Speed		m/s	ft/s
Stall Speed	V_s	13.0	42.7
Take-off Speed	V_{TO}	14.3	46.9
Cruise Speed	V_c	25.0	82.0

Loiter Speed	V_{loi}	25.0	82.0
Sustain Turn Speed	V_{turn}	25.0	82.0
Maximum Speed	V_{max}	39.0	128.0

Table 3.3 : Altitude inputs [5].

Altitude		m	ft
Take-off altitude	h_{TO}	0	0
Cruise altitude	h_c	4286	14061
Loiter altitude	h_{loi}	4286	14061
Sustain Turn Altitude	h_{turn}	4286	14061
Maximum speed altitude	h_{max}	4286	14061
Service ceiling	h_{sc}	6000	19685

Table 3.4 : Climb performance inputs [5].

Rate of Climb		m/s	ft/s	ft/min
Maximum rate of climb	ROC	2.5	8.2	492
Rate of climb at service ceiling	ROC_c	0.5	1.667	100

Table 3.5 : Performance parameters input [6].

Parameters	Symbol	Value	Unit
Aspect ratio	AR	14	-
Maximum lift to drag ratio	$(L/D)_{max}$	15	-
Oswald efficiency	e	0.658	-
Propeller efficiency	η_{prop}	0.7	-
Propeller efficiency at take off	η_{propTO}	0.5	-
Range	R	100	km
Range (Return)	R	100	km
Endurance	E	20	h

Table 3.6 : Specific fuel consumption inputs [6]

Specific fuel consumptions at		m/s	ft/s	ft/min
Cruise	SFC_c	0.6	8.2	492
Loiter	SFC_{loi}	0.6	1.667	100

Table 3.7 : Lift and drag inputs [6]

Lift			Drag		
Maximum lift	C_{Lmax}	2.00	Take of drag	$C_{D_{TO}}$	0.103
Cruise lift	C_{Lc}	0.80	Zero-lift drag	$C_{D0,TO}$	0.035
Flap down	ΔC_{Lflap}	0.60	Clean-zero lift drag	C_{D0}	0.021
Take-off lift	C_{LTO}	1.40	High lift drag	$C_{D0,HLD}$	0.005
Take-off rotation lift	C_{LR}	1.65			

3.2 Initial Weight Estimation

Initial weight estimation is performed using given formulas (3.1) and (3.2) [6]. Solving equations simultaneously by iteration gives initial take of weight of aircraft.

$$W_{TO} = \frac{W_{PL} + W_c}{1 - \left(\frac{W_f}{W_{TO}}\right) - \left(\frac{W_E}{W_{TO}}\right)} \tag{3.1}$$

$$\frac{W_E}{W_{TO}} = aW_{TO} + b \tag{3.2}$$

Here;

- W_{TO}: Maximum take-off weight
- W_E: Empty weight
- W_{PL}: Payload
- W_C: Crew weight
- W_f: Fuel weight

Payload is taken as 3.5 kg (from Requirements)

Crew weight is taken as 0.   (UAVs have no crew)

Empty weight and fuel weight estimations are performed at further chapters.

3.2.1 Empty weight

In equation (3.2) empty weight ratio of aircraft is represented linear combination of take-off weight. Thus, a and b data are calculated using UAVs have

Even if aircraft design books have a and b constant for specific aircraft types (fighter, general, home-built etc.), there no usable value for small unmanned aircrafts. Thus, a and b constants were obtained using the data of similar UAVs weighing between 15 kg and 40 kg and having an endurance of more than 5 hours. Results are plotted given Figure 3.1. Vertical axis of graph represents weight ratios and horizontal axis represents take-off weight of UAVs. Blue dots are representing data of UAVs which used in regression analysis. UAVs used in graph are numbered and list of them is given in Table 3.1

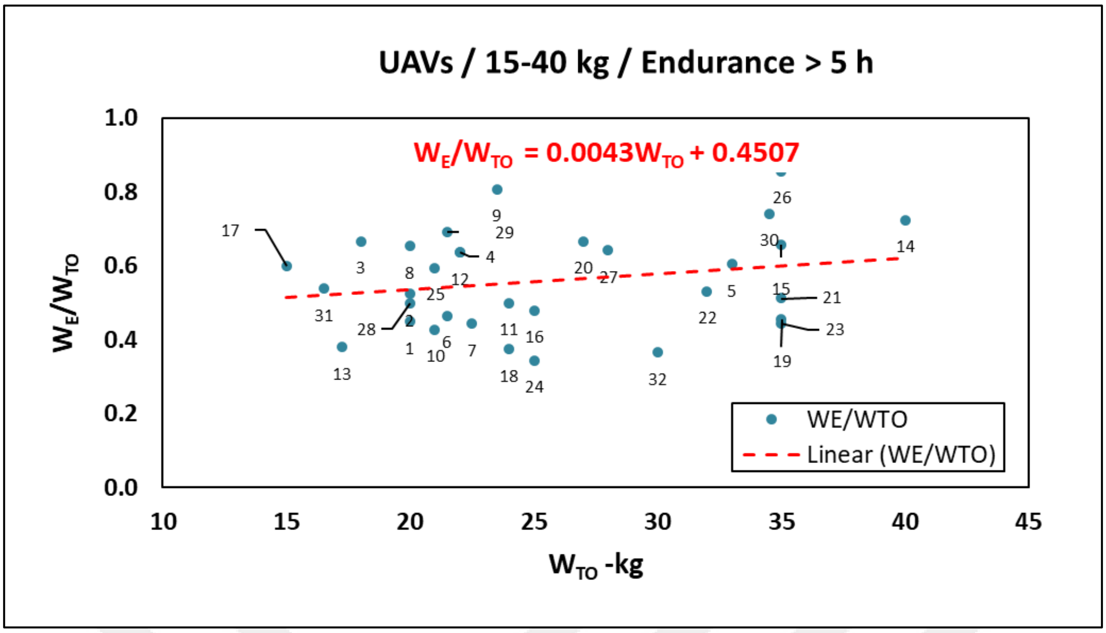

Figure 3.1 : Empty weight ratio to take-off weight.

Red dotted line in graph shows trend line of data and constants of equation 0.0043 and 0.4507 gives constant a and b, respectively. Thus, equation (3.2) is written as given below.

$$\frac{W_E}{W_{TO}} = 0.0043W_{TO} + 0.4507 \tag{3.3}$$

3.2.2 Fuel ratio

Fuel ratio is directly dependent to mission profile. From Figure 2.1, it can be seen that mission profile has 9 segments and 10 points. Similarly, the weight of the aircraft can be quantified at various stages throughout the flight mission. Hence, W_1 is the weight of aircraft before take-off and W_2 is end of take-off which is beginning of the climb. Therefore, it is easy to see that W_1 is equal to W_{TO} and W_{10} is equal to $W_{landing}$. Fuel weight is:

$$W_f = W_{TO} - W_{landing} \tag{3.4}$$

$$\frac{W_f}{W_{TO}} = \frac{W_{TO} - W_{landing}}{W_{TO}} = 1 - \frac{W_{landing}}{W_{TO}} \tag{3.5}$$

Therefore, for the case of a mission with nine segments as shown in Figure 2.1, the fuel weight fraction is obtained as follows:

$$\frac{W_f}{W_{TO}} = 1.05\left(1 - \frac{W_{10}}{W_1}\right) \tag{3.6}$$

The term inside the brackets is multiplied with 1.05 since the extra fuel required for safety purposes is almost 5% of the aircraft total weight, so it is applied to formula [6].

Where $\frac{W_{10}}{W_1}$ can be written as:

$$\frac{W_{10}}{W_1} = \frac{W_2}{W_1}\frac{W_3}{W_2}\frac{W_4}{W_3}\frac{W_5}{W_4}\frac{W_6}{W_5}\frac{W_7}{W_6}\frac{W_8}{W_7}\frac{W_9}{W_8}\frac{W_{10}}{W_9} \tag{3.7}$$

The phases in which the fuel consumption is minimal and almost negligible in comparison to the Maximum Takeoff Weight (MTOW) encompass taxi, take-off, climbing, descending, approach, and landing. Estimations for the fuel weight fractions during these mission segments are taken from [6]. Fuel ratio for these segments is shown in Table 3.8.

Table 3.8 : Typical average segment weight fractions [6].

No	Mission segment	
1	Taxi and take-off	0.98
2	Climb	0.97
3	Descent	0.99
4	Approach and landing	0.997

The cruise weight fraction for a prop-driven aircrafts can be calculated using (3.8) [8]:

$$\frac{w_i}{w_{i-1}} = e^{\frac{-RC}{n_P (L/D)_{max}}} \tag{3.8}$$

Here n_P refers to propeller efficiency; C value refers to specific fuel consumption; R value refers to range. The loiter weight fraction for a prop-driven aircrafts can be calculated using (3.9) [6]:

$$\frac{w_i}{w_{i-1}} = e^{\frac{-ECV_{E_{max}}}{n_P (L/D)_{max}}} \tag{3.9}$$

Here E refers to endurance. The speed for maximum endurance ($V_{E_{max}}$) is accepted that is equal to loiter speed given in Table 3.2.

Outputs for fuel fraction for each mission segment is given Table 3.9.

Table 3.9 : Fuel ratios

No	Path	Mission Segment	Fuel fractions
1	1-2	Taxi and take-off	1.00
2	2-3	Climb	0.97
3	3-4	Cruise	0.99
4	4-5	Descent	0.99
5	5-6	Loiter	0.82
6	6-7	Return Climb	0.97
7	7-8	Return Cruise	0.99
8	8-9	Return Descent	0.99
9	9-10	Approach and landing	1.00

Multiplying fuel fractions as described at Equation (3.7) and substitutes it in Eq (3.6):

$$\frac{W_f}{W_{TO}} = 0.27 \tag{3.10}$$

3.2.3 Summary of initial weight

In previous chapters fuel ratio required for Eq (3.1) and a, b coefficient required for Eq (3.2) is determined. Consequently, Eq (3.1) and Eq (3.2) can be solve together to find maximum take-off weight of aircraft. Summary for this chapter can be seen in Table 3.10.

Table 3.10 : Summary of initial weight

		kg	W/W_{TO}
Maximum take-off weight	W_{TO}	16.93	1
Payload	W_{PL}	3.50	0.21
Fuel weight	W_f	4.60	0.27
Empty weight	W_E	8.83	0.52

3.3 Constraint Diagram (Matching Plot)

One of the initial steps in designing a new aircraft is to create a constraint diagram. This diagram helps to evaluate the required wing area and power plant needs of the aircraft so that all performance requirements can be met [6][7].

Constraint diagram is created using equations derived for each aircraft performance requirement given below.

- stall speed (V_s);
- maximum speed (V_{max});

- maximum rate of climb (ROC_{max});
- take-off run (S_{TO});
- ceiling (h_c);
- turn requirements (turn radius and turn rate).

Equations can be found in below [2]:

$$\left(\frac{W}{P_{SL}}\right)_{V_{Max}} = \frac{\eta_p}{\frac{1}{2}\rho_0 V_{max}^3 C_{D_0}\frac{1}{\left(\frac{W}{S}\right)} + \frac{2k}{\rho\sigma V_{Max}}\left(\frac{W}{S}\right)} \tag{3.11}$$

$$\left(\frac{W}{P}\right)_{ROC} = \frac{1}{\frac{ROC}{\eta_P} + \sqrt{\frac{2}{\rho\sqrt{\frac{3C_{D_0}}{k}}}\left(\frac{W}{S}\right)}\left(\frac{1.155}{(L|D)_{max}\eta_P}\right)} \tag{3.12}$$

$$\left(\frac{W}{P}\right)_{S_{TO}} = \frac{1 - exp\left(0.6\rho g C_{D_G} S_{TO}\frac{1}{w/s}\right)}{\mu - \left(\mu + \frac{C_{D_G}}{C_{L_R}}\right)\left[exp\left(0.6\rho g C_{DG} S_{TO}\frac{1}{(w/s)}\right)\right]}\frac{\eta_P}{V_{TO}} \tag{3.13}$$

HavaKaşifi doesn’t have take-off requirement thus, take-of run equation isn’t plotted in constraint diagram. Constraint diagram of HavaKaşifi can be found in Figure 3.2. Design point can be seen on figure. This point determined as given below:

- Stall speed requirements met in the region on left of the curve
- Maximum speed, maximum rate of climb, take-off run, ceiling, and turn requirements met in the region below of their curves.

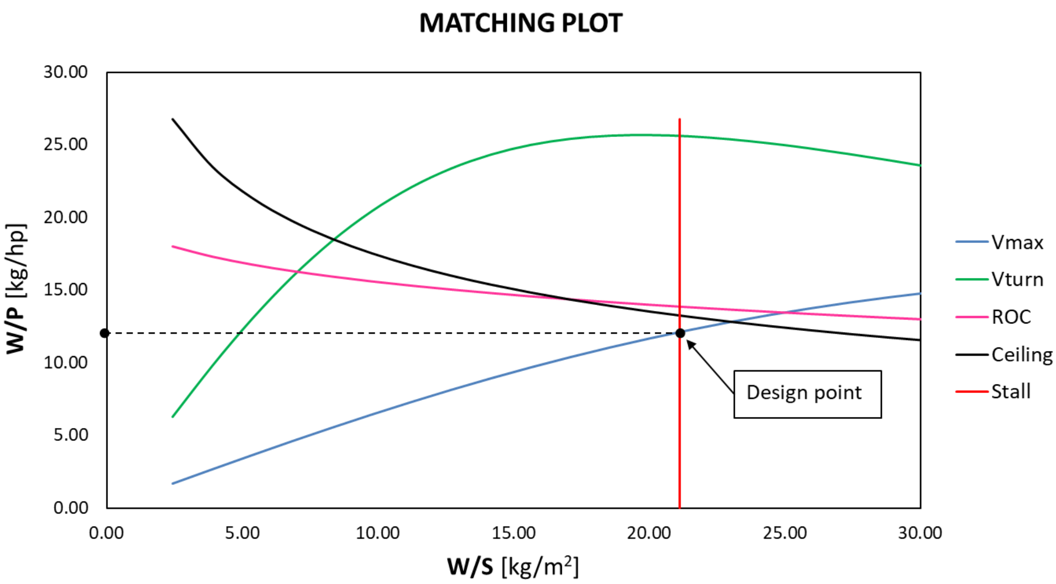

Figure 3.2 : Constraint plot (Matching plot)

Corresponding power loading and wing loading are, respectively:

$$\frac{W}{S} = 21.13\frac{kg}{m^2} \quad , \quad \frac{W}{P} = 11.68\frac{kg}{hp} \tag{3.14}$$

And weight is equal to 16.93 kg. Wing area and engine power are obtained as below.

$$S = 0.8\,m^2 \quad , \quad P = 1.45hp \tag{3.15}$$

3.4 Wing Design

The wing design study is undoubtedly the most important part of the aircraft design. Since the determination of the wing geometry, which has quite different appearances according to the flight characteristics, in accordance with the performance requirements, has a great impact on the success of the design to be obtained at the end of the process, it is important that it is done through a detailed examination. This stage can be expressed in two different parts. The first one is the selection of the airfoil, and the second one is the determination of the geometric properties of the wing such as taper ratio, aspect ratio, sweep angle. While the choice of airfoil has a great influence on the aerodynamic coefficients of the wing to be designed, the wing geometry determines the distribution of the transport on the wing, the regions where stall will start, the placement and shape of the control surfaces.

3.4.1 Airfoil selection

In the airfoil selection phase, a candidate pool was created by first considering the airfoils in the literature that meet the performance characteristics to meet our mission parameters. Since the main focus of the design in question here is to have a high endurance time, the performance criterion at the focal point will be to provide as high aerodynamic efficiency (L/D ratio) as possible.

The MH-114 has been chosen as a wing profile since it provides very high aerodynamic efficiency values according to [8].

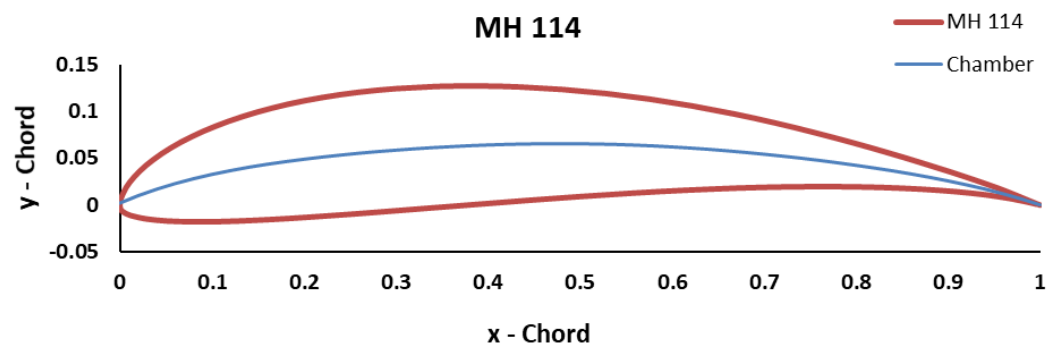

Figure 3.3 : MH 114(Scaled).

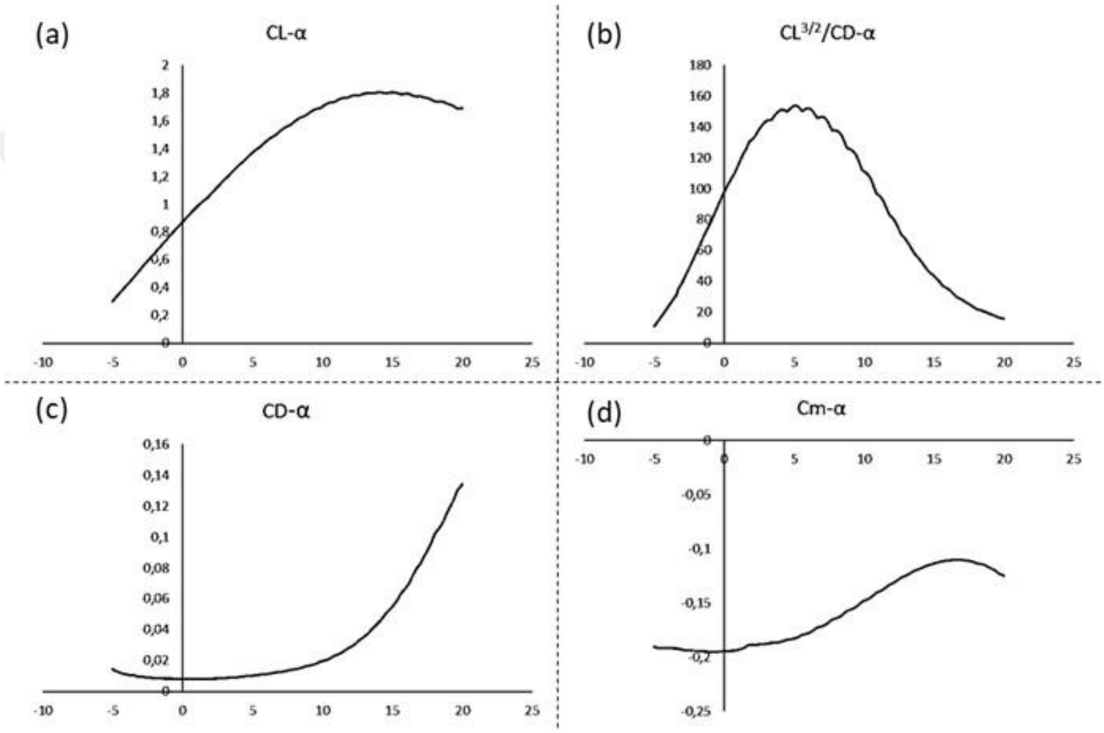

Figure 3.4 : Aerodynamic curves of MH-114: (a) lift curve. (b) $C_L^{3/2}/C_D$-α curve (c) drags curve (d) pitching moment curve.

Table 3.11 : Aerodynamic properties of MH-114

Parameter	Symbol	Value	Unit
Maximum lift	$C_{l_{max}}$	1.80	
Zero-angle lift	C_{l_0}	0.88	
Zero-angle moment	C_{m_0}	0.1935	
Minimum profile drag	C_{dmin}	0.00823	
Maximum lift to drag ratio-	$(C_l/C_d)_{max}$	134	
-	$(C_l^3/C_d^2)_{max}$	154	
Profile lift curve coefficient	C_{l_α}	0.1093	1/der
Zero-lift angle	α_{l_0}	-7.34	der
Stall angle	α_{stall}	14.58	der
Thickness ratio	% (t/c) r	12.85	

As can be seen in Fig3.1 where the aerodynamic coefficients are given, our airfoil has a very high $L^{3/2}/D$ ratio and the maximum values of this value are very close to the 0-degree angle of attack. When the aerodynamic efficiency of jet engine propulsion aircraft is analyzed, the L/D ratio is taken into consideration, whereas when the aerodynamic efficiency of propeller type propulsion aircraft is analyzed, the $L^{3/2}/D$ ratio is taken into consideration. Therefore, when considering airfoils in terms of aerodynamic efficiency, the base aerodynamic coefficient is the $L^{3/2}/D$ expression. In this airfoil, the magnitude of the moment coefficient in the negative direction seems to be a disadvantage, but since in this case it is not possible to achieve both a low moment coefficient value and an airfoil with high aerodynamic efficiency, the first priority is the high aerodynamic efficiency. Considering the relatively large moment coefficient compared to the other airfoils, it can be said that a larger tail area or a longer tail arm will be required when tail sizing is done in the future. This will be discussed in more detail in the following sections.

3.4.2 3D wing sizing

In this section where the wing will be handled in 3D, geometric properties such as span ratio, arrow angle, taper ratio will be emphasized. Then, when a result is reached in these parameters, the 3D external geometry of the wing will be obtained using these features. In the next stage, the aerodynamic coefficients of the 3D wing design will be obtained by using the 2D aerodynamic data of the airfoil.

3.4.2.1 Geometric properties of wing

In the previous sections, a design point was selected from the constraint diagram and ratios such as T/W and W/S were obtained based on this point. The weight estimation was also done after obtaining the fuel fractions. With this data known, it is now possible to determine the wing area. In this case, the wing area is obtained as follows:

$$\frac{W}{S} = 21.13\frac{kg}{m^2} \quad , \quad W = 16.93\ kg$$

Thus; wing area is:

$$S = 0.8\ m^2 \tag{3.16}$$

Considering Figure 3.5. Mathematical expressions for important properties of the wing are presented subsequent formulas [7].

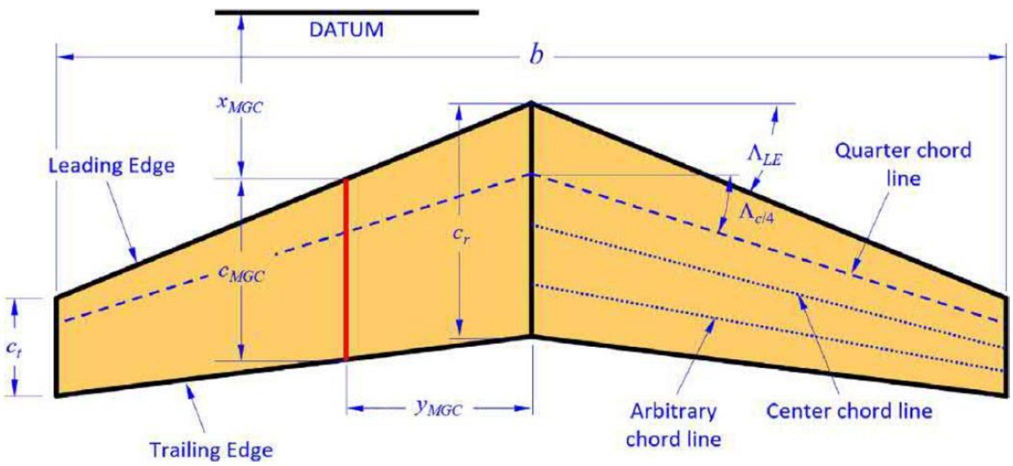

Figure 3.5 : Fundamental definitions of a trapezoidal wing planform [7].

Aspect ratio:

$$AR = \frac{b^2}{S} \tag{3.17}$$

Taper ratio:

$$\lambda = \frac{c_t}{c_r} \tag{3.18}$$

Root chord

$$c_r = \frac{2b}{(1+\lambda)AR} \tag{3.19}$$

Average chord

$$\bar{c} = \frac{c_r + c_t}{2} = \frac{c_r}{2}(1+\lambda) \tag{3.20}$$

Mean Geometric Chord (or Mean Aerodynamic Chord)

$$c_{MGC} = \left(\frac{2}{3}\right) c_r \left(\frac{1+\lambda+\lambda^2}{1+\lambda}\right) = \left(\frac{4b}{3AR}\right)\left(\frac{1+\lambda+\lambda^2}{1+2\lambda+|\ \lambda^2}\right) \tag{3.21}$$

Chord for a straight-tapered wing:

$$c(y) = c_r\left(1 + \frac{2(\lambda-1)}{b} y\right) \tag{3.22}$$

Y-location of MGC

$$y_{MGC} = \left(\frac{b}{6}\right)\left(\frac{1+2\lambda}{1+\lambda}\right) \tag{3.23}$$

X-location LE of MGC

$$x_{MGC} = y_{MGC}\, tan\, \Lambda_{LE} \tag{3.24}$$

Angle of quarter chord line

$$tan\, \Lambda_{c/4} = tan\, \Lambda_{LE} + \frac{c_r}{2b}(\lambda - 1) \tag{3.25}$$

Angle of an arbitrary chord - line:

$$tan\, \Lambda_n = tan\, \Lambda_m - \frac{4}{AR}\left[(n-m)\frac{1-\lambda}{1+\lambda}\right] \tag{3.26}$$

Where m and n are chordwise ratios of the chord lines such that m is the ratio for a known angle and n for the unknown angle. For instance, if it’s known the quarter chord angle and the half chord is unknown: m and n equal to 0.25 and 0.5, respectively [7].

Span efficiency e is defined as given below:

$$e = \frac{2}{2 - AR + \sqrt{4 + AR^2(1 + tan\Lambda_{tmax}^2}} \tag{3.27}$$

Where, $tan\lambda_{tmax}$: Swept angle at maximum chord thickness line

All geometric properties can be calculated using formulas given above with governing variables. These governing variables are: wing area (S), aspect ratio (AR), taper ratio

(λ) and angle of leading edge (Λ_{LE}). Wing area is obtained from constraint diagram. Other variables are selected considering similar aircrafts at Table 3.1. For HAWK these parameters are listed in Table 3.12.

Table 3.12 : Governing variables for obtaining wing geometrical properties.

Parameter	Symbol	Value	Unit
Wing area	S	0.8	m2
Taper ratio	λ	0.70	
Aspect ratio	AR	14	
Leading edge-swept angle	Λ_{LE}	7	deg

Thus, geometrical parameters of wing are obtained as given in Table 3.13.

Table 3.13 : Geometric properties of wing

Parameter	Symbol	Value	Unit
Span	b	3.349	m
Root chord	c_r	0.281	m
Tip chord	c_t	0.197	m
Mean geometric chord	c or MGC	0.242	m
Angle of leading-edge line	Λ_{LE}	7.00	der
Angle of trailing edge line	Λ_{TE}	4.14	der
Angle of quarter chord line	$\Lambda_{0.25c}$	6.29	der
Angle of half chord line	$\Lambda_{0.5c}$	5.57	der
X-location LE of MGC	X_{MGC}	0.097	m
Y-location of MGC	Y_{MGC}	0.788	m
X-location LE of 0.25MGC	$X_{0.25MGC}$	0.157	m
Distance between wing root LE and tip LE	l_{r2t}	0.206	
Thickness ratio	% (t/c)	12.846	
Maximum thickness at root	t_r	0.036	
Maximum profile thickness at tip	t_t	0.025	
Maximum profile thickness at MGC	t_{MGC}	0.031	
Chord corresponding to tail span	c_{w_h}	0.264	
Profile thickness corresponding to tail span	t_{w_h}	0.034	
Chordwise position of wing root LE from airplane nose	X_{LE}	0.460	
Span efficiency	e	0.906	

3.4.2.2 Control surface sizing - aileron

Aileron chord ratio is set at 0.265c to be consistent with flaps (see section 3.11.2.4) Aileron span ratio is taken at 0.45 to 0.70 for preliminary design phase.

Rear and Front spar location is determined according to [9]

- Rear spar location: (1-0.265-0.005) c = 0.73c

- Front spar location: 0.20c

Figure 3.6 shows a dimensioned drawing of the proposed wing platform.

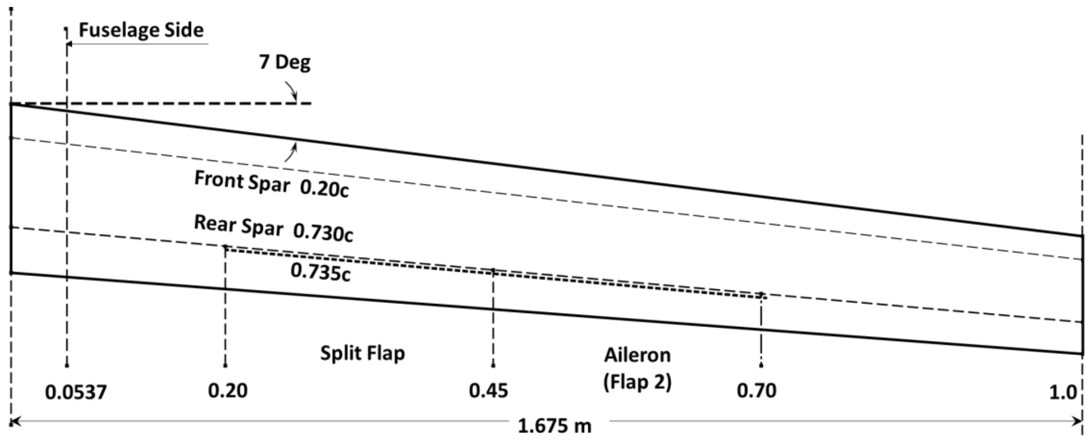

Figure 3.6 : Wing planform geometry (Scaled).

3.5 Empennage Design

In this chapter empennage sizing is presented. Sizing the empennage start by deciding on the magnitude of S_h and S_v. The so-called Volume-method represented equations 3.28 and 3.29 is used for it. Volume coefficients and moment arms for both horizontal tail and vertical tail represented at given Figure 3.8.

$$V_h = \frac{x_h S_h}{Sc} \tag{3.28}$$

$$V_v = \frac{x_v S_v}{Sb} \tag{3.29}$$

Considering similar aircraft geometrical data parameters are determined and areas are calculated. Result can be found in Table 3.14.

Table 3.14 Governing variables for obtaining tail geometrical properties.

Parameter	Symbol	HT	VT	Unit
Volume coefficient	V	0.47	0.025	
Tail arm	l	0.952	0.952	m
Control surface area (elevator or rudder) to tail (HT or VT)	S_e/S_h or S_r/S_v	0.234	0.17	
Area	S	0.096	0.038	m^2
Taper ratio	λ	1	0.68	
Aspect ratio	AR	4.8	1.7	
Leading edge-swept angle	Λ_{LE}	0	28	deg

Geometric parameters for horizontal and vertical tail calculated exactly as it is for the wing. Except for vertical tail aspect ratio and area for twin tail.

- Span of vertical tail is defined as height of the vertical tail (VT) from its base to tip.
- AR for a twin tail is calculated considering one tail only, where S_v refers to one half the total are of the vertical tail.

Table 3.15 Geometric properties of horizontal tail and vertical tail.

Parameter	Symbol	HT	VT	Unit
Span	b	0.677	0.25	m
Root chord	c_r	0.141	0.208	m
Tip chord	c_t	0.141	0.141	m
Mean geometric chord	c or MGC	0.141	0.176	der
Angle of trailing edge line	Λ_{TE}	0	15.19	der
Angle of quarter chord line	$\Lambda_{0.25c}$	0	22.76	der
Angle of half chord line	$\Lambda_{0.5c}$	0	17.10	der
X-location LE of MGC	X_{MGC}	0.00	0.064	m
Y-location of MGC	Y_{MGC}	0.00	0.120	m
X-location LE of 0.25MGC	$X_{0.25MGC}$	0.04	0.108	m
Thickness ratio	% (t/c)	12.84		
Maximum thickness at root	t_r	0.016		
Maximum thickness at tip	t_t	0.016		
Maximum thickness at MGC	t_{MGC}	0.016		

Furthermore, arm definitions for horizontal and vertical tail can be seen from Figure 3.7 and Figure 3.8. l_a, l_b, l_c and l_d are calculated from equation 3.30 to 3.33.

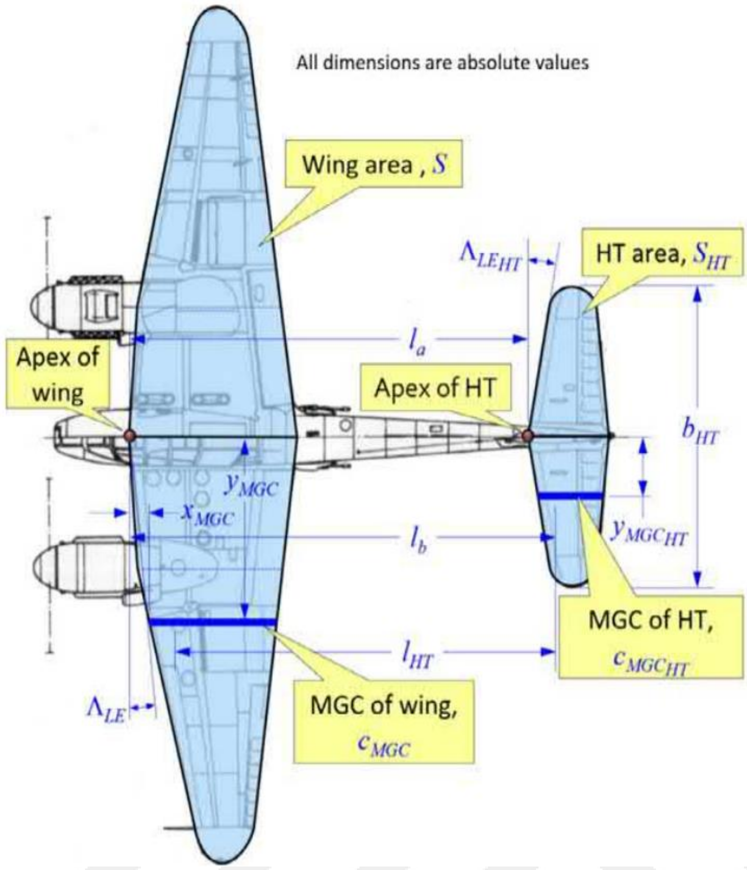

Figure 3.7 : Representation of horizontal tail geometric parameters [7]

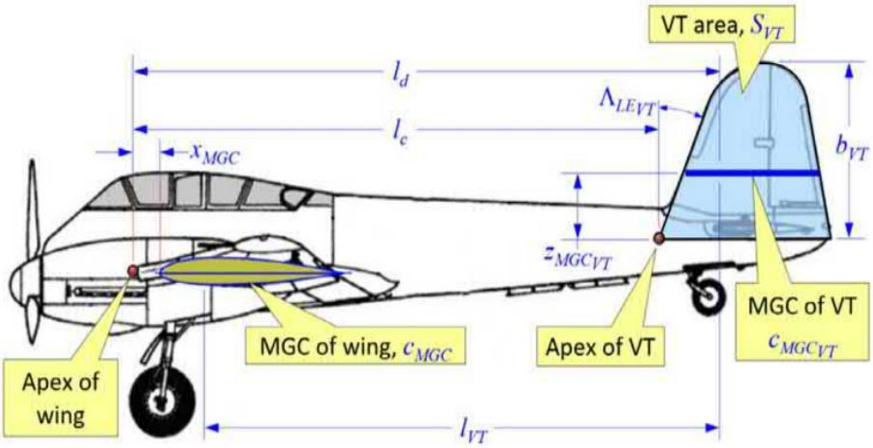

Figure 3.8 : Representation of vertical tail geometric parameters [7]

$$l_b = l_a + y_{MGC_{HT}} \tan \Lambda_{LE_{HT}} \tag{3.30}$$

$$l_d = l_c + z_{MGC_{VT}} \tan \Lambda_{LE_{VT}} \tag{3.31}$$

$$l_{HT} = l_a - \left(y_{MGC} \tan \Lambda_{LE} + \frac{1}{4} c_{MGC} \right) + \left(y_{MGC_{HT}} \tan \Lambda_{LE_{HT}} + \frac{1}{4} c_{MGC_{HT}} \right) \tag{3.32}$$

$$l_{VT} = l_c - \left(y_{MGC} \tan \Lambda_{LE} + \frac{1}{4} c_{MGC} \right) + \left(z_{MGC_{VT}} \tan \Lambda_{LE_{VT}} + \frac{1}{4} c_{MGC_{VT}} \right) \tag{3.33}$$

Tail arm geometric properties can be found in Table 3.16. Tail boom radius is determined considering wing and horizontal tail thickness.

Table 3.16 : Geometric properties of tail arm

Parameter	Symbol	Value	Unit
Radius of boom at wing quarter chord	R_1	0.019	m
Radius of boom at HT quarter chord	R_2	0.008	m
Distance between wing root chord LE and HT root chord LE	l_a	1.07	m
Distance between wing root chord LE and HT MGC quarter chord	l_b	1.11	m
Distance between wing root chord LE and VT root chord LE	l_c	0.92	m
Distance between wing root chord LE and VT MGC quarter chord	l_d	1.03	m

3.5.1 Control surface sizing – elevator and rudder

Elevator and rudder sizing performed considering area ratio given in Table 3.17.

Table 3.17 : Elevator and rudder geometrical properties.

Parameter	Symbol	Elevator	Rudder	Unit
Control surface area (elevator or rudder) to tail (HT or VT)	S_e/S_h or S_r/S_v	0.234	0.17	
Area	S_e or S_r	0.022	0.0065	m^2

3.6 Fuselage Design

3.6.1 Fuselage segmentation

Fuselage sizing is performed considering aircraft requirements. Firstly, fuselage contain payload, avionics equipment and propulsion system equipment. Considering these fuselages can be separated 4 modules. Starting from nose:

- Payload module
- Avionic module
- Fuel tank module
- Engine module

These modules are represented simply in Figure 3.9.

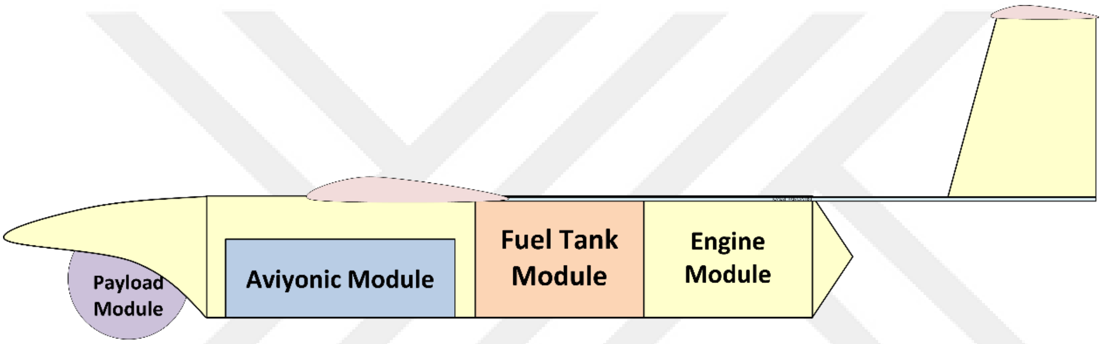

Figure 3.9 : Fuselage segmentation

Using similar aircraft data, length of fuselage (L_{fus}) and diameter of fuselage (D_{fus}) is determined 1.3 m and 0.18 m, respectively.

3.6.2 Payload module sizing

Payload module length is determined according to payload dimensions. From Table 3.24, payload width is 18 mm. Front of payload should cover radome. Radome can be idealized as a hemisphere has a diameter of fuselage so that length of it is equal to 9 mm. Considering structure length after payload, payload module length (L_p) can be formulated as below:

$$\begin{matrix} Payload \\ Module \\ Lenght \end{matrix} = \begin{matrix} Radome \\ Lenght \end{matrix} + \begin{matrix} Payload \\ Lenght \end{matrix} + \begin{matrix} Rear \\ Structure \\ Lenght \end{matrix} \tag{3.34}$$

Rear structure length is accepted as 9 mm. Hence payload module length is found as 36 mm.

$$L_p = 9 + 18 + 9 = 36\ mm \tag{3.35}$$

3.6.3 Fuel tank and engine module sizing

Fuel tank sizing is performed considering fuel weight and fuel density.

Fuel weight (W_f) is 4.6 kg, from **Table 3.10**. Fuel density (ρ_f) is 740 kg/m^3 (average density of gasoline) [10]. Hence, fuel volume (V_f) is;

$$V_f = \frac{W_f}{\rho_f} = \frac{4.6}{740} = 0.006216\ m^3 = 6.21\ L \tag{3.36}$$

Fuel tank length can be calculated assuming fuel tank has a wall thickness of 1 mm. Thus, diameter of fuel tank (D_f) is taken as 16 mm and fuel tank length (L_f) is calculated as below:

$$S_f = \frac{\pi D_f^2}{4} = \frac{\pi (0.16)^2}{4} = 0.02011\ m^2 \tag{3.37}$$

$$L_f = \frac{V_f}{S_f} = \frac{0.006216}{0.02545} = 0.309\ m \tag{3.38}$$

This calculation gives fuel tank size considering only its volume. Considering fuel hose, other sub systems and difficulties in perfect system integration total L_f is accepted as 0.40 m.

3.6.4 Summary of fuselage design

After L_P and L_f are determined remaining fuselage length is divided between avionic and engine module.

Thus, engine module length (L_E) and avionic module length (L_A) are calculated as below.

$$L_A = L_E = 0.5\left(L_{fus} - L_P - L_f\right) = 0.5(1.3 - 0.36 - 0.40 \\ = 0.27\ m \tag{3.39}$$

Hence, sizing for fuselage can be summarize in Table 3.18.

Table 3.18 : Summary of fuselage sizing

Parameter	Symbol	Value	Unit
Fuselage diameter	D_{fus}	0.18	mm
Fuselage length	L_{fus}	1.30	mm
Payload module length	L_P	0.36	mm
Avionics module length	L_A	0.27	mm
Fuel tank volume	V_f	6.21	L
Fuel tank module length	L_f	0.40	mm
Engine module length	L_E	0.27	mm

3.7 Propulsion System Design

3.7.1 Engine selection

Engine type and location is determined at section 2.5.2 and required engine power is calculated as 1.45 hp at section 3.3. Considering propulsion system requirements for HAVK, the Sky Power GmbH SP-28 CR engine is selected because it's known for being robust and lasting a long time. This engine has been used in similar small planes for over ten years, and one user even reported flying it for more than 1,000,000 hours without major issues [11]. As a summary it is selected since it fits perfectly with HAVK size and requirements, and it's proven to work well for long flights and different flying conditions. Specifications can be found in Table 3.19.

Figure 3.10 : Sky Power GmbH SP-28 CR [7]

Table 3.19 : Specification of SP-28 CR [11]

Specification	Value
Type	1-cylinder gas engine
Capacity	28 cc / 1.71 cu in
Power	2.2 HP / 1.6 KW
Speed Range	2,500 – 10,000 RPM
Weight	2.95 lbs (1.34 kg) incl. ignition
Crankshaft	3 ball bearings
Oil/Gasoline Ratio	1:50 / 2% mix
Operating Voltage	6 – 8.4 V DC
Bore Diameter	1.42 inch (36.00 mm)
Stroke	1.10 inch (28.00 mm)
Torque	2.3 Nm at 6,600 RPM

3.7.2 Propeller sizing

Propeller sizing perform considering statistical analysis based given aircraft data in Table 3.20 [9]. Even if these aircrafts are much bigger then HAWK using these values power to power loading graph is plotted and linear regression is applied to calculated corresponding propeller diameter for HAWK.

Table 3.20 : Aircraft's power and propeller data [9]

Airplane Type	**Pitch**	**Max. Power per Engine, Pmax (hp)**	**Prop. Diam., D' (ft)**	**Number of Prop. Blades, n_b'**	**Power Load. per Blade, Pbl (hp/ft²)**
Homebuilt					
Jurca MJ5	Fixed	115	6.1	2	2
Piel CP130	Fixed	160	5.9	2	2.9
Piel CP301	Fixed	90	5	2	2.3
Pottier P70S	Fixed	60	4.3	2	2.1
Pazmany PL4A	Fixed	50	5.7	2	1
Variviggen	Fixed	150	5.8	2	2.8
Rand/ KR-1	2-pos.	90	4.4	2	3
Van's RV-3	Fixed	125	5.7	2	2.5
Sequoia F8L	Fixed	135	6.2	2	2.2
Per. Osprey II	Fixed	150	5.5	2	3.2
FAR23 Certified					
Cessna 152	Fixed	108	5.8	2	2

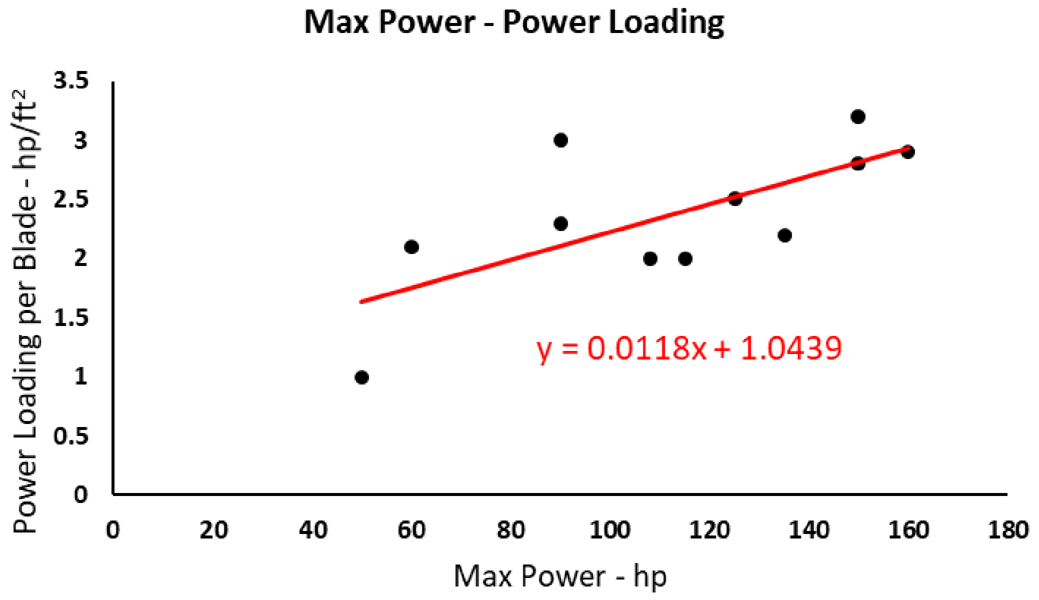

Figure 3.11 : Propellers maximum power to power loading chart.

From linear regression given equation 3.40 is obtained.

$$P_{bl} = 0.0118 * P_{max} + 1.0439 \tag{3.40}$$

For P_{max} is 2.2 hp, P_{bl} is calculated as 1.07 hp/ft^2. Furthermore, power loading is defined as given below.

$$P_{bl} = \frac{P_{max}}{n_b A_{prop}} = \frac{P_{max}}{n_b \frac{\pi D_{prop}^2}{4}} \tag{3.41}$$

Propeller sizing results can be found in Table 3.21.

Table 3.21 : Summary of propeller sizing

Specification	Value
Propeller Pitch	Fixed
Number Blades	2
Propeller Diameter	0.356 m/14 in
Power Loading per Blade	1.07 hp/ft^2
Propeller Pitch	7 in

3.7.3 Static thrust

Static thrust is calculated as following [7]:

$$T_{STATIC} = K_P P_{req}^{\frac{2}{3}} (2\rho A_P)^{\frac{1}{3}} \left(1 - \frac{A_{spinner}}{A_P}\right) \tag{3.42}$$

Kp scale-based correction factor is selected from Table 3.22. For HAVK average of RC aircraft application which is 0.375 is selected [7].

Table 3.22 : Scale-based correction factor.[7]

Application	Range of Kp
RC aircraft	0.2–0.45
Small, fixed-pitch propellers (kit planes)	0.5–0.65
Medium, fixed and constant speed propellers	0.7–0.75
Large turboprops, constant speed propellers	0.75–1.0

Result summary given table following:

Table 3.23 : Summary of static thrust

Specification	Value
T_{STATIC}	**7 lb / 30 N (h=1000 m)**
D_P	14 in/356 mm
$D_{spinner}$	3.5 in/89 mm (assumed)
P_{req} or P_{BHP}	2.2 hp
ρ	1.111 kg/m^3(h=1000 m.)

3.8 Payload

HavaKaşifi should perform intelligence, surveillance and reconnaissance missions. Thus, payload type of it selected as Electro-Optical/Infrared (EO/IR) Systems. These payloads provide day and night vision capabilities, important for ISR missions. They often come with features like target tracking, geolocation, and zoom capabilities [12].

Ukrspec Systems' USG-400 camera system is selected as payload. Fundamental features of it are given below.

- Full HD EO with 30x optical zoom
- Scene lock
- Target tracking
- Digital video stabilization
- Anti-fog feature
- On-board recording and storage
- Laser rangefinder

Figure 3.12 : Ukrspec Systems' USG-400 camera [13].

Table 3.24 : Physical data of USG-400 camera [13].

Attribute	Value
Width	180 mm
Height	180 mm
Depth	250 mm
Power consumption	50 W
Power voltage	12-24 V
Environmental protection	IP65

3.9 Weight Analysis

3.9.1 Component weight estimation

Component weight estimations are performed considering both Class 1 and Class 2 method of [14]

3.9.2 Class 1 method for estimating airplane component weights

According to the Class I weight estimating method, within each airplane category, gross take-off weight can be used as a base to calculate the weight of major airplane components (or groups) as a simple fraction [14].

The weight fraction data of the Bede BD5B homebuilt aircraft was used for weight estimates as it is the only aircraft among all homebuilt and single-engine propeller aircraft categories represented in [14] with a similar empty weight fraction value of 0.52 (see Table 3.10) as the HAVK. Bede BD5B homebuilt aircraft weight data shown in Table 3.25.

Table 3.25 : Group Weight Data for Bede BD5B [14].

Type	Bede BD5B
Flight Design Gross Weight, GW, kg	477
Fuselage Group/GW	0.085
Wing Group/GW	0.083
Empenn. Group/GW	0.016
Land. Gear Group/GW	0.03
Structure Weight/GW	**0.214**
Fixed Equipmt/GW	0.119
Power Plant/GW	0.18
Nacelle Group/GW	0
Empty Weight/GW	**0.513**

Using fraction value shown in Table 3.25. Weight of components group of HAVK is obtained and results are listed Table 3.27.

Table 3.26 : Group Weight Data for HAVK

Type		Weight, kg
Flight Design Gross Weight		16.930
Fuselage Group		1.436
Wing Group		1.402
Empenn. Group		0.271
Land. Gear Group		0.000
	Structure Weight	**3.109**
Fixed Equipmt.		2.011
Power Plant		3.041
Nacelle Group		0.000
	Empty Weight	8.160

Separating weight groups in to components is performed a s given below:

- Empennage group of HAVK consist of horizontal and vertical tail. These two separated considering planform area ratios.
- There is no landing gear usage in HAVK so separating them is not a concern for this study.
- Fuselage weight is separated in to fuselage and booms considering their wetted area ratio. See Table 3.63

Table 3.27 : Weight of Separated Components

Weight	Symbol	kg
Wing	W_w	1.402
Horizontal tail	W_h	0.152
Vertical tail	W_v	0.118
Fuselage	W_{fus}	1.045
Boom	W_{boom}	0.391
Fixed Equipmt.	W_{feq}	2.011
Power Plant	W_{pwr}	3.041

3.9.3 Class 2 method for estimating airplane component weights

Class 2 method is detailed version of Class 1 method. It includes methods for component weight estimation provided by Cessna, Torenbeek and USAF [14]. In following chapter inputs required for each component are listed. Results are obtained considering each three methods then with an average they are listed in tables.

3.9.3.1 Structural weight

Wing weight

In this chapter weight estimation inputs for wing and results are listed.

Table 3.28 : Wing weight estimation inputs

Parameter	Symbol	Value	Unit
Maximum speed	V_{max}	38.97	m/s
Take-off weight	W_{TO}	16.91	kg
Wing area	S	0.801	m^2
Wing aspect ratio	A	14.00	
Taper ratio	λ	0.70	
Wing quarter-cord sweep angle	$\Lambda_{c/4}$	6.29	der
Wing half-cord sweep angle	$\Lambda_{c/4}$	5.57	der
Thickness ratio (root)	$\%(th / ch)_r$	12.85	
Thickness ratio (tip)	$\%(th / ch)_t$	12.85	
Ultimate load factor	N_{ult}	3.60	

Table 3.29 : Wing weight estimation outputs

Parameter	Value	Unit
Cessna method	65.00	lb
Torenbeek method	2.50	lb
USAF method	2.90	lb
Average value	23.50	lb
Selected value	2.70	lb
Selected value	1.22	kg

Cessna method gives un realistic result; thus, average of Torenbeek and USAF method is selected.

Horizontal tail weight

In this chapter weight estimation inputs for horizontal tail and results are listed.

Table 3.30 : Horizontal tail weight estimation inputs

Parameter	Symbol	Value	Unit
Take-off weight	W_{TO}	16.91	kg
Horizontal tail area	S_h	0.083	m2
Vertical tail area	S_v	0.057	m2
Horizontal tail aspect ratio	A_h	4.50	
Horizontal tail thickness ratio (root)	$\%(t_h/c_h)_r$	12.85	
Ultimate load factor	N_{ult}	3.60	
Distance between wing quarter-MGC and horizontal tail quarter-MGC	L_h	1.18	m

Table 3.31 : Horizontal tail estimation outputs

Parameter	Value	Unit
Cessna method	0.99	lb
Torenbeek method	0.104	lb
USAF method	0.642	lb
Average value	0.579	lb
Selected value	0.579	lb
Selected value	0.262	kg

Average value is selected as design value.

Vertical tail weight

In this chapter weight estimation inputs for vertical tail and results are listed.

Table 3.32 : Vertical tail weight estimation inputs

Parameter	Symbol	Value	Unit
Take-off weight	W_{TO}	16.91	kg
Horizontal tail area	S_h	0.077	m2
Vertical tail area	S_v	0.057	m2
Horizontal tail aspect ratio	A_h	1.30	
Horizontal tail quarter-cord sweep	$\Lambda_{c/4}$	28.50	der
Horizontal tail thickness ratio (root)	$\%(t_h/c_h)_r$	12.85	
Ultimate load factor	N_{ult}	3.60	

Table 3.33 : Vertical tail weight estimation outputs

Parameter	Value	Unit
Cessna method	0.062	lb
Torenbeek method	0.077	lb
USAF method	0.386	lb
Average value	0.175	lb
Selected value	0.386	lb
Selected value	0.175	kg

Average value is selected as design value. Be careful that HAVK has twin tail thus average value is multiplied.

Fuselage weight

In this chapter weight estimation inputs for fuselage and results are listed.

Table 3.34 : Fuselage weight estimation inputs

Parameter	Symbol	Value	Unit
Cruise Speed	Vc	25.00	m/s
Take-off weight	W_{TO}	16.91	kg
Fuselage Length	Lf	1.300	m
Fuselage Height	wf	0.180	m
Fuselage Width	hf	0.180	m
Ultimate load factor	Nult	3.6	

Table 3.35 : Fuselage weight estimation outputs

Parameter	Value	Unit
Cessna method	No method	lb
Torenbeek method	No method	lb
USAF method	0.991	lb
Average value	0.5	lb
Selected value	0.991	lb
Selected value	0.449	kg

USAF method's result is selected since its only available one.

Boom weight

Boom weight is estimated considering wetted area of booms and fuselage. Fuselage weight is multiplied by booms wetted area to fuselage wetted area. Wetted areas taken from Table 3.63.

Table 3.36 : Boom weight estimation inputs

Parameter	Symbol	Value	Unit
Fuselage weight	W_{fus}	0.499	kg
Fuselage wetted area	S_{wetfus}	0.604	m^2
Boom wetted area	$S_{wetboom}$	0.226	m^2

$$W_{boom} = \frac{S_{wet_{boom}}}{S_{wet_{fus}}} W_{fus} = \frac{0.226}{0.604} 0.449 = 0.168\ kg \qquad (3.43)$$

Structural weight summary

In this chapter structural components of weight estimated from Class 1 and Class 2 method are compared and design structural weight value selection is performed.

Table 3.37 shows Class 2 method structural component weight summary; furthermore, Class 1 and Class 2 structural weight estimating results can be shown in Table 3.38.

Design structural weights are selected considering average of Class 1 and Class 2 method.

Table 3.37 : Class 2 method structural components weight summary.

Weight	Symbol	kg	ratio
Wing	W_w	1.226	0.537
Horizontal tail	W_h	0.263	0.115
Vertical tail	W_v	0.175	0.077
Fuselage	W_{fus}	0.450	0.197
Boom	W_{boom}	0.168	0.074
Total structural	W_{st}	2.282	1.000

Table 3.38 : Class 1 and Class 2 methods structural components weight summary

Weight	Symbol	Class 1 kg	Class 2 kg	Average kg
Wing	W_w	1.402	1.226	1.314
Horizontal tail	W_h	0.152	0.263	0.208
Vertical tail	W_v	0.118	0.175	0.147
Fuselage	W_{fus}	1.045	0.450	0.748
Boom	W_{boom}	0.391	0.168	0.280
Total structural	W_{st}	3.108	2.282	2.695

3.9.3.2 Installed engine weight

The airplane installed engine weight, W_{pwr} is assumed to consist of the following components [14]:

$$W_{pwr} = W_e + W_{ai} + W_{prop} + W_{fs} + W_p \tag{3.44}$$

W_e: Engines

W_{ai}: Air induction system

W_{prop}: Propellers

W_{fs}: Fuel System

W_p: Propulsion System

- engine controls
- starting systems
- propeller controls
- provisions for engine installation

Roskam gives three methods for engine weight estimations [14]. Cessna method estimates W_e , while USAF method is $W_{pwr} - W_{fs}$ and Torenbeek is W_{pwr}

In this study W_e is directly taken from Table 3.19 as 1.34 kg and W_{pwr} will be calculated using Torenbeek method from Eq 6.4 of [14].

Table 3.39 : Installed engine weight estimation

Parameter	Symbol	Value	Unit
Engine weight	W_e	1.34	kg
Engine power	P_{TO}	2.2	hp
Installed engine weight	W_{pwr}	1.78	kg

3.9.3.3 Fixed equipment weight

Fixed equipment list for HAVK and estimated weights are listed in Table 3.40.

Table 3.40 : Fixed equipment list and estimated weight

Parameter	Weight, kg	Ref.
Flight Control System (FCS)	0.301	[15]
GPS and INS (Inertial Navigation System)	0.101	[16]
Communication System	0.98	[17]
Power System	0.437	[18]
Autopilot	0.073	[19]
Telemetry System	0.014	[20]
Fixed Equipment Weight	1.024	

3.9.3.4 Component weight summary

Component weight summary is given in Table 3.41.

Table 3.41 : Component Weight Summary

Weight	W_i	kg	Wi/WTO
Empty Weight	W_E	7.647	0.48
Trap. Fuel Oil	W_{tfo}	0.230	0.01
Op. Weight Emp.	W_{oe}	7.876	0.49
Fuel weight	W_f	4.594	0.29
Payload	W_p	3.489	0.22
Take-Off Weight	W_{TO}	15.960	1.00

3.9.4 Component CG estimation

In previous chapter component’s weight are estimated. Further step of weight analysis is to enter appropriate x, y, and z coordinates for each component. Figure 3.13 taken from [5] shows how CGs of major components can be determine. For other components CG is selected considering below:

- Boom: Half of its length is considered as CG
- Fuel system: Center of fuel system module described in section 0 is taken as CG.
- Engine: Center of engine module described in section 0 is taken as CG.
- Payload: Center of payload module described in section 0 is taken as CG.

List of components CG's can be found in Table 3.42.

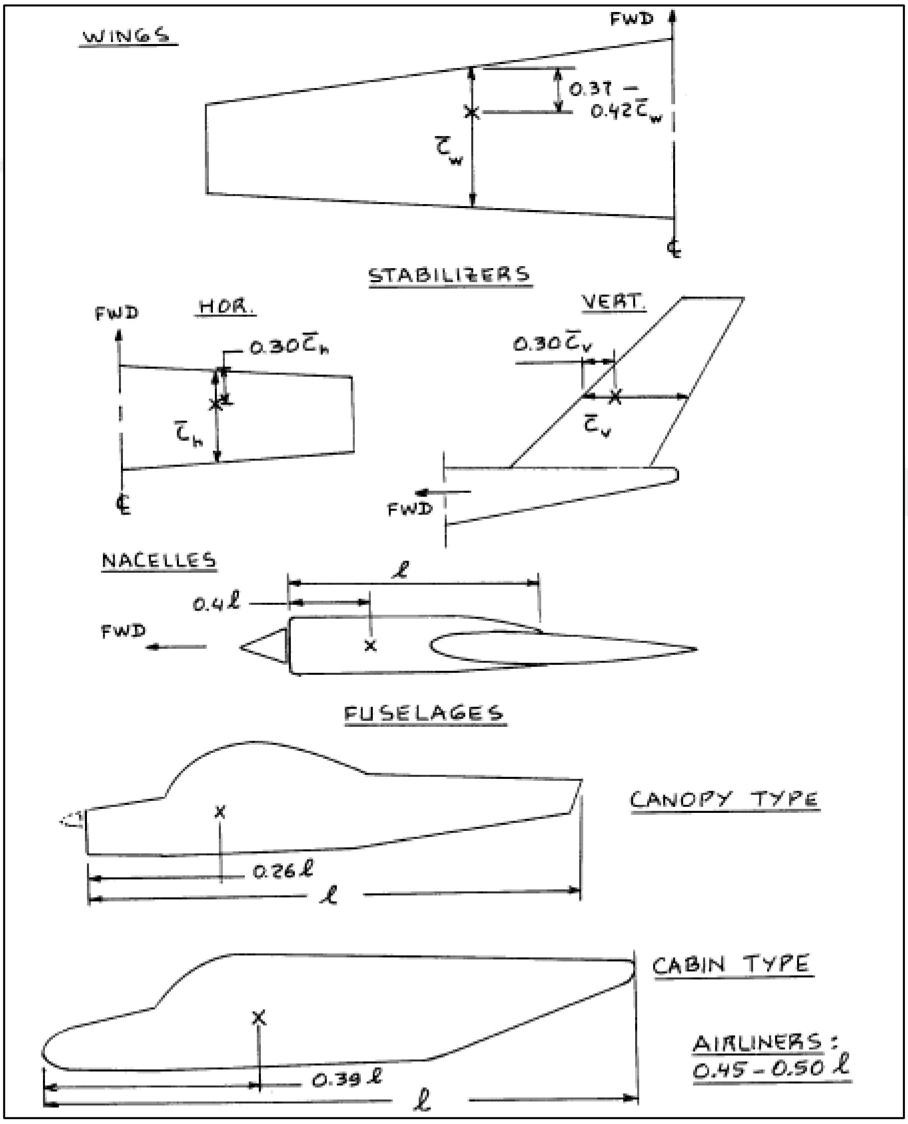

Figure 3.13 : Location of CGs of Major Components [9]

Table 3.42 : Component CG's.

Weight	CG (x axis)
Wing	$0.37C_w$
Horizontal tail	$0.30C_h$
Vertical tail	$0.30C_v$
Fuselage	$0.5L_{fus}$
Boom	$0.5L_{bom}$
Inst. Engine	$0.5L_E$
Trap. Fuel Oil	$0.5L_f$
Fuel	$0.5L_f$
Payload	$0.5L_P$

3.9.5 Component weigh locations

Figure below represents an aircraft weight and balance coordinate frame. Origin of coordinate frame should be selected so that all x and z coordinates are positives [9]. In this study origin of coordinate frame is determined that radome coordinates of an aircraft are written as (1000, 0, 1000) mm, as can be seen in Table 3.43.

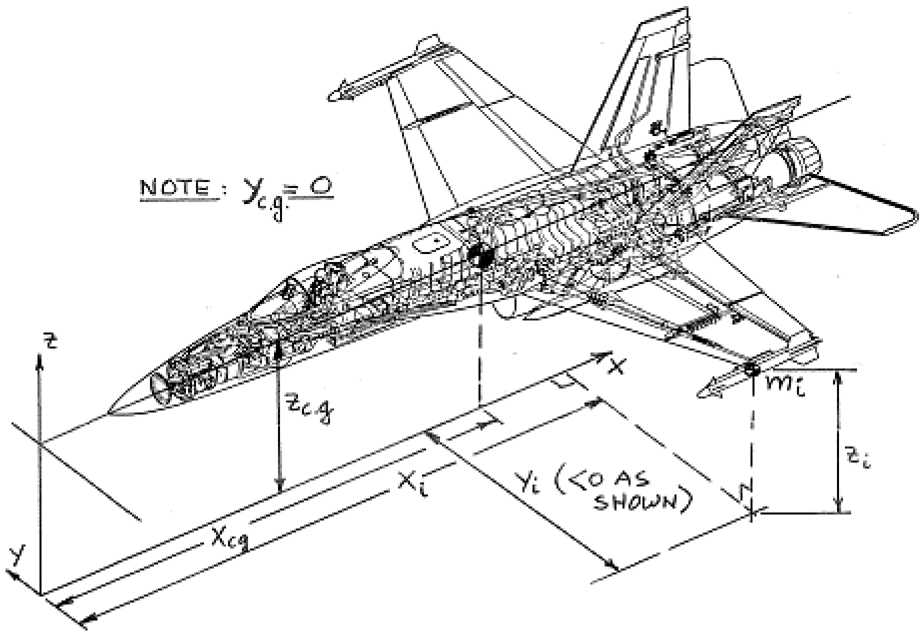

Figure 3.14 : Definition of Coordinates. [9]

Table 3.43 : Radome nose coordinates of an aircraft.

Xi (mm)	Yi (mm)	Zi (mm)
1000	0	1000

The overall center of gravity of the airplane is found from:

$$x_{cg} = \frac{\sum_{i=1}^{n} w_i x_i}{\sum_{i=1}^{n} w_i} \tag{3.45}$$

$$\sum_{i=1}^{n} W_i = W \tag{3.46}$$

Table 3.44 shows the results of calculated CGs. It can be seen that CG locations are calculated for all feasible locations:

A. Empty weight

B. Empty weight + trapped fuel and oil weight = Operational weight empty

C. Operational weight empty + fuel

D. Operational weight empty + payload = Take-off weight

E. Take-off weight – fuel weight

Summary of center cg gravity locations for given scenario above are listed in Table 3.45.

Table 3.44 : Component Weight and Coordinate Data

No	Component		Weight kg	x mm	Wx kg.mm	y mm	Wy kg.mm	z mm	Wz kg.mm
1	Wing	W_w	1.314	1625	2136	0	0	1080	1419
2	Horizontal tail	W_h	0.208	2754	571	0	0	1080	224
3	Vertical tail	W_v	0.147	2754	403	0	0	1134	166
4	Fuselage	W_{fus}	0.748	1493	1116	0	0	991	740
5	Boom	W_{boom}	0.280	2126	594	0	0	1080	302
6	Inst. Engine	W_{pwr}	1.780	2145	3817	0	0	1080	1922
7	Fixed equip.t	W_{feq}	3.172	1481	4697	0	0	946	3001
	Empty Weight	$\mathbf{W_E}$	**7.647**	**1744**	**13335**	**0**	**0**	**1017**	**7774**
8	Trap. Fuel Oil	W_{tfo}	0.230	1625	373	0	0	973	223
	Op. Weight Emp.	$\mathbf{W_{oe}}$	**7.876**	**1740**	**13709**	**0**	**0**	**1015**	**7997**
9	Fuel weight	W_f	4.594	1625	7468	0	0	973	4469
10	Payload	W_p	3.489	1169	4078	0	0	955	3332
	Take-Off Weight	$\mathbf{W_{TO}}$	**15.960**	**1582**	**25255**	**0**	**0**	**990**	**15798**
	Op. Weight Emp.	W_{oe}	7.876	1740	13709	0	0	1015	7997
	Fuel weight	W_f	4.594	1625	7468	0	0	973	4469
	$\mathbf{W_{oe} + W_f}$		**12.471**	**1698**	**21177**	**0**	**0**	**1000**	**12467**
	Take-Off Weight	W_{TO}	15.960	1582	25255	0	0	990	15798
	Fuel weight	W_f	4.594	1625	7468	0	0	973	4469
	$\mathbf{W_{TO} - W_f}$		**11.365**	**1565**	**17787**	**0**	**0**	**997**	**11329**

Table 3.45 CG Locations Summary

	Wi	Wi (kg)	Xi (mm)	Yi (mm)	Zi (mm)
A	W_E	7.647	1745	0	1016
B	Woe	7.876	1740	0	1016
C	Woe + W_f	12.471	1697	0	1001
D	W_{TO}	15.960	1582	0	991
E	W_{TO} - W_f	11.365	1565	0	998

3.9.6 CG envelope

CG locations given in Table 3.45 can be nondimensionalize with mean geometric chord of an airplane as represented in Figure 3.15

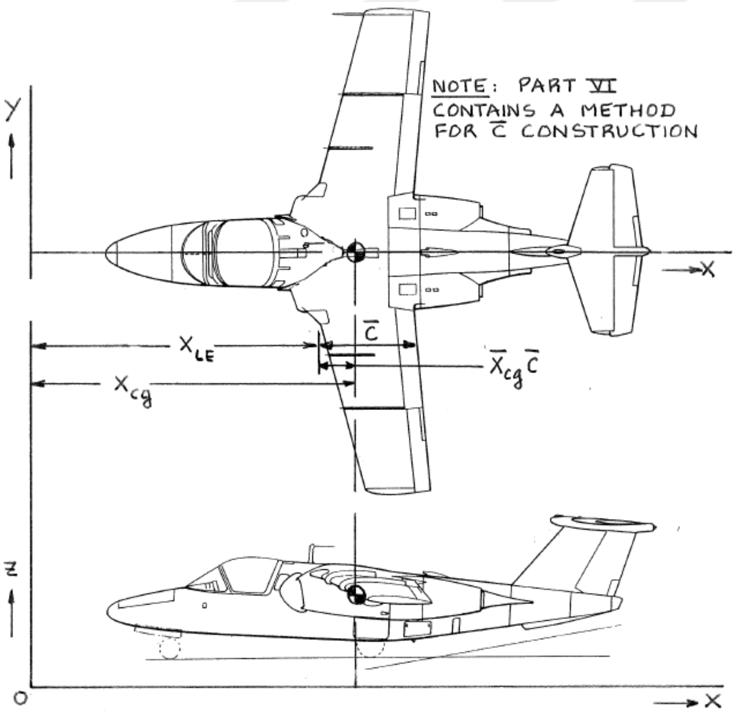

Figure 3.15 : Definition of Mean geometric Chord ($\bar{c}$) Location and Overall CG Location [9]

$$\bar{x}_{cg} = (x_{cg} - x_{LE})/\bar{c} \quad (3.47)$$

CG locations for all feasible loading scenarios can be found in Table 3.46. Using this table CG excursion diagram of HAVK which is shown in Figure 3.17 is plotted. Forward and aft CG limit of diagram is determined considering single engine propeller driven aircraft category, 0.06$\bar{C}$ and 0.27$\bar{C}$, respectively, from Figure 3.16. [9]

Table 3.46 : CG Envelope

	Wi	$(X_{cg} - X_{LE})/c$	W_i / W_{TO}
A	W_E	0.992	0.45
B	Woe	0.988	0.47
C	Woe + W_f	0.935	0.77
D	W_{TO}	0.336	1
E	W_{TO} - W_f	0.105	0.7

Type	C.G. Range (in.)	$fr.\bar{c}_w$	Type	C.G. Range (in.)	$fr.\bar{c}_w$
Homebuilts	5	0.10	Military Trainers	8	0.10
Single Engine Prop. Driven	7-18	0.06-0.27	Fighters	15	0.20
Twin Engine Prop. Driven	9-15	0.12-0.22	Mil.Patr. Bomb and Transp.	26-90	0.30
Ag. Airpl.	5	0.10	Fl.Boats, Amph. and Float Amph. and	7-28	0.25
Business Jets	8-17	0.10-0.21			
Regional TBP	12-20	0.14-0.27			
Jet Transp.	26-91	0.12-0.32	Supersonic Cruise	20-100	0.30

Figure 3.16 : Examples of Center of Gravity Ranges [14]

It can be seen that W_{TO} is out of aft limit. This can be fixed changing location of wing fuselage connection. However, calculation is performed considering current scenario.

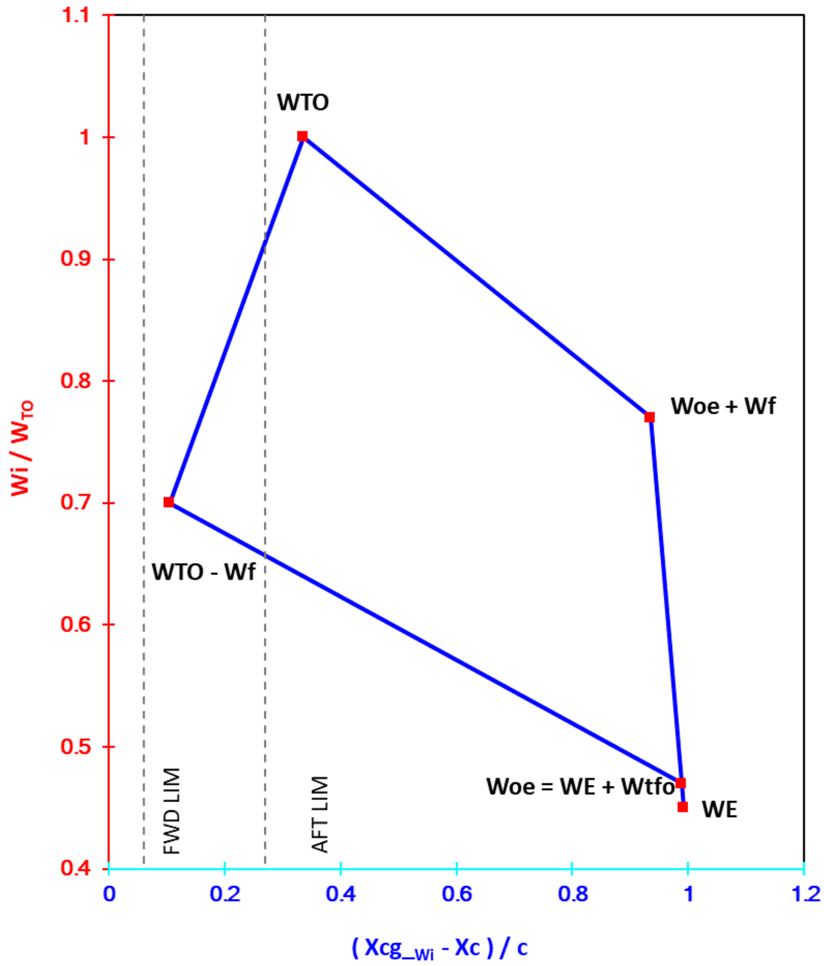

Figure 3.17 : Weight-CG Excursion Diagram

3.9.7 Inertia

In this chapter moments and products of inertia are estimated. The following equations are used [14].

$$I_{xx} = \underset{i=1}{i=n}\, Sum_i \left(\left(y_i - y_{cg}\right)^2 + \left(z_i - z_{cg}\right)^2\right\} \tag{3.48}$$

$$I_{yy} = Sum_{i=1}^{i=n}\, m_i \left(\left(z_i - z_{cg}\right)^2 + \left(x_i - x_{cg}\right)^2\right) \tag{3.49}$$

$$I_{zz} = Sum_{i=1}^{i=n}\, m_i \left\{\left(x_i - x_{cg}\right)^2 + \left(y_i - y_{cg}\right)^2\right\} \tag{3.50}$$

$$I_{xy} = Sum_{i=1}^{i=n}\, m_i \left(x_i - x_{cg}\right)\left(y_i - y_{cg}\right) \tag{3.51}$$

$$I_{yz} = Sum_{i=1}^{i=n}\, m_i \left(y_i - y_{cg}\right)\left(z_i - z_{cg}\right) \tag{3.52}$$

$$I_{zx} = Sum_{i=1}^{i=n}\, m_i \left(z_i - z_{cg}\right)\left(x_i - x_{cg}\right) \tag{3.53}$$

Figure 3.14 defines the coordinates used in these equations. Weight a coordinate values for components and full aircraft are taken from Table 3.44 and Table 3.45, respectively.

Calculations are performed for Take-Off Weight.

Results are presented at table following.

Table 3.47 : Moment and product of Inertia (All units are kgm^2).

Ixx	Iyy	Izz	Ixy	Ixz	Iyz
0.797	1.990	2.675	0	0.170	0

It can be seen that Ixy and Iyz are 0, since aircrafts have symmetry axis according to xy and yz plane.

3.10 Stability and Control

Stability and control analysis of the aircraft performed according to [9][21]. In this thesis only static longitudinal stability (Longitudinal x-plot). is checked Other important stability and control characteristics such as directional stability, take-off rotation, cross-wind controllability, trim through the c.g. range and a variety of dynamic stability considerations are not covered by this study but it’s noted as a further study.

3.10.1 Longitudinal stability

Figure 3.18 presents examples of longitudinal x-plots [9]. The two legs are representative of:

1. The c.g. leg represents the rate at which the c.g. moves aft (fwd) as a function of horizontal tail area.
2. The a.c. leg represents the rate at which the a.c. moves aft (fwd) as a function of horizontal tail area.

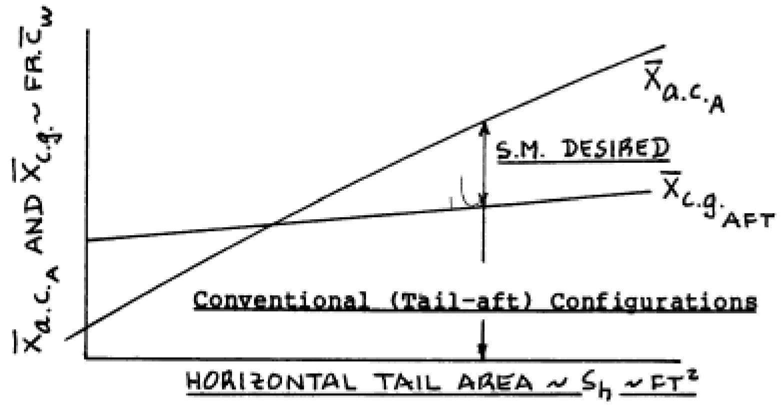

Figure 3.18 : Examples of Longitudinal X-Plots [9]

The cg leg is calculated with the help of the weight and balance analysis performed at previous chapter.

The a.c leg is calculated with the following equations [9]:

$$\bar{x}_{ac_A} = \left[\bar{x}_{ac_{wf}} + c_{L_{a_h}}(1 - d\varepsilon_h/da)(S_h/S)\,\bar{x}_{ac_h}/C_{L_{a_{wf}}}\right]/F \qquad (3.54)$$

where:

$$F = \left[1 + C_{L_{\alpha_h}}(1 - d\varepsilon_h/da)(S_h/S)\,/C_{L_{a_{wf}}}\right] \qquad (3.55)$$

Figure 3.19 defines required geometric quantities in these equations. The aerodynamic quantities are computed subsequent chapters.

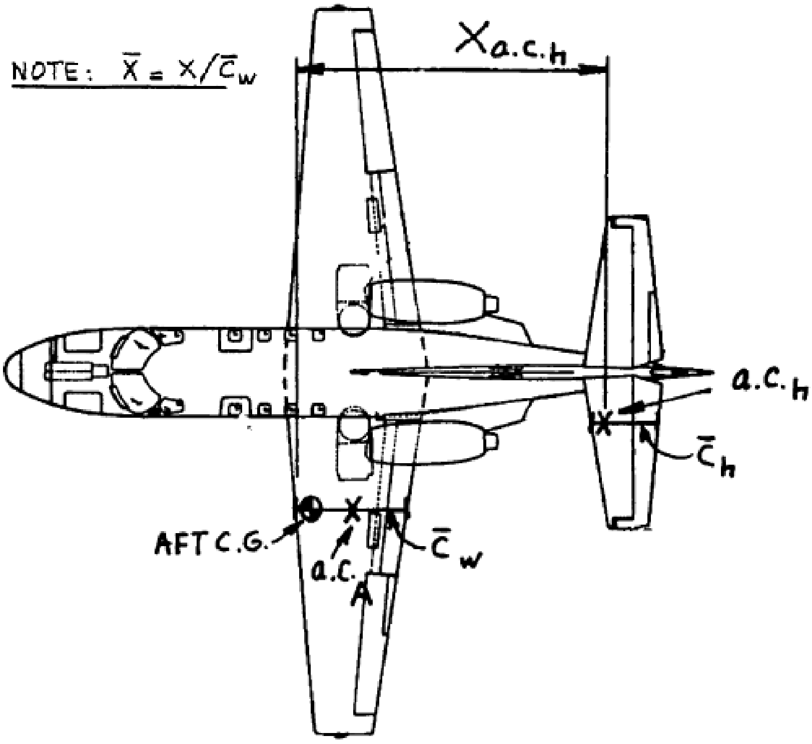

Figure 3.19 : Geometric Quantities for AC Calculations [9]

Static margin defined at Figure 3.18 should be minimum 10 percent [9].

$$S.M. = \frac{dC_m}{dC_L} = \bar{x}_{\text{cg}} - \bar{x}_{\text{ac}} = -0.10 \qquad (3.56)$$

Longitudinal x-plot for HAVK shown in Figure 3.20. It can be easily seen that horizontal tail is which is 0.0966 m2 gives static margin of -0.1088.

Condition is satisfied.

Results used in this section are obtained at following chapters.

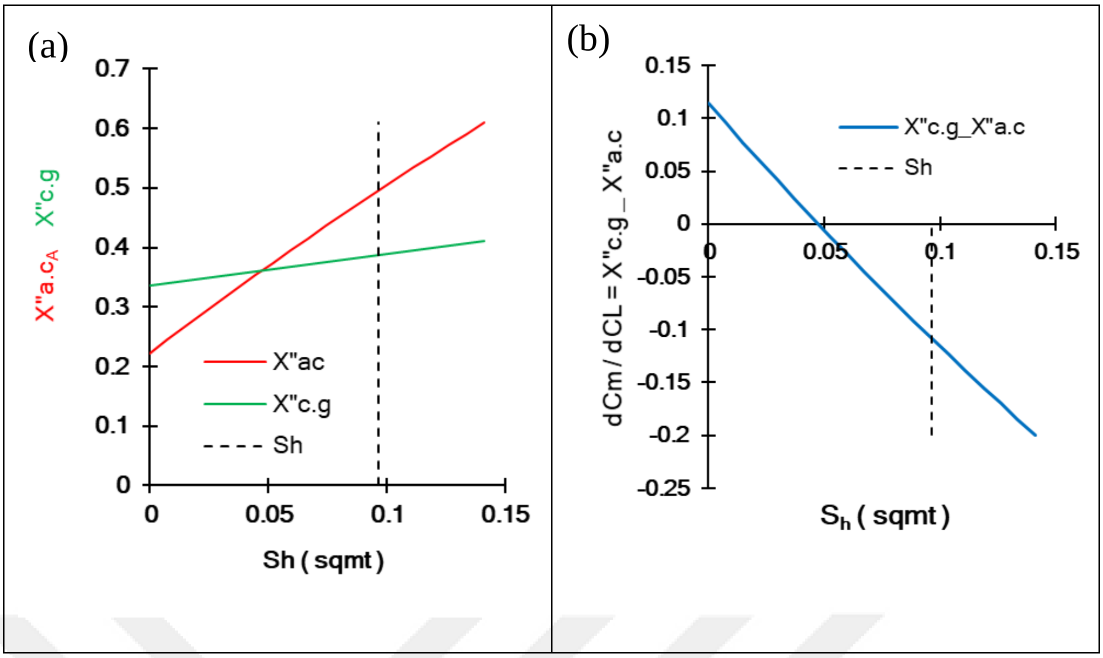

Figure 3.20 : Longitudinal stability: (a)Longitudinal x-plot, (b) Static Margin Plot

3.10.1.1 Aircraft aerodynamic center

Aircraft aerodynamic center calculation formula given below [21].

$$\bar{x}_{ac_A} = \left[\bar{x}_{ac_{wf}} + c_{L_{a_h}}(1 - d\varepsilon_h/da)(S_h/S)\,\bar{x}_{ac_h}/C_{L_{a_{wf}}}\right]/F \qquad (3.57)$$

$where$:

$$F = \left[1 + C_{L_{a_h}}(1 - d\varepsilon_h/da)(S_h/S)\,/C_{L_{a_{wf}}}\right] \qquad (3.58)$$

$$\bar{x}_{ac_{wf}} = \bar{x}_{ac_w} + \Delta\bar{x}_{ac_f} \qquad (3.59)$$

All values required are calculated at subsequent chapters. Results are listed at Table 3.48 as a summary.

Table 3.48 : Aircraft Aerodynamic Canter Calculation Summary

Parameter	Symbol	Value	Unit
Aircraft AC location	$\bar{x}_{ac_A}$	**0.657**	**MGC**
Wing fuselage ac location	$\bar{x}_{ac_{wf}}$	0.222	MGC
Horizontal tail ac location	$\bar{x}_{ac_h}$	4.191	MGC
Aircraft lift curve slope	C_{La}	0.1069	1 / der
Wing fuselage lift curve slope	C_{LawF}	0.0952	1 / der
Wing lift curve slope	C_{Law}	0.0951	1 / der
Horizontal tail lift curve slope	C_{Lah}	0.0733	1 / der
Wing downwash gradient	$d\varepsilon / d\alpha$	0.203	der

Wing aerodynamic center calculation

Wing aerodynamic center is taken as wing profile aerodynamic center. This value is represented in terms of wing mean geometric(aerodynamic) chord.

$$\frac{X_{ac_w}}{c} = X"_{ac_w} = 0.25 \tag{3.60}$$

Wing-fuselage aerodynamic center calculation

$\Delta\bar{x}_{ac_f}$ the shift in aerodynamic center caused by adding the fuselage to the wing is calculated using "Munk" method [21].

$$\Delta\bar{\mathrm{x}}_{\mathrm{ac_f}} = -\frac{\sum_{1}^{i=13} W_{f_i}^2\,(d\bar{\varepsilon}/\mathrm{d}\alpha)_i \Delta x_i}{36.5 * 0.08 * \mathrm{Sc}} \tag{3.61}$$

Here Wfi and Xi are defined in Figure 3.21. To calculate fuselage contribution to MGC the fuselage should divided into stations.

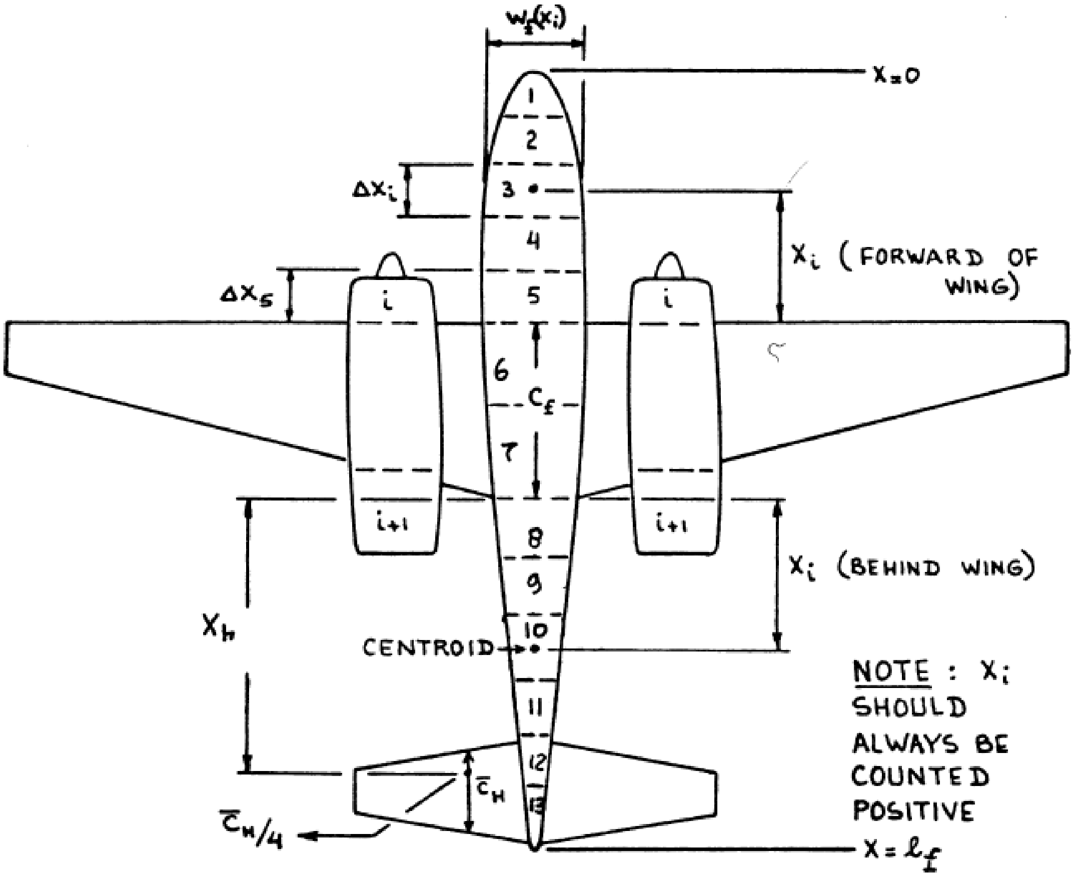

Figure 3.21 : Fuselage contribution to Airplane Aerodynamic Center Location [21].

In Figure 3.22, fuselage top view of HAVK is shown with its stations.

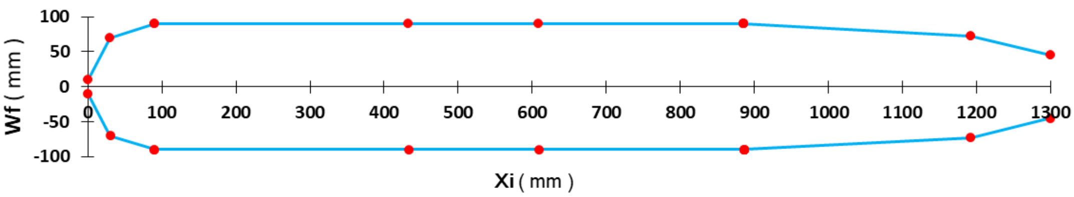

Figure 3.22 : HAVK fuselage top view drawing [21].

For each station Xi and Wfi values are listed at Table following.

Table 3.49 : Horizontal tail inputs

Station	Xi -mm	Wfi-mm
0	0	20
1	30	140
2	90	180
4	433	180
5	609	180
6	886	180
7	1192	145
l_{fus}	1300	90

Details of Munk method and its application on HAVK didn't discuss at this study. Detailed information can be found at [21]

The shift in aerodynamic center caused by adding the fuselage to the wing is calculated as[21]:

$$\Delta\bar{x}_{ac_f} = -0.03 \tag{3.62}$$

$$\bar{x}_{ac_{wf}} = \bar{x}_{ac_w} + \Delta\bar{x}_{ac_f} = 0.25 - 0.03 = 0.22 \tag{3.63}$$

3.11 Lift Analysis

3.11.1 Aerodynamic properties of wing

In this chapter aerodynamic properties of wing are obtained.

3.11.1.1 Wing zero lift angle of attack

The wing angle of attack, α_w, is defined as follows:

$$\alpha_w = \alpha + i_w \tag{3.64}$$

$where: \alpha\ is\ the\ airplane\ angle\ of\ attack\ and$

$i_w\ \ is\ the\ wing\ incidence\ angle$

Figure 3.23 shows how these angles are defined on an airplane.

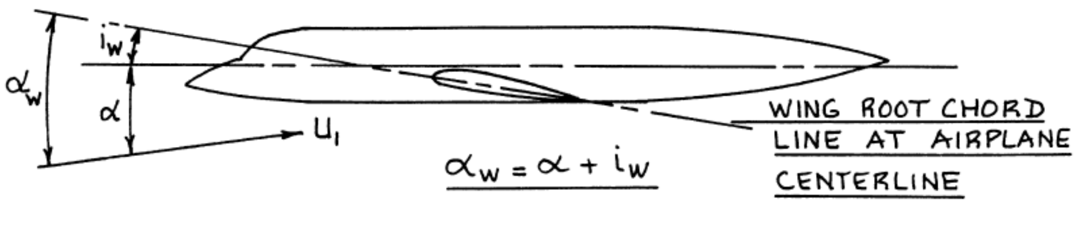

Figure 3.23 : Wing angles relationship[21].

If there is no twist wing zero lift angle of attack, $\alpha_{0_{L_W}}$, is equal to profile zero lift angle of attack, α_{0_l}, from Table 3.11:

$$\alpha_{0_{L_W}} = \alpha_{0_l} = -7.34\ \text{deg} = -0.128\ rad \tag{3.65}$$

3.11.1.2 Wing incidence angle

Wing incidence angle is selected as 1.5 degree considering similar aircrafts data at Table 3.1. This value should check with minimum wing incidence requirement of HAVK. Minimum wing incidence angle is calculated as below. [7]

$$C_{L_c} = \frac{W_1 + W_2}{\rho_c V_c^2 S}$$

$$C_{L_{W_c}} = 1.075 C_{L_c}$$

Table 3.50 : Wing Cruise Lift Coefficient Calculation

Parameter	Symbol	Value	Unit
Wing Cruise Lift Coefficient	$\boldsymbol{C_{L_{W_c}}}$	**0.76**	
Aircraft Cruise Lift Coefficient	C_{Lc}	0.72	
Launch Weight	W_1	16.93	kg
Recovery Weight	W_2	12.33	kg
Cruise Altitude Density	ρ_c	0.79	kg/m3
Cruise Speed	V_c	25	m/s
Wing Area	S	0.80	m2

$$C_{L_{W_C}} = C_{L_0} + C_{L_\alpha} i_w$$

$$C_{L_0} = C_{L_\alpha} |\alpha_{L=0}|$$

$$i_{w_{min}} = \frac{C_{L_{W_C}}}{C_{L_\alpha}} - |\alpha_{L=0}| = \frac{0.76}{0.69} - 0.13 = 0.6 \text{ deg} < 1.5 \; deg$$

Condition is satisfied.

3.11.1.3 Wing lift curve slope calculations

For conventional, straight tapered wing with moderate sweep angles, lift curve slope calculation is performed as following:

From Polhamus equation [7],

$$C_{L_\alpha} = \frac{2\pi * AR}{2 + \sqrt{\left(\frac{AR * \beta}{k}\right)^2 * \left(1 + \frac{\tan\Lambda_{\frac{c}{2}}^2}{\beta^2}\right) + 4}}$$

$\beta = \text{Mach number parameter} = (1 - M^2)^{0.5}$

$k = \text{ratio of 2D lift curve slope to } 2\pi = \frac{C_{l_\alpha}}{2\pi}$

$\Lambda_{\frac{c}{2}} = \text{middle chord swept angle}$

Table 3.51 : Wing Lift Curve Slope Calculation Summary

Symbol	Value	Unit
$\boldsymbol{C_{L_{\alpha_w}}}$	**5.41**	**1/rad**
$C_{l_{\alpha_w}}$	6.26	1/rad
AR	14	
k	1	
β	1	
$\Lambda_{C/2}$	5.57	deg

3.11.1.4 Wing fuselage lift curve slope calculation

$C_{L_{wf}}$ is the wing-fuselage lift curve slope calculated from Eq. (8.43) of [21].

where: K_{wf} is the wing-fuselage interference factor

$$C_{L_{\alpha_{wf}}} = K_{wf} C_{L_{a_w}} \tag{3.66}$$

$$K_{wf} = 1 + 0.025\left(d_{fus}/b\right) - 0.25\left(d_{fus}/b\right)^2 \tag{3.67}$$

Table 3.52 : Wing Fuselage Lift Curve Slope Calculation Summary

Symbol	Value	Unit
$\boldsymbol{C_{L_{\alpha_{wf}}}}$	**5.45**	**1/rad**
d_{fus}	0.59	in
b	10.99	in
K_{wf}	1.001	
$C_{L_{wf}}$	5.45	1/rad

3.11.2 Aerodynamic properties of airplane

3.11.2.1 Airplane zero lift angle of attack

The airplane zero angle of attack, α_{0_L}, is defined as follows [21]:

$$\alpha_{O_L} = \left(\frac{-C_{L_O}}{C_{L_\alpha}}\right) = \left(\frac{-0.82}{0.106}\right) = -7.67 \text{ deg} = -\ 0.134 \text{ rad} \tag{3.68}$$

Parameters are calculated on following chapters.

3.11.2.2 Airplane zero angle of attack lift coefficient

The airplane zero-angle-of-attack lift coefficient may be estimated from:

$$C_{L_O} = C_{L_{O_{wf}}} + C_{L_{\alpha_h}} \eta_h \left(\frac{S_h}{S}\right)\left(-\alpha_{O_{L_h}} - \epsilon_{O_h}\right) \tag{3.69}$$

Also wing-fuselage zero-angle-of-attack lift coefficient is:

$$\begin{aligned} C_{L_{O_{wf}}} &= \left(i_w - \alpha_{O_{L_w}}\right) C_{L_{\alpha_{wf}}} \\ &= \left(1.5 - (-7.34)\right)0.095 \\ &= 0.84 \end{aligned} \tag{3.70}$$

Summary of calculations for C_{L_O} can be found on table, following;

Table 3.53 : Airplane Zero Angle of Attack Lift Coefficient Calculation Summary

Symbol	Value	Unit
C_{L_O}	**0.82**	
$C_{L_{O_{wf}}}$	**0.84**	
$C_{L_{\alpha_h}}$	0.073	1/deg
η_h	1.68	
S	0.801	m^2
S_h	0.096	m^2
$\alpha_{O_{L_h}}$	1.5	deg
ϵ_{O_h}	0	deg

$\epsilon_{O_h}$is taken as 0 since according to Roskam, for most airplanes its acceptable take it zero [21].

3.11.2.3 Aircraft maximum lift coefficient

Aircraft maximum lift coefficient calculated according given relations and results are listed at Table 3.54[21].

$$C_{L_{max_W}}{=}1.075 C_{L_{max}}$$

$$C_{L_{max_{W(unswept)}}}=\frac{C_{L_{max_{W(swept)}}}}{\cos\Lambda_{\frac{c}{4}}}$$

$$C_{L_{max_W}}=0.915C_{l_{max}}$$

Table 3.54 : Maximum Lift Coefficients

Parameter	Symbol	Value
Aircraft maximum lift coefficient	$C_{L_{max}}$	1.52
Wing maximum lift coefficient	$C_{L_{max_W}}$	1.64
Unswept wing maximum lift coefficient	$C_{L_{max_{W(unswept)}}}$	1.65
2D wing maximum lift coefficient	$C_{l_{max}}$	1.80

3.11.2.4 High lift device sizing

High lift device sizing is performed considering Roskam Class 1 Method [21] . Takeoff and landing of HAWK is not conventional type so that take of is performed with catapult. It's assumed that:

Catapult will accelerate HAWK to 14.7 m/s, which is take off speed of it.

First step of sizing is calculated required take-off lift coefficient; $C_{L_{To}}$. This is performed by using given values in Table 3.55.

Table 3.55 : Take of Parameters

Parameter	Symbol	Value	Unit
Lift Coefficient – Take off	$C_{L_{To}}$	1.73	
Weight – Take off	W_{TO}	16.93	kg
Speed – Take off	V_{TO}	14.7	m/s
Altitude – Take off	h_{TO}	1000	m
Air density -Take off	ρ_{TO}	1.11	kg/m3
Dynamic pressure – Take off	q_{TO}	120.10	

Step 2 is calculating $C_{L_{\max_W}}$. It is taken as 1.075 times $C_{L_{\max}}$[21].

Step 3 is determining the incremental value of maximum lift coefficient which need to be produced by HLD:

$$\Delta C_{L_{max_{TO}}} = 1.05 * \left(C_{L_{max_{TO}}} - C_{L_{max}}\right) \tag{3.71}$$

Step 4 is calculation required incremental 2D maximum lift coefficient with flaps down from:

$$\Delta C_{l_{max}} = \frac{(\Delta C_{L_{max}})(S/S_{wf})}{K_{\Lambda}} \quad (3.72)$$

$$K_{\Lambda} = (1 - 0.08\, cos^2 \Lambda_{c/4})\, cos^{3/4} \Lambda_{c/4} \quad (3.73)$$

Area ratio S/S_{wf} is defined given in Figure 3.24.

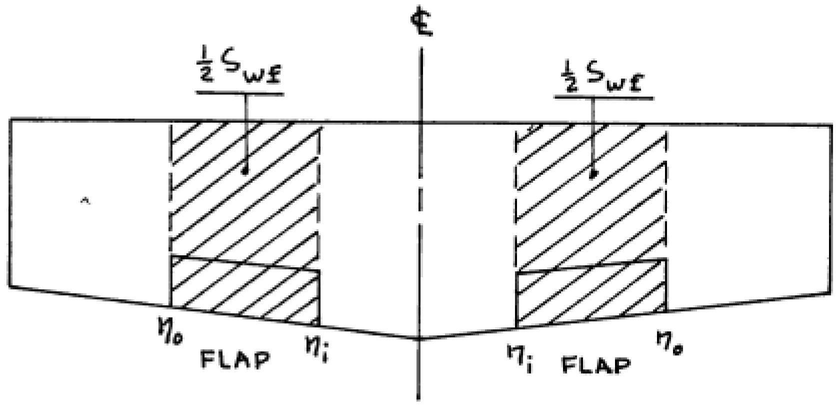

Figure 3.24 : Definition of Flapped Wing Area [21].

Area ratio is taken as 4 considering similar aircrafts at Table 3.1.

Step 5 is computing required value of incremental 2D lift coefficient, with ΔC_l, which flaps must generate and relate this value to flap type flap angle and flap chord. Using Figure 3.25 required flap parameter is determined and results are listed in Table 3.56.

Table 3.56 : Flap ratio calculation summary.

Symbol	Value
c_f/c	**0.265**
S/S_{wf}	**4.00**
δ_f	**25**
K_Λ	0.92
$\Delta C_{L_{max_{TO}}}$	0.21
$\Delta C_{L_{max}}$	0.94
K	0.72
K'	0.700
$C_{l_{\delta_f}}$	4.25
ΔC_l	1.30

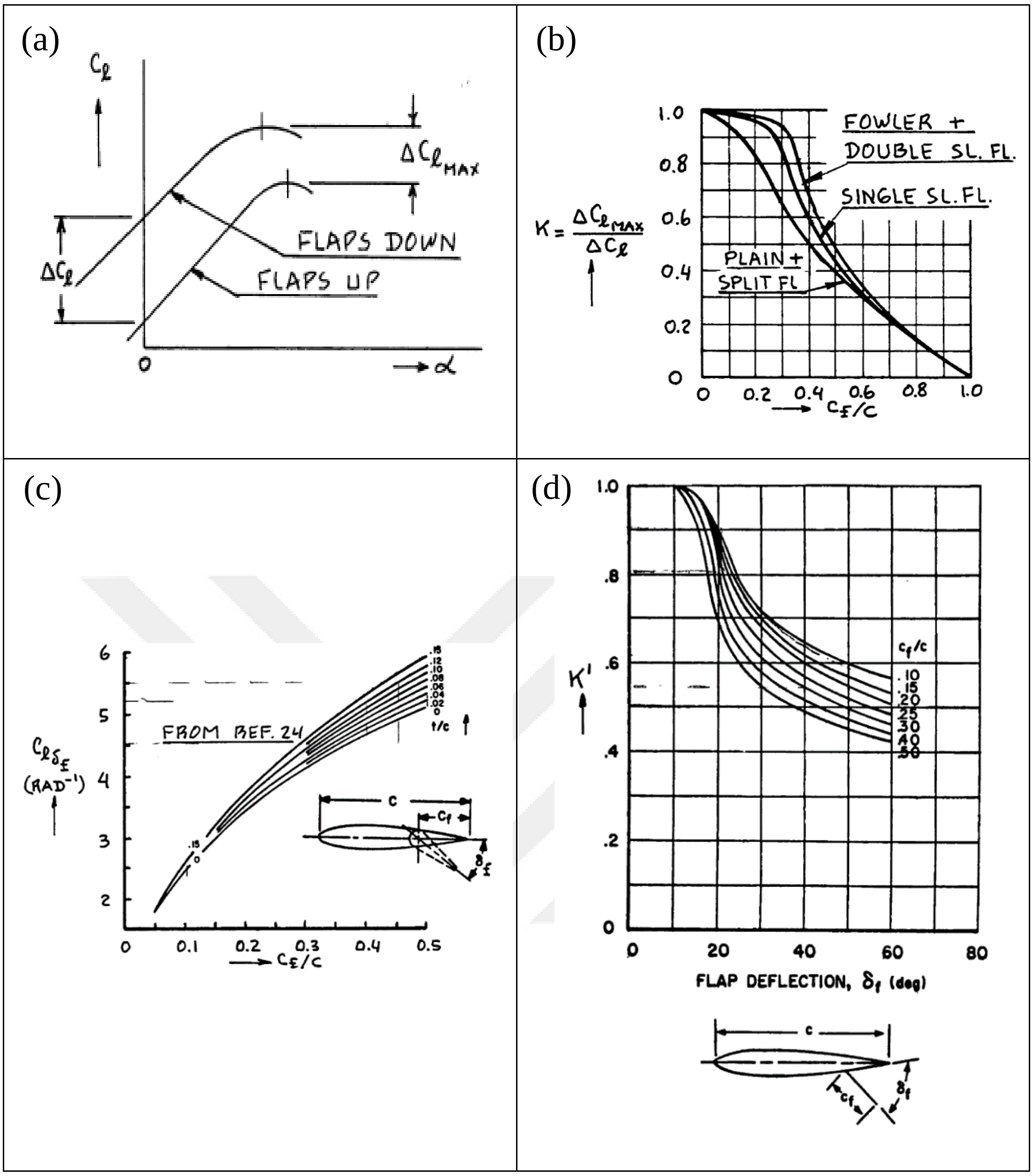

Figure 3.25 : (a)Relation between ΔC_l and $\Delta C_{l_{max}}$. (b)Effect of Flap Chord Ratio and Flat Type on K. (c)Effect of thickness ratio and Flap Chord Ratio on $C_{l_{\delta_f}}$.(d)Effect of Flap Chord Ratio and Flat Deflection on K' [21].

3.11.3 Lift curve slope calculation

Airplane lift curve slope is calculated given formula below [21].

$$C_{L_a} = C_{L_{\alpha_{wf}}} + C_{L_{a_h}} \eta_h \left(\frac{S_h}{S}\right)\left(1 - \frac{d\epsilon}{da}\right) \tag{3.74}$$

All values required are calculated at subsequent chapters. Results are listed at Table 3.57 as a summary.

Table 3.57 : Wing Lift Curve Slope Calculation Summary

Symbol	Value	Unit	Value	Unit
$\boldsymbol{C_{L_\alpha}}$	**6.125/**	**1/rad**	**0.107**	**1/deg**
$C_{L_{\alpha_{wf}}}$	5.45	1/rad	0.095	1/deg
$C_{L_{\alpha_h}}$	4.2	1/rad	0.073	1/deg
η_h	1.68			
S_h/S	0.119			
$d\epsilon/da$	0.203			

3.11.3.1 Horizontal tail lift curve slope calculation

Same calculation performed for wing at previous chapter is applied to the horizontal tail. Summary can be seen from Table 3.58.

Table 3.58 : Horizontal Tail Lift Curve Slope Calculation Summary

Symbol	Value	Unit
$\boldsymbol{C_{L_{\alpha_h}}}$	**4.2**	**1/rad**
$C_{l_{\alpha_h}}$	6.28	1/rad
AR	4.8	
k	1	
β	1	
$\Lambda_{\frac{C}{2}}$	0	deg

3.11.3.2 Downwash gradient calculation

Downwash gradient at horizontal tail, $\frac{d\epsilon}{da}$, calculated as below:

$$\frac{d\epsilon}{da} = 4.44\left[\left\{\mathrm{K_A K_\lambda K_h}\left(\cos\Lambda_{C/4}\right)^{\frac{1}{2}}\right\}^{1.19}\right] \tag{3.75}$$

$$where:\ K_A = 1/AR - \frac{1}{(1+AR^{1.7})} \tag{3.76}$$

$$K_\lambda = (10-3\lambda)/7 \tag{3.77}$$

$$K_h = \left(1-\frac{h_h}{b}\right)/(2l_h/b)^{\frac{1}{3}} \tag{3.78}$$

h_h, l_h parameters are defined given Figure 3.26.

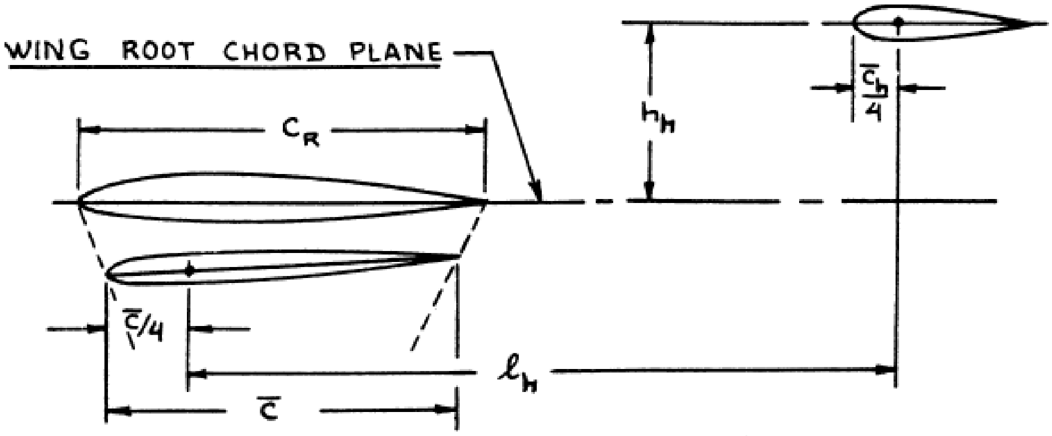

Figure 3.26 : Geometric Characteristics for Horizontal Tail Location [21]

Geometric characteristics of horizontal tail listed in Table 3.59;

Table 3.59 : Geometric Characteristics for Horizontal Tail

Parameter	Symbol	Value	Unit
Horizontal tail area	S_h	1.029	ft^2
Horizontal tail aspect ratio	A_h	4.8	
Horizontal tail taper ratio	λ_h	1	
Horizontal tail quarter chord swept angle	$\Lambda_{ch/4}$	0	der
Distance between horizontal aerodynamic chord and wing aerodynamic chord	x_{ac_h}	1.013	m
Distance between horizontal aerodynamic chord and wing leading edge at fuselage interference	x_h	0.822	m
	h_h	0.255	m
	l_h	0.953	m

Calculation summary given following table:

Table 3.60 : Downwash Calculation Summary

K_A	K_λ	K_h	$\Lambda_{c/4}$
0.06	1.129	1.11	6.29

Downwash gradient is found as below:

$$\frac{d\epsilon}{da} = 0.203$$

3.11.3.3 Horizontal tail dynamic pressure ratio calculation

η_h horizontal tail dynamic pressure ratio depends on where the horizontal tail is located relative to the propeller. From equation 3.79, η_h is calculated.

$$\eta_h = 1 + \left(S_{h_{slip}}/S_h\right)(2200\mathrm{P_{av}})/\left(qU_1\pi D_p{}^2\right) \tag{3.79}$$

Inputs for formula given in Table 3.61. Using these inputs η_h is calculated as 1.68.

Table 3.61 : Horizontal Tail Dynamic Pressure Ratio Calculation Summary

Parameter	Symbol	Value	Unit
Horizontal tail dynamic pressure ratio	η_h	**1.68**	
The area of the tail which is submerged in the propeller slipstream	S_{h_slip}	0.049	m2
Horizontal tail area	S_h	0.096	m2
Cruise speed of the airplane	U_1	25	m/s
Dynamic pressure	q	248	N/m^2
The available horsepower	P_{av}	1.08	hp
Propeller Diameter	D_P	0.35	m

Dynamic pressure and available horse power is calculated considering cruise speed altitude air density value. Horizontal tail slipstream is found help of the Figure 3.27.

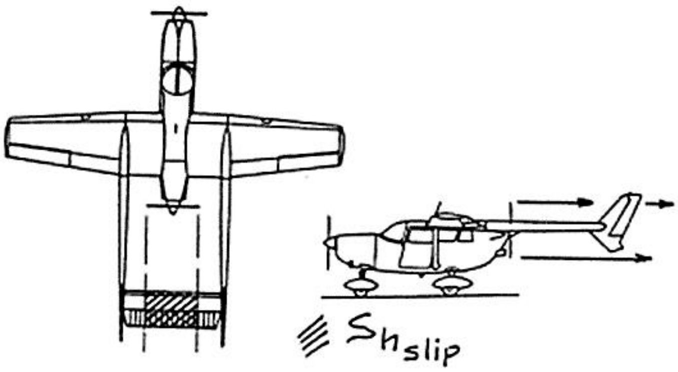

Figure 3.27 Definition of tail area which is submerged in propeller slipstream [21].

3.11.4 Airplane lift model

Airplane lift model written as given below.

$$C_L = C_{L_O} + C_{L_\alpha}\alpha + C_{L_{\delta e}}\delta_e \tag{3.80}$$

$$C_L = 0.82 + 6.125\alpha + 0.37\delta_e \tag{3.81}$$

Angles are unit of radian.

Table 3.62 : Lift Coefficients

Symbol	Value	Unit
C_{L_O}	0.82	
C_{L_α}	6.125/	1/rad
$C_{L_{\delta e}}$	0.37	1/rad

3.12 Drag Analysis

3.12.1 Wetted area calculation

Wing, horizontal and vertical tail wetted areas are calculated using equation (12.1) of [22]

$$S_{wet\,plf} = 2S_{exp.plf}\{1 + 0.25(t/c)_r(1 + \tau\lambda)/(1 + \lambda)\} \quad (3.82)$$

$$\text{where } \frac{t}{r} = \frac{(t/c)_t}{(t/c)_r} \text{ and } \lambda = \frac{c_t}{c_r}.$$

Fuselage wetted area is calculated using equation (12.3) of [22].

$$S_{\text{wet fus}} = \pi D_{f\,f}^{1}\left(1 - 2/\lambda_f\right)^{2/3}\left(1 + 1/\lambda_f^2\right) \quad (3.83)$$

Where $\lambda_f = \frac{L_{fus}}{D_{fus}}$, the fuselage finess ratio. From Table 3.18, diameter is 0.18 m and length are 1.3.

Boom wetted area is calculated simply assuming boom geometry as a cylindrical tube, diameter is 0.036 m and length is 1.0 m (l_{vt}-0.75C_{MGC}). From cylinder area wetted area of booms (two of them) are calculated as below:

$$S_{wet_{boom}} = 2 * \pi D_{boom} L_{boom} \quad (3.84)$$

$$S_{wet_{boom}} = 0.226\, m^2 \quad (3.85)$$

Summary table can be found in Table 3.63.

Table 3.63 : Wetted area results.

Wetted area		m2	ft2	ratio
Wing	S_{wet_w}	1.536	16.53	0.581
Vertical tail	S_{wet_h}	0.159	1.71	0.060
Horizontal tail	S_{wet_v}	0.117	1.26	0.044
Fuselage	S_{wet_fus}	0.604	6.50	0.229
Boom	S_{wet_boom}	0.226	2.43	0.086
Total	S_{wet}	2.641	28.432	1.000

3.12.2 Drag polar

From Roskam the method for estimating drag polars at low speed drag coefficient of airplane is written as [22]:

$$C_D = C_{D_0} + \frac{C_L^2}{\pi A e} = C_{D_0} + K C_L^2 \tag{3.86}$$

The zero-lift coefficient, C_{D_0} can be expressed as:

$$C_{D_0} = \frac{f}{S} \tag{3.87}$$

Where f is the equivalent parasite area. f is calculated given equation below.

$$\log f = a + b * logS_{wet} \tag{3.88}$$

a and b coefficients are taken from Table 3.64. for the equivalent skin friction constant, C_f. C_f is selected as 0.006 from Figure 3.28.Thus; a is

$$\log f = -2.2218 + 1 * log28.432$$

$$C_{D_0} = 0.17/8.62 = 0.0197$$

From Table 3.65; C_D for takeoff and cruise conditions are written as below, respectively:

$$C_D = 0.0347 + 0.028294 * C_L^2 \tag{3.89}$$

$$C_D = 0.0197 + 0.026526 * C_L^2 \tag{3.90}$$

Drag polar summary given Table 3.66 and chart can be found in Figure 3.29, Figure 3.30, and Figure 3.31.

Table 3.64 : Correlation coefficients for parasite area versus wetted Area [22].

C_f	a	b
0.0090	-2.0458	1.0000
0.0080	-2.0969	1.0000
0.0070	-2.1549	1.0000
0.0060	-2.2218	1.0000
0.0050	-2.3010	1.0000
0.0040	-2.3979	1.0000
0.0030	-2.5229	1.0000
0.0020	-2.6990	1.0000

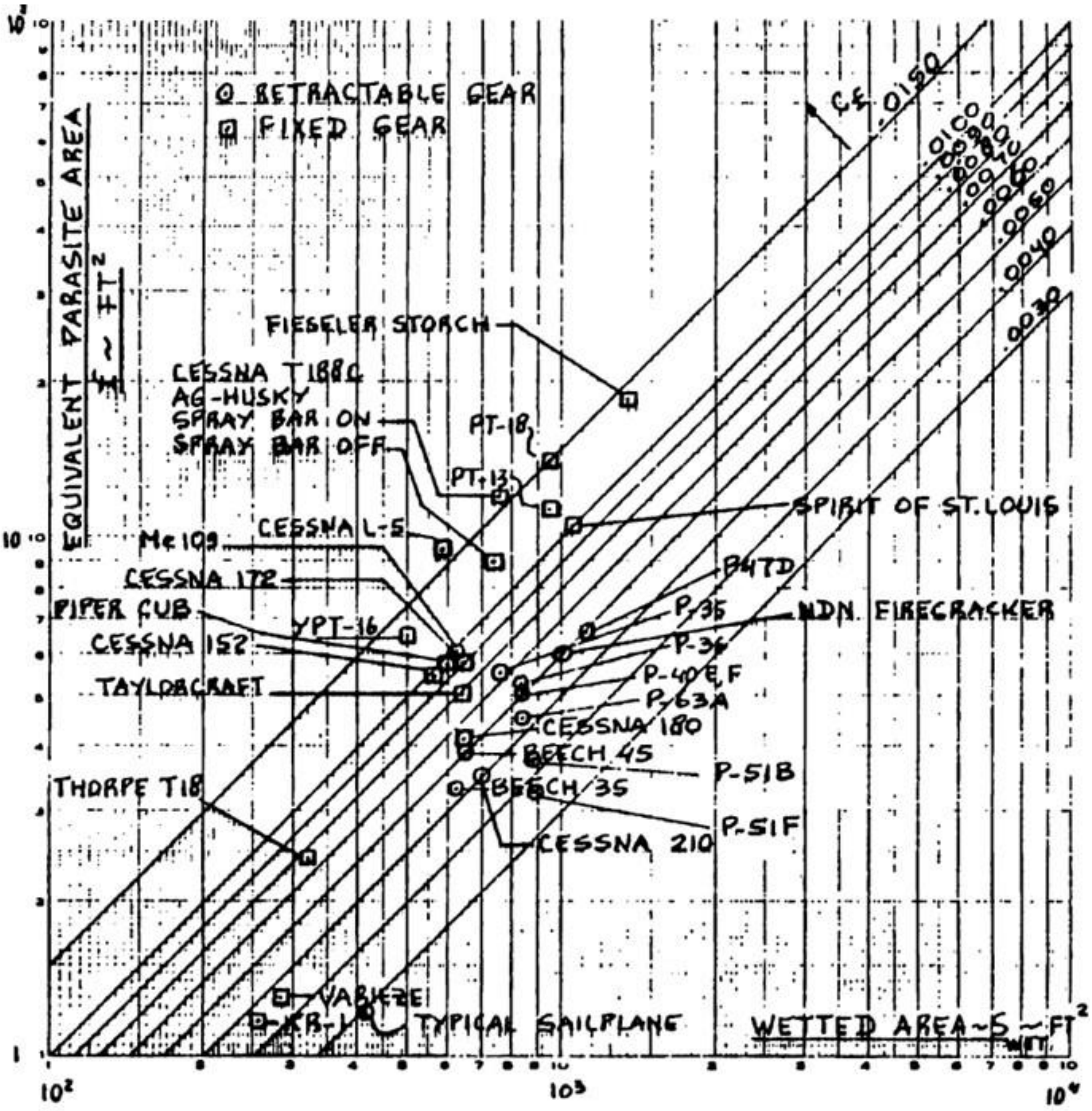

Figure 3.28 Effect of equivalent skin friction and wetted area on equivalent parasite area for single engine propeller driven airplanes [22]

Table 3.65 : First estimates for ΔC_D and e with flaps [22].

Configuration	ΔC_D	e
Clean	0	0.8
Take-off flaps	0.015	0.75

Table 3.66 : Drag Summary

Condition	ΔC_D	e	C_{D_0}	K	$\frac{C_L}{C_D}$	$\frac{C_L^3}{C_D^2}$
Take-off	0.015	0.75	0.0347	0.0283	15.96	19.14
Cruise	0	0.8	0.0197	0.0265	21.87	23.15

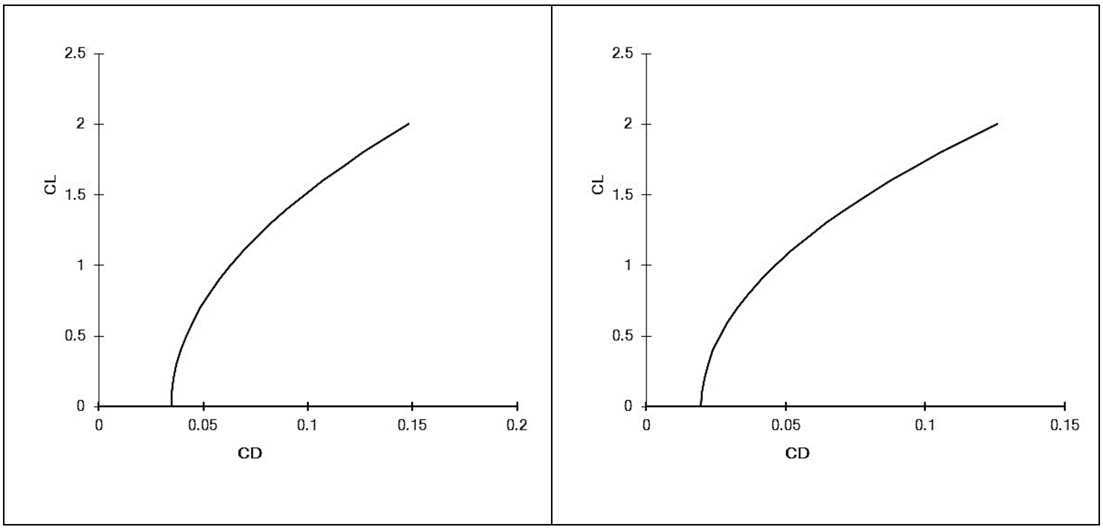

Figure 3.29 : L/D Polar of Take-off (Left) and Cruise (Right)

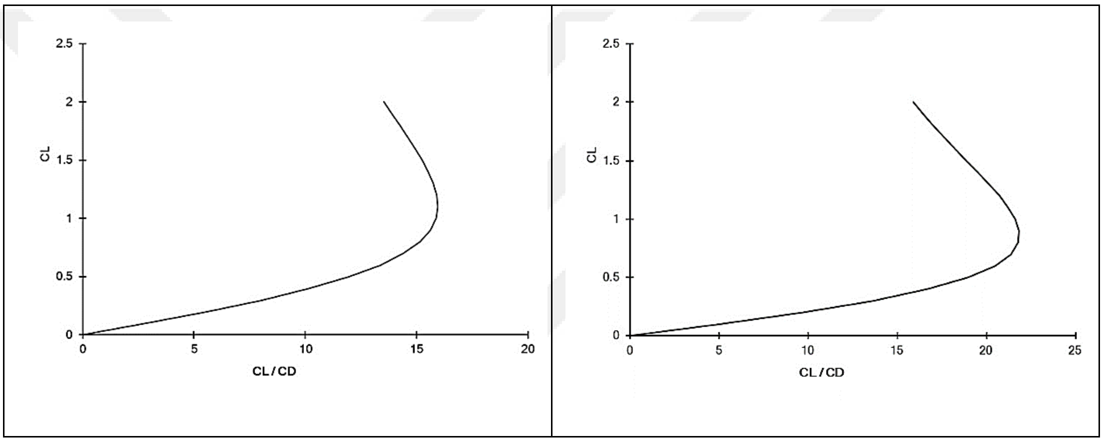

Figure 3.30 : L/D Polar of Take-off (Left) and Cruise (Right)

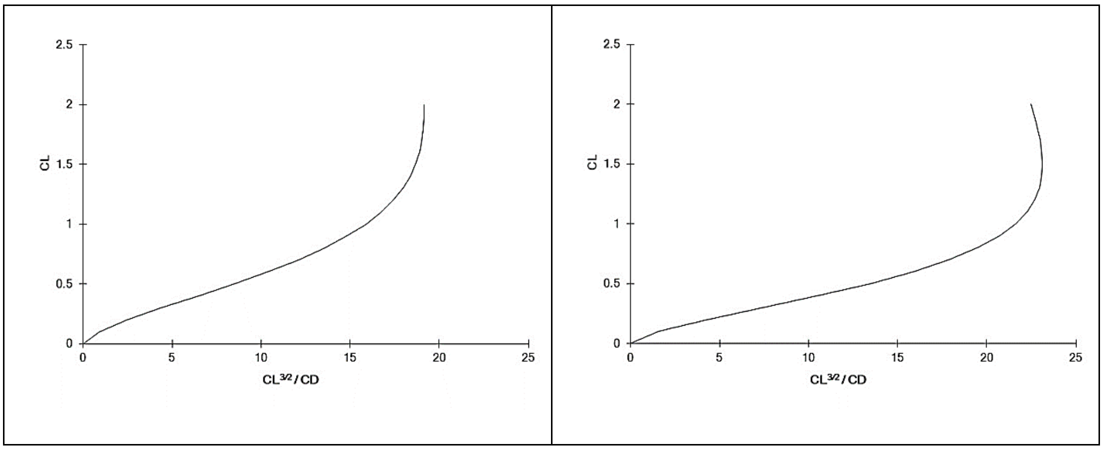

Figure 3.31 : L^3/D^2 Polar of Take-off (Left) and Cruise (Right)

3.13 Pitching Moment Analysis

3.13.1 Airplane zero angle of attack pitching moment coefficient

$C_{M_0}$is calculatede as below [21]:

$$C_{M_O} = C_{M_{O_{wf}}} + C_{M_{O_h}} \tag{3.91}$$

Where:

$$C_{M_{O_{wf}}} = \left(C_{M_{O_w}} + C_{M_{O_f}}\right) + C_{L_{O_{wf}}}\left(\bar{x}_{\mathrm{cg}} - \bar{x}_{ac_{wf}}\right) \tag{3.92}$$

Summary of calculations given table following:

Table 3.67 : Airplane Zero Angle of Attack Pitching Moment Coefficient Calculation Summary

Symbol	Value	Unit
C_{M_O}	-0.023	
$C_{M_{O_{wf}}}$	-0.108	
$C_{M_{O_w}}$	-0.168	
$C_{M_{O_f}}$	-0.035	
$C_{M_{O_h}}$	0.084	
$C_{L_{O_{wf}}}$	0.84	
$\bar{x}_{ac_{wf}}$	0.222	
$\bar{x}_{cg}$	0.336	

3.13.1.1 Contribution by the horizontal tail

Horizontal contribution to $C_{M_0}$is calculatede as below [21].

$$C_{M_{O_h}} = -\left(C_{L_{O_h}}\right)\left(\bar{x}_{ac_h} - \bar{x}_{\mathrm{cg}}\right) \tag{3.93}$$

Where:

$$C_{L_{O_h}} = C_{L_{\alpha_h}}\eta_h\left(\frac{S_h}{S}\right)\left(-\alpha_{O_{L_h}} - \epsilon_{O_h}\right) \tag{3.94}$$

Summary of calculations given table following:

Table 3.68 : Horizontal Tail Contribution to Airplane Zero Angle of Attack Pitching Moment Coefficient Calculation Summary

Symbol	Value	Unit
$C_{M_{O_h}}$	**0.084**	
$C_{L_{O_h}}$	**-0.022**	
$C_{L_{\alpha_h}}$	0.073	1/deg
η_h	1.68	
S	0.801	m^2
S_h	0.096	m^2
$\bar{x}_{ac_h}$	4.191	
$\bar{x}_{cg}$	0.336	
$\alpha_{O_{L_h}}$	1.5	deg
ϵ_{O_h}	0	deg

ϵ_{O_h} is taken as 0 since according to Roskam for most airplanes its acceptable take it zero [21].

3.13.1.2 Contribution by the fuselage

Fuselage contribution to C_{M_0} is calculatede as below. Detailed about formulation can be found in [7]

$$C_{M_{FUS}} = \frac{k_2 - k_1}{36.5 \times S \times C_{MGC}} \sum_{x=0}^{l} w_f^2 (\alpha_{O_W} + i_f) \Delta x$$
$$= \frac{0.9}{36.5 \times 8.62(12 \times 12) \times 0.793(12} (7.8 \text{ deg}) 2164 \qquad (3.95)$$
$$= -0.035$$

i_f, relative angle of fuselage is zero for fuselage of HAVK since its symmetric. Here; $k_2 - k_1$ is found 0.9 from Figure 3.32. The formula uses feet as a unit of length and degree as a unit of angle.

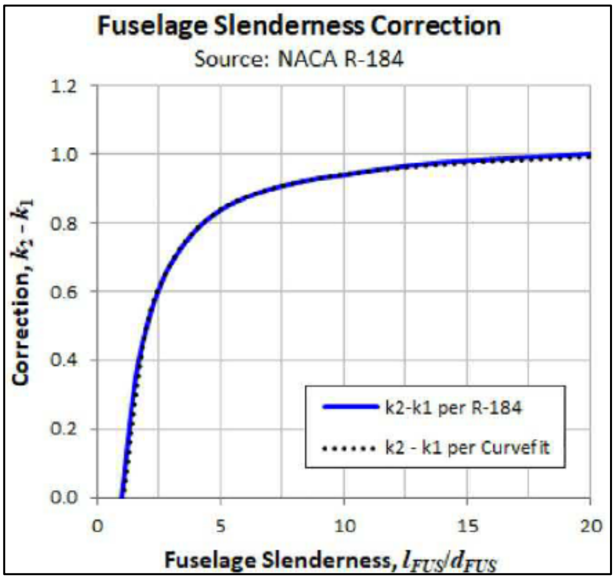

Figure 3.32 : Fuselage Slenderness Correction [7].

3.13.2 Airplane pitching moment curve slope

The pitching moment due to angle of attack derivative, C_{M_α} is computed from:

$$C_{M_\alpha} = (dC_M/dC_L)C_{L_\alpha} \tag{3.96}$$

Summary of calculations given table following:

Table 3.69 : C_{M_α} Calculation Summary

Symbol	Value	Unit
$\boldsymbol{C_{M_\alpha}}$	**-0.6125**	**1/rad**
$\frac{dC_M}{dC_L}$	-0.10	
C_{L_α}	6.125	1/rad

3.13.3 Airplane pitching moment model

Airplane pitching moment model written as given below [21].

$$C_M = C_{M_O} + C_{M_\alpha}\alpha + C_{M_{\delta e}}\delta_e + C_{M_q}\frac{c}{2V}q + C_{M_{\dot\alpha}}\frac{c}{2V}\dot\alpha \tag{3.97}$$

$$C_M = -0.023 + 0.6125\alpha + 0.56\delta_e - 25.57\frac{c}{2V}q - 5.19\frac{c}{2V}\dot\alpha \tag{3.98}$$

Pitching moment coefficients can be found in Table 3.70.

Table 3.70 : Pitching Moment Coefficients

Symbol	Value	Unit
C_{M_O}	-0.023	
C_{M_α}	-0.6125	1/rad
$C_{M_{\delta e}}$	0.56	1/rad
$C_{M_{\dot\alpha}}$	-5.19	
C_{M_q}	-25.57	

Derivatives used in Pitching Moment Coefficients calculated following chapters.

3.14 Derivatives

3.14.1 Angle of attack rate derivatives

The pitching moment due to angle of attack derivative, $C_{M_{\dot\alpha}}$ is computed from [21]:

$$C_{M_{\dot\alpha}} = -2\left(C_{L_{\alpha_h}}\right)\eta_h(\overline{V_h})(\bar{x}_{ac_h} - \bar{x}_{\mathrm{cg}})\left(\frac{d\epsilon}{d\alpha}\right) \tag{3.99}$$

Summary of calculations given table following:

Table 3.71 : $C_{M_{\dot\alpha}}$, Angle of Attack Rate Calculation Summary

Symbol	Value
$C_{M_{\dot\alpha}}$	-5.19
$C_{L_{\alpha_h}}$	4.2
η_h	1.68
V_h	0.47
$\bar{x}_{ac_h}$	4.191
$\bar{x}_{cg}$	0.336
$d\epsilon/d\alpha$	0.203

3.14.2 Pitch rate derivatives

The pitching moment due to pitch angle derivative, C_{M_q} is computed from [21]:

$$C_{M_q} = -2.2\left(C_{L_{\alpha_h}}\right)\eta_h(\overline{V_h})(\bar{x}_{ac_h} - \bar{x}_{\mathrm{cg}}) \tag{3.100}$$

Summary of calculations given table following:

Table 3.72 : C_{M_q}, Pitch Rate Calculation Summary

Symbol	Value
$\boldsymbol{C_{M_q}}$	**-25.57**
$C_{L_{\alpha_h}}$	4.2
η_h	1.68
V_h	0.47
$\bar{x}_{ac_h}$	4.191
$\bar{x}_{cg}$	0.336

Elevator control derivatives

Elevator control derivatives are calculated as given following.

3.14.2.1 $C_{L_{\delta e}}$

The rate of change of the lift coefficient of the aircraft due to deflection of the elevator is calculated according to 3.101 [7]:

$$C_{L_{\delta e}} = \eta_h \frac{S_h}{S} \frac{\partial C_{L_h}}{\partial \delta e} \tag{3.101}$$

Where: $$\frac{\partial C_{L_h}}{\partial \delta e} = \frac{\partial C_{L_h}}{\partial \alpha_h} \frac{\partial \alpha_h}{\partial \delta e} = C_{L\alpha_h} \tau_e \tag{3.102}$$

Elevator effectiveness $\tau_e$is calculated from Figure 3.33:

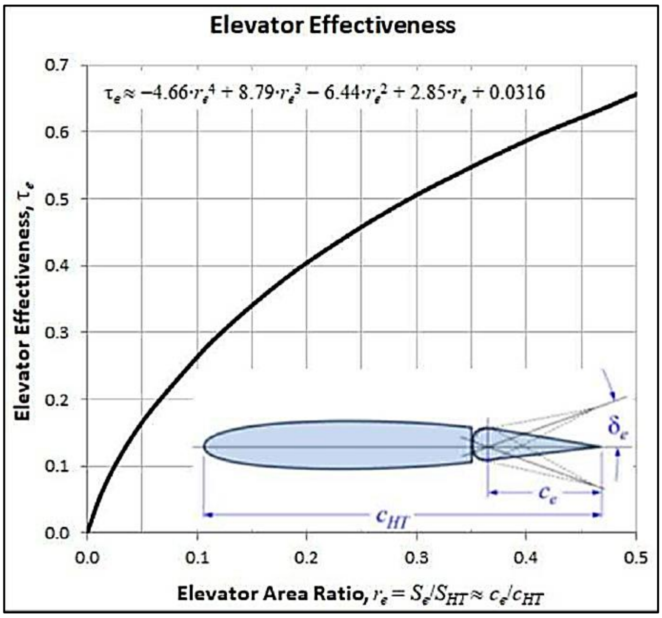

Figure 3.33 : Elevator effectiveness can be approximated using the polynomial shown [7].

Polynomial representation of chart given in 3.103:

$$\tau_e \approx -4.66r_e^4 + 8.79r_e^3 - 6.44r_e^2 + 2.85r_e + 0.0316 \tag{3.103}$$

Summary of calculations can be found on Table 3.73;

Table 3.73 : $\boldsymbol{C_{L_{\delta e}}}$, Elevator Derivative Calculation Summary

Symbol	Value
$\boldsymbol{C_{L_{\delta e}}}$	**0.37**
$C_{L_{\alpha_h}}$	4.2
η_h	1.68
V_h	0.47
S	0.801
S_h	0.096
$\partial C_{L_h}/\partial \delta e$	**1.86**
$C_{L_{\alpha_h}}$	4.2
τ_e	0.44
r_e	0.234

3.14.2.2 $\boldsymbol{C_{M_{\delta e}}}$

The rate of change of the pitching moment coefficient of the aircraft due to deflection of the elevator is calculated according to equation 3.104 [21]:

$$C_{M_{\delta e}} \equiv \frac{\partial C_M}{\partial \delta e} \approx C_{L_{\delta e}}\left(\bar{x}_{ac_h} - \bar{x}_{\mathrm{cg}}\right) - V_h \frac{\partial C_{L_h}}{\partial \delta e} \tag{3.104}$$

Summary of calculations can be found on table, following;

Table 3.74 : $\boldsymbol{C_{M_{\delta e}}}$, Elevator Derivative Calculation Summary

Symbol	Value
$\boldsymbol{C_{M_{\delta e}}}$	**0.56**
$C_{L_{\delta e}}$	0.37
$\partial C_{L_h}/\partial \delta e$	1.86
V_h	0.47
$\bar{x}_{ac_h}$	4.191
$\bar{x}_{cg}$	0.336

3.15 Summary of Preliminary Design

In this chapter the work done in chapters before is combined into a preliminary three view of the configurations. Figure 3.34 shows three views of HAVK (HavaKaşifi). Geometric characteristics of HAVK are summarized in Table 3.75.

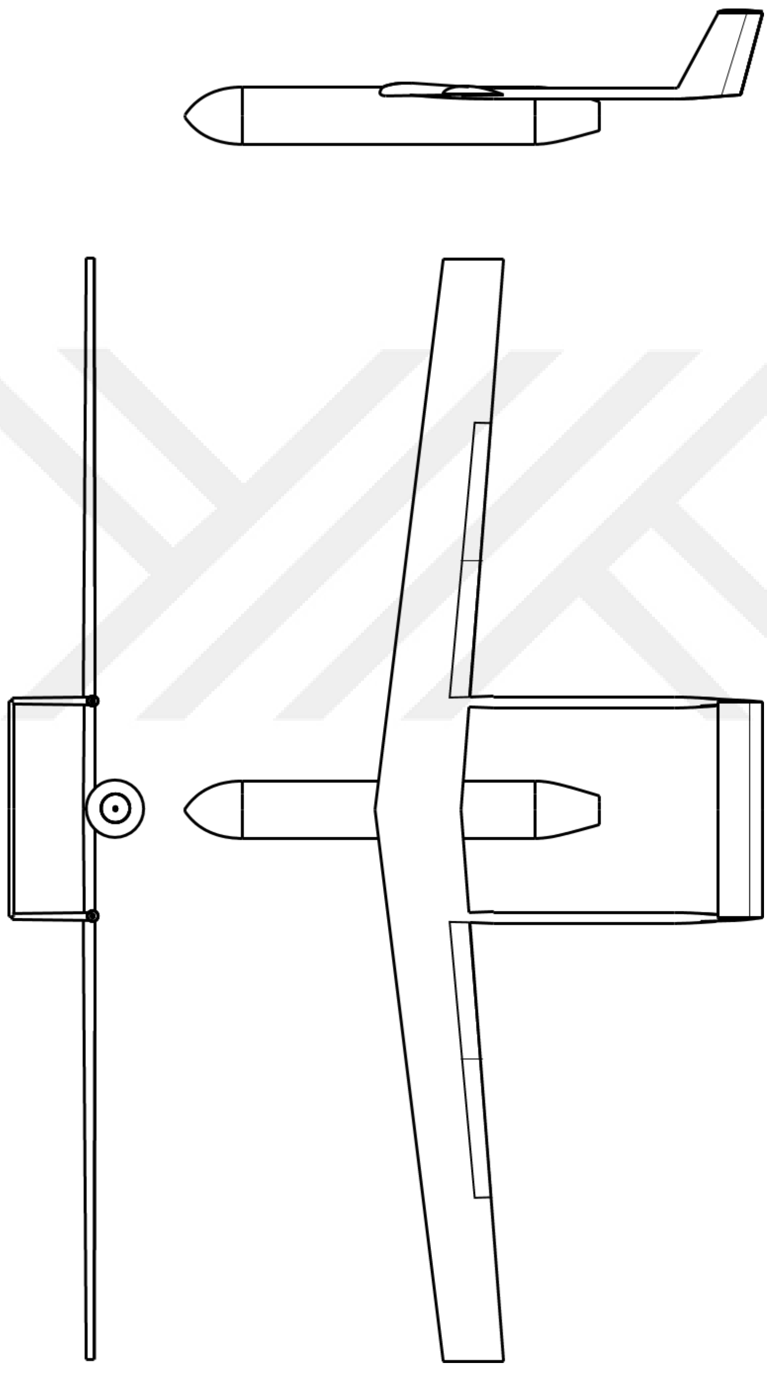

Figure 3.34 : HavaKaşifi : Three view

Table 3.75 : Preliminary Design Summary

Parameter	Symbol	Value	Unit
Take-Off Weight	W_{TO}	15.960	kg
Empty Weight	W_E	7.647	kg
Fuel weight	W_f	4.594	kg
Payload	Wp	3.489	kg
Wing area	S	0.8	m2
Taper ratio	λ	0.70	
Aspect ratio	AR	15	
Leading edge-swept angle	L_{LE}	7	deg
Fuselage diameter	D_{fus}	0.18	mm
Fuselage length	L_{fus}	1.30	mm
Take-Off Weight	W_{TO}	15.960	kg
	C_{L_O}	0.82	
	C_{L_α}	6.125/	1/rad
	$C_{L_{\delta e}}$	0.37	1/rad
	C_{M_O}	-0.023	
	C_{M_α}	-0.6125	1/rad
	$C_{M_{\delta e}}$	0.56	1/rad

4. LAUNCH AND RECOVERY

4.1 Catapult Launch

Catapult launching mechanisms offer enhanced maneuverability for UAV applications. These mechanisms are set at specific angles towards the ground surface to enable UAVs to lift off in straight paths. They help to reduce the take-off speed, eliminate to need of a paved runway. Thus; they allow an aircraft to take off from anywhere a transportation vehicle can reach [23][24].

Considering requirements of HAVK specifications for the launching mechanism is listed Table 4.1:

Table 4.1 : Required Specifications for Launcher

Specification	Value
Launch angle	>6 degrees
Weight	<70kg
Maximum plane mass	>20kg
Maximum allowed launch velocity	>25m/s
Puller configuration aircraft	YES
Pusher configuration aircraft	YES
Typical set-up time	<10min

Detailed market research and trade-off analysis for selecting launcher are not performed in this study but Eli Airborne Solutions PL-40 UAV launcher is selected to use in calculations since it satisfies general requirements given above [25].

Table 4.2 Launcher Specifications PL-40[25]

Specification	Value
Launch angle	11 degrees
Overall rail length when assembled	5m
Rail length when disassembled	1.28m
Weight of catapult set, 2 boxes	Total 56kg
Launcher case external dimensions	1480x440x170mm
Compressor case external dimensions	650x325x520mm
Maximum plane mass	45kg
Maximum allowed launch velocity	25m/s
Puller configuration aircraft	YES
Pusher configuration aircraft	YES
Typical set-up time	5min

Figure 4.1 PL-40 UAV Launcher [25]

4.1.1 Equation of take -off motion

A takeoff of from catapult launcher has the same equations of motion as take-off from a ramp. The main difference is that aircraft taking off from the ramp have landing gear, but catapult-launched aircraft do not.

Figure 4.2 represents the motion of catapult launch. This can be split in to two main phases; before take-off and after -take off. In first phase of the launch, from 1 to 2, aircraft is accelerated to its take-off speed. This acceleration can be performed by catapult mechanism or engine thrust or like in this case their combinations.

In the second phase, as specified by Silkov and Zirka (2014)," the aircraft moves on a trajectory close to a ballistic one" [23]. Because of the angle of ramp its velocity has vertical component that helps aircraft to gain height which means potential. If take-off speed is not high enough to maintain straight climb, the aircraft reaches maximum height shown by 3 then it will start to go down. The aircraft is accelerated while it goes down from point 3 to 4 also its angle of attack increases with the help of these two phenomena the lift increases up to value required for flight. If the aircraft reaches enough lift before it touches the ground it can perform climb.

Thus, a takeoff speed that cause H4 to be zero is minimum speed to achieve theoretical flight will be called $V_{takeoff\_min}$.

IF $V_{takeoff} < V_{takeoff\_min}$. → $H4 < 0$, the plane will crash.

IF $V_{takeoff} > V_{takeoff\_min}$. → $H4 > 0$, the plane will climb.

To select $V_{takeoff}$ as much as low helps to reduce g force which is used accelerate the aircraft. However, for safety concern $V_{takeoff}$ is selected such that:

<u>Condition: Altitude of an aircraft after launch will not decrease or vertical speed of the aircraft cannot be zero.</u>

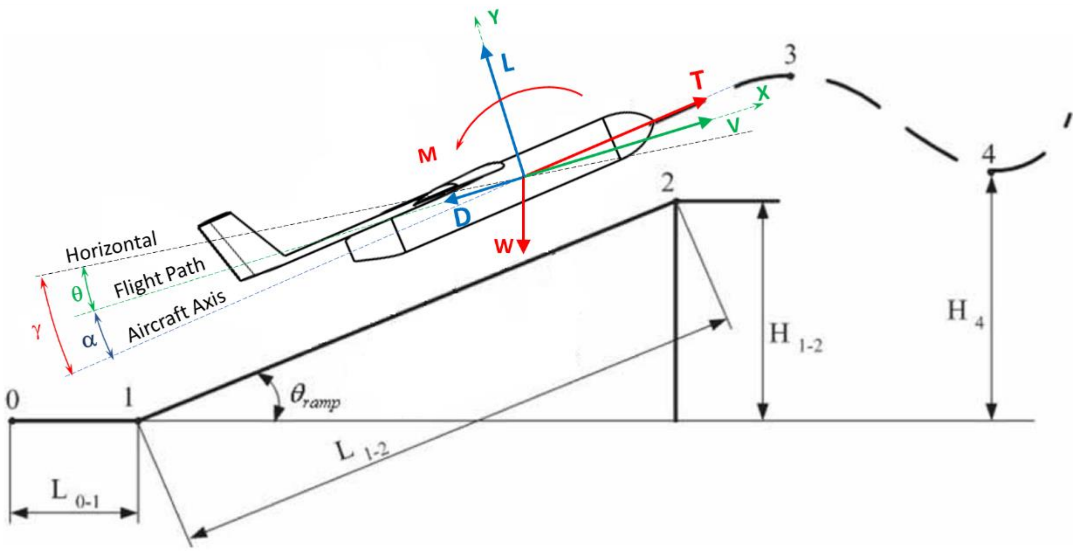

Figure 4.2 : FBD of take-off

Take-off speed, $V_{takeoff}$, which satisfy this condition is determined as 13.89 m/s. Calculations are performed considering equation of motion of the aircraft given

Appendix B [26]. Initial elevator angle is taken 5 degrees, to trim aircraft positive angle of attack. Overall parameter used in calculations can be found Appendix C. Outputs are plotted and represented in Figure 4.3 and Figure 4.4. Horizontal axis of plots shows horizontal distance after take-off from ramp. It can be easily seen that altitude of aircraft increases first then at some point the aircraft stops to goes up and preserves its height (where Vy is zero). Thus, it is shown that condition which mentioned before is satisfied.

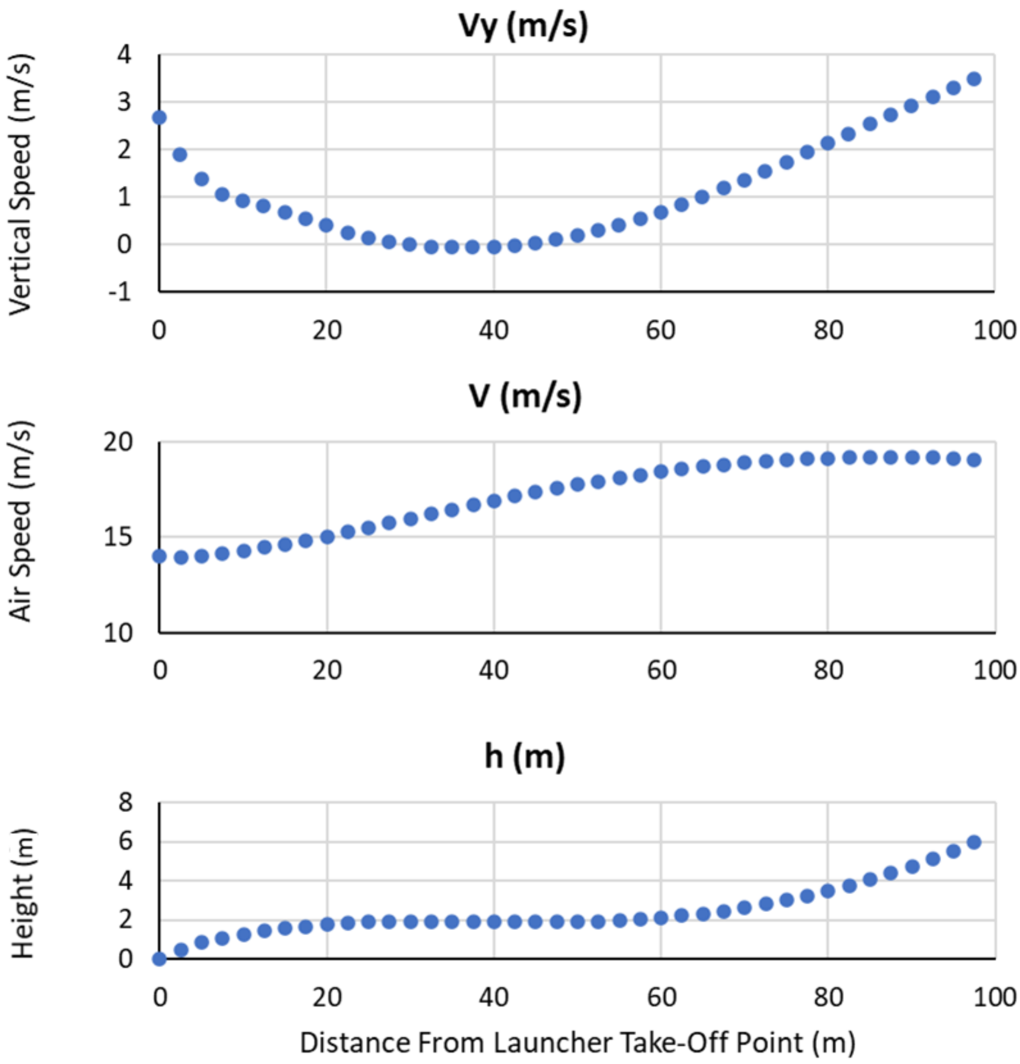

Figure 4.3 : Vertical speed, air speed and height characteristics of HAVK. $\delta e = 5^{o}$ and $\theta_I = 11^{o}$

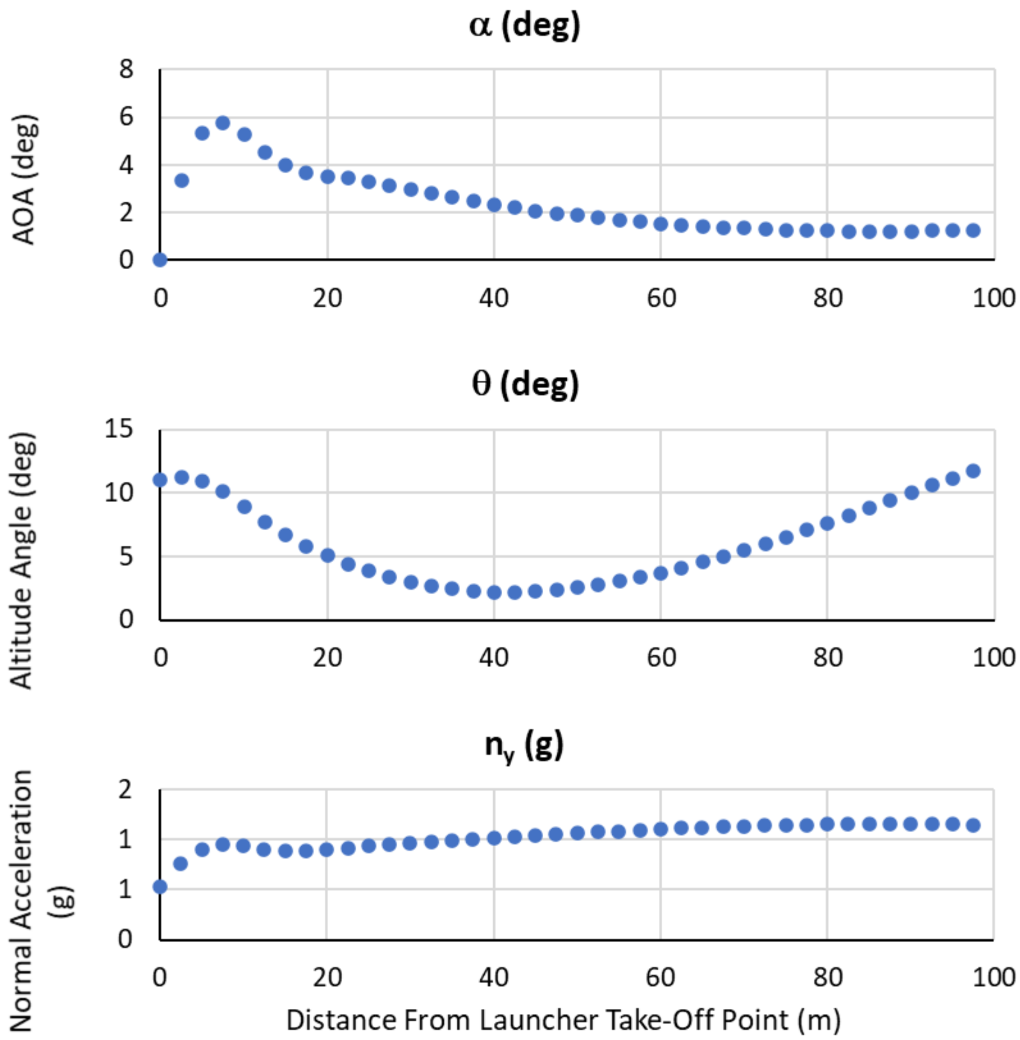

Figure 4.4 : AOA, atitude angle and normal acceleration characteristics of HAVK. $\delta e = 5°$ and $\theta_l = 11°$

4.2 Vertical Rope-type Recovery

A vertical rope-type recovery system is a specialized method used to recover unmanned aerial vehicles (UAVs), particularly in environments where landing space is limited or traditional runway landings are impractical. Figure 4.5 shows SkyHook recovery system used by InSitu, which is an example of vertical arresting rope type recovery system[27].

Figure 4.5 : SkyHook/Insitu [34]

System components are defined and system requirements are determined subsequent chapters.

4.2.1 Part of vertical arresting system

Vertical arresting rope recovery system main components are represented Figure 4.6. Following Table shows name of components pointed on Figure.

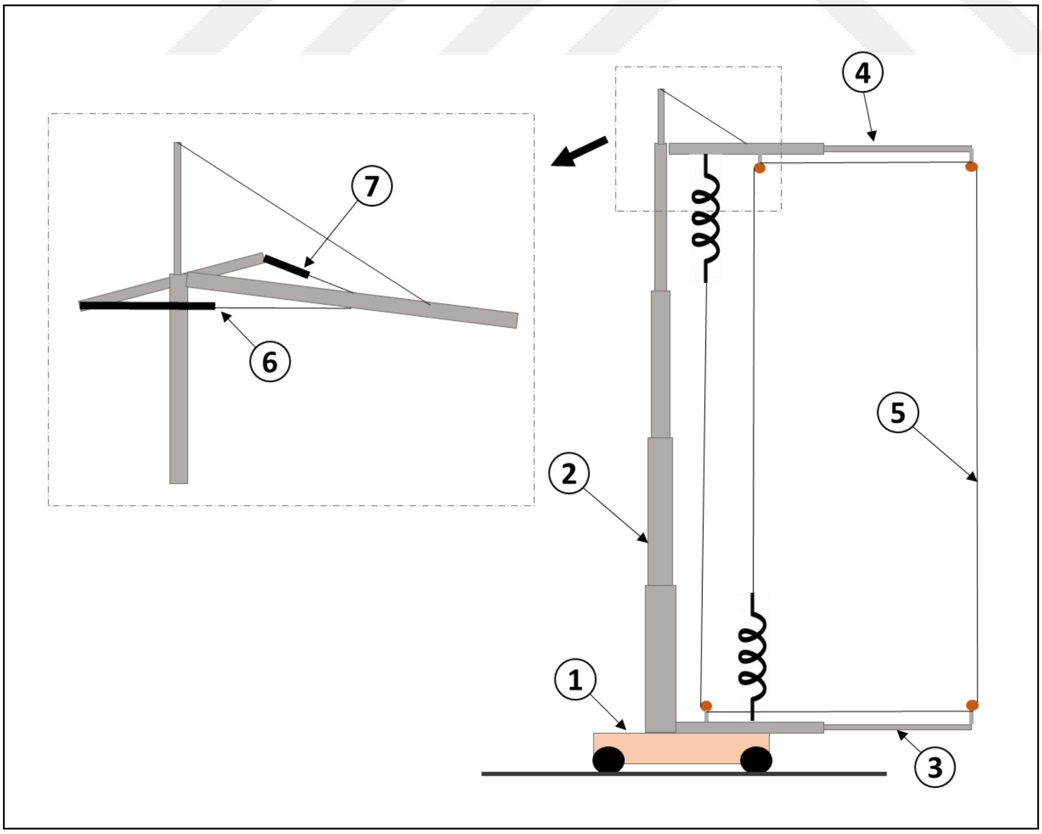

Figure 4.6 : Schematic representation of main components of vertical arresting system

Table 4.3 : List of main components of vertical arresting system

No	Part
1	Support
2	Vertical bar
3	Lower cross bar
4	Upper cross bar
5	Arresting rope
6	Damping rope 1
7	Damping rope 2

4.2.2 Motion analysis

Motion analysis of vertical recovery type cable is based on study of Ma et al (2018), provides a comprehensive study on the mechanics and dynamics involved in the vertical rope-type recovery of unmanned aerial vehicles (UAVs) [28]. The aircraft parameters used in analysis at Ma et al (2018) given Table 4.4.

Table 4.4 : Parameters for Recovery Analysis [28].

Description	Value	Unit
Aircraft weight	60	kg
Wingspan:	5	m
Leading edge sweep angle	11	deg
Recovery velocity of aircraft	25	m/s
Arresting rope length	16	m
Rope stiffness coefficient	500	N/m
Rope damping coefficient	40	N//m/s)
Distance between first contact point and bottom end of the rope	8	m
Distance between first contact point and CG of the aircraft at spanwise direction	2	m

The recovery process split into two main phases by Ma et al, (2018): the arresting rope hitting the wing leading edge and then its interaction with the wingtip [28].

Figure 4.7, represent trajectory of CG of the aircraft in horizontal plane. Starting point represents the CG location the aircraft when it hits to rope. It can be seen that the aircraft moves along x direction then tension force on the rope force the aircraft to enter circular trajectory.

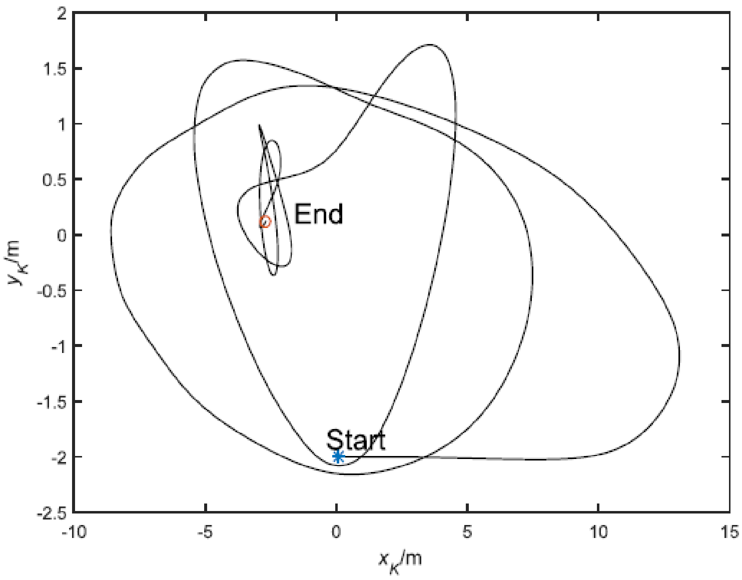

Figure 4.7 : Trajectory of UAV's center of gravity in horizontal plane [28].

Considering motion envelope of the aircraft on recovery, length criteria about upper and lower cross bar can be determined as given below:

$$L_{cbar} = SF * \left(y_{cg_{rec}} + \frac{b}{2}\right) \tag{4.1}$$

- Where; L_{cbar}: Length of cross bar (upper/or lover)
- $y_{cg_{rec}}$: Maximum spanwise direction value at recovery (Positive value is important which is from arresting rope to vertical rod)
- SF: Safety factor. It is assumed as 1.5

$y_{cg_{rec}}$ is 1.7 m (See from Figure above) for the aircraft has 5 m wingspan. Non-dimensioning $y_{cg_{rec}}$ with span b, then, $\bar{y}_{cg_{rec}}$ is obtained as 0.34.

Thus, L_{cbar} for HAVK is calculated as:

$$\begin{aligned} L_{cbar} &= 1.5 * \left(0.34 * b + \frac{b}{2}\right) \\ &= 1.5 * \left(0.34 * 3.35 + \frac{3.35}{2}\right) \\ &= 4.22\ m \end{aligned} \tag{4.2}$$

Ma et al (2018) also explores how different parameters, like the initial conditions of the rope impact, the stiffness, and damping coefficients of the arresting rope affect the recovery performance [28]. Results suggest that these parameters significantly influence; the maximum resistance force, load factor and radius of the recovery trajectory. Findings can be summarized as given below:

- Recovery velocity and maximum resistance force have linear relationship. Resistance force increases by recovery velocity
- Increasing stiffness coefficient increases maximum resistance force decreases maximum radius
- Increasing damping coefficient decreases maximum resistance force decreases maximum radius

The resistance force acting on the aircraft as a function of time is shown in Figure 4.8. Here x is fuselage direction and y are spanwise direction.

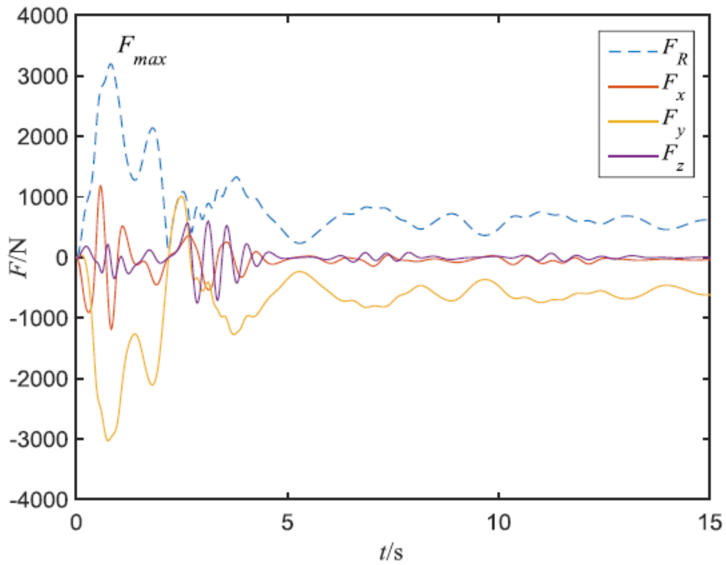

Figure 4.8 : Curve of resistance force [28].

It can be seen that from Figure 4.8;

- Resisting force increases rapidly after the aircraft hit the rope then it reaches its maximum when aircraft reached longest distance it can.
- Force in x direction increases after the contact then it drops since the aircraft starts turn around its wing tip which cause increment in force y direction.

Maximum resistance forces and load factors are listed in Table 4.5.

Table 4.5 : Forces and Load Factors

Description	Value	Unit
$F_{x_{max}}$	1217	N
$F_{x_{min}}$	-1217	N
$F_{y_{max}}$	3083	N
$F_{r_{max}}$	3200	N
$n_{x_{max}}$	2.1	g
$n_{x_{min}}$	-2.1	g
$n_{y_{max}}$	5.2	g
$n_{r_{max}}$	5.4	g

These load factors are conservative for HAVK since it has lower weight and slower recovery speed (not calculated yet but certainly smaller than its cruise speed 25 m/s) Thus, these load factors are assumed to be the same for HAVK until specific analysis for it is performed.

Furthermore, requirements for vertical arresting system defined Table 4.6. Rope length, rope stiffness and damping coefficient is taken same with [28].

Ma et al (2018) show that increasing the stiffness of the arresting rope decreases the maximum radius of UAV motion but increases load factor. Conversely, adjusting the damping coefficient affects the energy absorption, improving the buffering characteristics and reducing load factor [28].

These insights are crucial for optimizing the design and function of UAV recovery systems, particularly in constrained environments like ships or islands, where precision in recovery is critical.

Table 4.6 : Requirements of vertical arresting system.

Description	Symbol	Value	Unit
Vertical var height	H_{vr}	16	m
Cross bar height	L_{cbar}	4.22	m
Stiffness constant	k	500	N/m
Damping constant	c	40	N/(m/s)

5. LOADS

5.1 Flight Loads

5.1.1 v-N diagram

In this section, where the maneuver envelope, also referred to as the V-n envelope, is created, the load coefficients that the aircraft will be exposed to at different speeds will be emphasized. The V-n envelope, also referred to as the maneuver envelope, is a diagram showing the load that the aircraft is subjected to during flight phases. It consists of two parts, negative and positive. This envelope provides pilots with information on which flight speeds are safe during flight and in which situations and provides the necessary information for safe flight.

There are a few basic points in the drawing of the envelope, the most important of which is the maximum load coefficients to be selected for the lower and upper limits. In determining the load factors, there are standard values for different aircraft types in documents such as FAR.23 and CS-VLA. The standard load coefficients determined according to these documents are 3.8 at the positive limit and -1.9 at the negative limit. However, these values are quite high for the HAVK being designed. CS-VLA (Certification Specifications for Very Light Airplanes) is a standard based on aircraft weighing 750 kg or less [29]. The platform being designed here has a take-off weight of around 18 kg and can be defined as a mini-class UAV. In this case, since it would not be appropriate to determine the load coefficients to be selected according to the CS-VLA, studies on platforms of similar sizes were taken as a basis.

Based on the studies mentioned in [30-33] , the positive and negative load factor limits in the maneuver envelope were determined as 2.4 and -1 and the maneuver envelope was drawn within these limits.

Table 5.1 : Load factors

Parameter	Value
Positive load limit	2.4
Negative load limit	-1
Ultimate load factor	1.5

Table 5.2 : Envelope specifications.

Parameter		Value	
Max. normal lift coef.	C_{Nmax}	1.76	
Min. normal lift coef.	C_{Nmax_neg}	-0.594	
Limit load factor	n^+	2.4	g
Negative limit load factor	n^-	-1	g
Stall speed	V_s	13.7	m/s
Negative stall speed	V_{s_neg}	23.8	m/s
Cruise Speed	V_C	26	m/s
Dive Speed	V_D	32.5	m/s
Maneuver speed	V_A	21.2	m/s

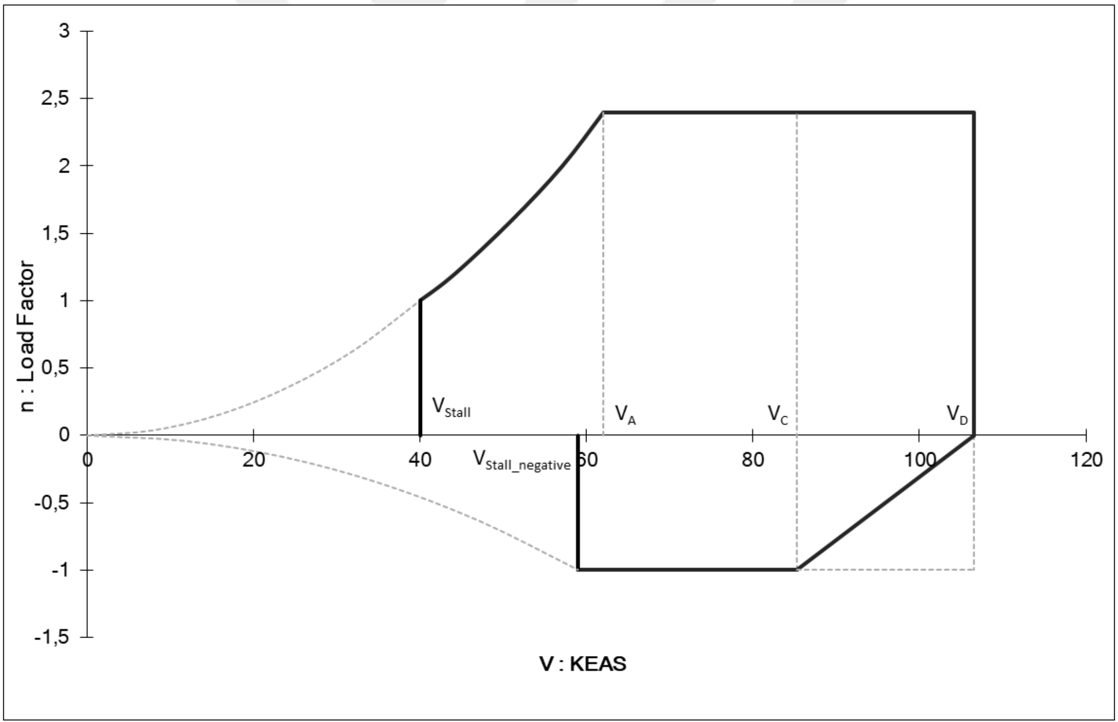

Figure 5.1 : HAVK structural flight envelope.

5.2 Launch Loads

Launch loads are determined considering launch pad force acting on the aircraft. In this process tangential and normal load are play active load. The tangential force is the force accelerating the aircraft its take-off speed. Its calculated considering launcher length. Assuming accelerations is constant kinematic equation of tangential motion written as given below [34]:

$$V^2 = 2 * a * l \tag{5.1}$$

For length of launcher is L =5 m and take-of velocity is $V_{takeoff}$ = 13.9 m/s, acceleration calculated as 19.321 m/s^2. Thus, load factor at x-direction is found as 1.97 g.

$$n_x = 1.97 \approx 2\ g \tag{5.2}$$

Since the launcher length, launching speed and slope will affect the take-off performance, this value can change by possible scenarios.

Furthermore; the normal force is calculated by formula as given below:

$$N = L - mgcos\theta \tag{5.3}$$

Where, L is lift and θ is launch angle.

Initially lift is zero thus, maximum load factor at normal direction equals to $cos\theta$;

$$n_z = -cos\theta = -cos11^o = 0.98\ \approx 1 \tag{5.4}$$

Maximum launch loads are given Table 5.3.

Table 5.3 : Launch Load Factors

Description	Value	Unit
n_x	2.0	g
n_z	1.0	g

5.3 Recovery Loads

Recovery load are determined at Table 4.5. Summary table can be found Table 5.4:

Table 5.4 : Recovery Load Factors

Description	Value	Unit
n_x	+/-2.1	g
n_y	5.2	g

6. COST ANALYSIS

6.1 Introduction

A cost analysis method named Eastlake model use special cost estimating relationships (CER) originally derived by the RAND Corporation to estimate the development cost of new military aircraft (. The CERs constitute a method commonly referred to as DAPCA-IV (development and procurement costs of aircraft) [7].

Even if the RAND model incorporates weight, speed, altitude, and thrust to provide a cost assessment Valerdi (2005) points out that, “Traditional software and hardware cost models are not effective for UAVs due to the new challenges presented by their operational attributes”, [35][36]

In this study, cost analysis is performed with Eastlake model presented in [7]. However, considering what mentioned paragraph above, unrealistic outputs of Eastlake model is changed by assumed value of the writer.

6.2 Development Cost of an Aircraft

A general flow chart of Eastlake model is presented in Figure. Required calculations are performed in subsequent chapters following the flow chart.

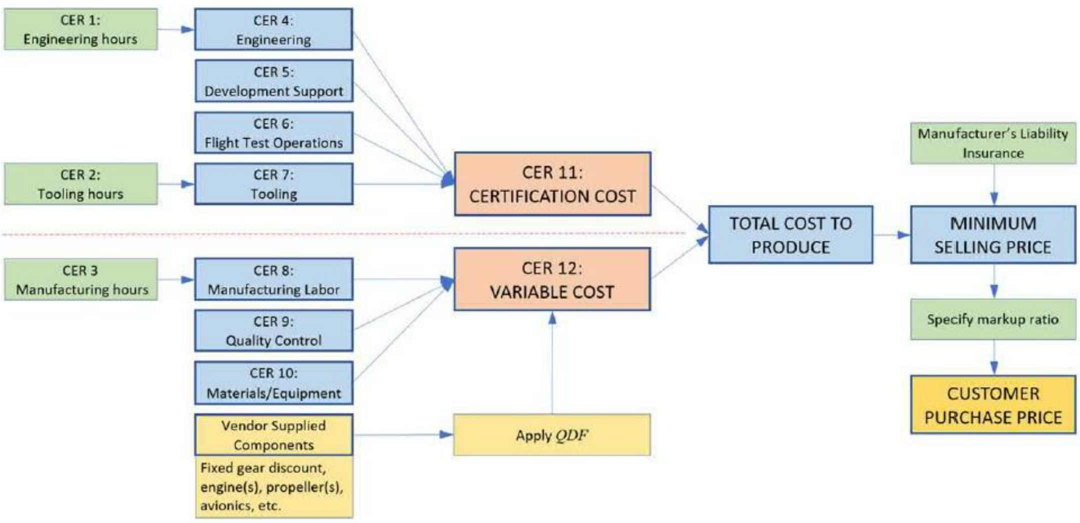

Figure 6.1 : A flow chart of the Eastlake Cost Model [7].

Main inputs required to perform calculations are airframe weight ($W_{airframe}$), maximum speed at unit of knot (V_H), and number of aircraft planning to produce (N).

- $W_{airframe}$ is assumed 0.5 of take-off weight (it taken 20 kg considering requirements)
- V_H is taken as 76.5 knot
- N should be selected considering planned aircraft to be produced over 5 years. Thus, its assumed that every month 2 aircraft will be produced which makes it 120 over 5 years.

Also, system of UAV is assumed consist of

- Airframe
- Payload
- Modular ground control station
- Modular light launcher
- Modular vertical cable recovery system

6.2.1 Quantity discount factor

For vendor supplied components (VSC) quantity discount factor is calculated as below:

$$QDF = (F_{EXP})^{1.4427.\ln N} \tag{6.1}$$

Where: F_{EXP} =Experience effectiveness (It was taken as 0.95)

N = Number of units produced

6.2.2 CER 1 – Engineering workhours

The estimation of engineering hours needed to design the aircraft and carry out the required Research, Development, Test, and Evaluation (RD&T&E) is calculated by formula (2-8) of [7] given below. Calculation summary can be found Table following.

$$H_{\mathrm{ENGR}} = 0.0396 \cdot W_{\mathrm{airframe}}^{0.791} \cdot V_H^{1.526} \cdot N^{0.183} \cdot F_{\mathrm{CERT}} \cdot F_{\mathrm{CF}} \cdot F_{\mathrm{COMP}} \cdot F_{\mathrm{PRESS}} \tag{6.2}$$

H_{ENGR} = the number of engineering work hours.

W_{airframe} = Weight of the structural skeleton

V_H = Maximum level airspeed in KTAS

N =Number of planned aircraft to be produced over a 5-year period

F_{CERT} = 0.67 if certified as LSA, =1 if certified as a 14 CFR Part 23 aircraft

F_{CF}= 1.03 for a complex flap system, =1 if a simple flap system.

F_{COMP} =1+f_comp a factor to account for the use of composites in the airframe

f_{COMP}= Fraction of airframe made from composites that range from 0 to 1 (=0 for aluminum aircraft, =1 for a complete composite aircraft)

F_{PRESS} = 1.03 for a pressurized aircraft, =1 if unpressurized

Table 6.1 : Required Engineering Hours Calculation Summary

	Value	Unit
H_{ENGR}	**1087**	**h**
$W_{airframe}$	22.05	lb
V_H	75.8	knot
N	120	
$F_{CERT\ 1}$	0.67	
F_{CF_1}	1	
F_{COMP_1}	2	
f_{comp}	1	
F_{PRESS_1}	1	

Required engineering workhours are calculated as 1087 hours for 120 aircraft, which makes 453 h for 1 aircraft. This is corresponded to 11 weeks or 3 months which is underestimated time for an engineer to design a small UAV.

It is assumed that total engineering time to design 1 aircraft cannot be less than 2 years (6 months for 4 engineers). Then H_{ENGR}:

$$H_{ENGR} = 2\,year \times\ 48\frac{week}{year} \times 40\frac{hour}{week} = 3840\ h \tag{6.3}$$

And for 120 aircrafts:

$$H_{ENGR} = 3840 * 120^{0.183} = 3840 * 2.4 = 9216\ h \tag{6.4}$$

This value is used in calculations. Considering first estimation which is1087 h, it can be seen that model underestimates engineering effort 8.5 times.

6.2.3 CER 2 – Tooling workhours

The estimation of tooling hours needed to design and build tools, fixtures, jigs molds, and so on is calculated by formula (2-9) of [7] given below. Calculation summary can be found Table following.

$$H_{\mathrm{TOOL}} = 1.0032 \cdot W_{\mathrm{airframe}}^{0.764} \cdot V_H^{0.899} \cdot N^{0.178} \cdot Q_m^{0.066} \cdot F_{\mathrm{CF2}} \cdot F_{\mathrm{COMP2}} \cdot F_{\mathrm{PRESS2}} \cdot F_{\mathrm{TAPER2}} \tag{6.5}$$

Where;

Q_m = Estimated production rate in number of aircraft per month = N/60 for 60months/5years

F_{CF2} = 1.02 for a complex flap system, =1 if a simple flap system

F_{COMP2} = 1+f_{comp} a factor to account for the use of composites in the airframe

F_{PRESS2} = 1.01 for a pressurized aircraft, =1 if unpressurized

F_{TAPER2} = 0.95 for a constant chord wing, =1 for a tapered wing

Table 6.2 : Required Toling Hours Calculation Summary

	Value	Unit
H_{TOOL}	**2562**	**h**
$W_{airframe}$	22.05	lb
V_H	75.8	knot
N	120	
Q_m	2	
F_{CF_2}	1	
F_{COMP_2}	2	
F_{PRESS_2}	1	
F_{TAPER_2}	1	

6.2.4 CER 3 – Manufacturing labor workhours

The estimation of tooling hours needed to design and build tools, fixtures, jigs molds, and so on is calculated by formula (2-10) of [7] given below. Calculation summary can be found Table following.

$$H_{\mathrm{MFG}} = 9.6613 \cdot W_{\mathrm{airframe}}^{0.74} \cdot V_H^{0.543} \cdot N^{0.524} \cdot F_{\mathrm{CERT3}} \cdot F_{\mathrm{CF3}} \cdot F_{\mathrm{COMP3}} \tag{6.6}$$

F_{CERT3}= 0.75 if certified as LSA, =1 if certified as a 14 CFR Part 23 aircraft

F_{CF3}= 1.01 for a complex flap system, =1 if a simple flap system

F_{COMP3}= 1+0.25f_comp a factor to account for the use of composites in the airframe

Table 6.3 : Required Manufacturing Labor Hours Calculation Summary

	Value	Unit
H_{MFG}	**11515**	**h**
$W_{airframe}$	22.05	lb
V_H	75.8	knot
N	120	
$F_{CERT\ 3}$	0.75	
F_{CF_3}	1	
F_{COMP_3}	1.25	

6.2.5 Hourly rate of labor

According to Gudmundsson (2021), when estimating costs in aircraft design, it is crucial to apply accurate hourly rates for engineering, tooling and manufacturing labor. At $92, $61 and $53 per hour as of June 2012, these rates include not only the direct wages of workers, but also overhead and benefits [7]. Gudmundsson (2021) cautions against the common tendency to underestimate these rates, emphasizing that they are comprehensive. For example, an engineer with a master's degree and 10 years of experience, earning about $100,000 a year, is paid about $48 per hour. However, when overhead costs are included, the cost to the company is $92 per hour, almost double the engineer's direct hourly wage [7]

Rate of labor in Turkey is calculated considering metrics of GDP-Nominal and GDP-PPP shown in Table 6.4. Ratio of GDP-Nominal and GDP-PPP is useful metric for understanding the relative cost of living and the purchasing power of a country's currency compared to a standard international dollar rate[37]. Thus, multiplying this ratio with rate of labors defined at [7], rates of labor in Turkey can be calculated as given Table 6.5

Table 6.4 : Turkey GDP (USD Million)[38].

GDP	Value
Nominal	1,113,561
PPP	3,831,533
PPP/Nominal	3.44

Table 6.5 : Rates of Labor in Turkey ($)

Labor	the USA ($)	Turkey ($)
Engineering	92	27
Tooling	61	18
Manufacturing	53	15

6.2.6 CER 4 – Total cost of engineering

Total cost of engineering is calculated by formula (2-12) of [7] given below. Calculation summary can be found Table following.

$$C_{\text{ENGR}} = H_{\text{ENGR}} \cdot R_{\text{ENGR}} \cdot CPI_{2012} \tag{6.7}$$

R_{ENGR}= Rate of engineering labor in dollars per hour (e.g., $92/h)

CPI_{2012} = Consumer Price Index relative to June 2012

Table 6.6 : Total Cost of Engineering Calculation Summary

	Value	Unit
C_{ENGR}	**338424**	$
H_{ENGR}	9216	h
R_{ENGR}	27	$/h
CPI_{2012}	1.36	

6.2.7 CER 5 – Total cost of development support

Total cost of development support is calculated by formula (2-12) of [7] given below. Calculation summary can be found Table following.

$$C_{\text{DEV}} = 0.06458 \cdot W_{\text{airframe}}^{0.873} \cdot V_H^{1.89} \cdot N_P^{0.346} \cdot CPI_{2012} \cdot F_{\text{CERT5}} \cdot F_{\text{CF5}} \cdot F_{\text{COMP5}} \cdot F_{\text{PRESS5}} \tag{6.8}$$

N_P= Number of prototypes

F_{CERT5} = 0.5 if certified as LSA, =1 if certified as a 14 CFR Part 23 aircraft

F_{CF5}= 1.01 for a complex flap system, =1 if a simple flap system

F_{COMP5}= 1+0.5f_comp a factor to account for the use of composites in the airframe

F_{PRESS5}= 1.03 for a pressurized aircraft, =1 if unpressurized

Table 6.7 : Total Cost of Development Support Calculation Summary

	Value	Unit
C_{DEV}	**4449**	**$**
$W_{airframe}$	22.05	lb
V_H	75.8	knot
N_P	2	
CPI_{2012}	1.36	
$F_{CERT\ 5}$	0.5	
F_{CF_5}	1	
F_{COMP_5}	1.5	
F_{PRESS_5}	1	

It can be seen from table, C_{DEV}, total cost of development support, is estimated $4449. Again, this amount is accepted as underestimated and multiplied by ratio of 8.5 discussed in CER 1-Engineering Workhours

$$C_{DEV} = 4449 * 8.5 = 37812\ \$ \tag{6.9}$$

6.2.8 CER 6 – Total cost of flight test operations

The total cost of flight test program is calculated by formula (2-13) of [7] given below. Calculation summary can be found Table following.

$$C_{\text{FT}} = 0.009646 \cdot W_{\text{airframe}}^{1.16} \cdot V_H^{1.3718} \cdot N_P^{1.281} \cdot CPI_{2012} \cdot F_{\text{CERT6}} \tag{6.10}$$

F_{CERT6}= 10 if certified as LSA, =5 if a 14 CFR Part 23 aircraft

Table 6.8 : Total Cost of Flight Test Operations Calculation Summary

	Value	Unit
C_{FT}	**2185**	**$**
$W_{airframe}$	22.05	lb
V_H	75.8	knot
N_P	2	
CPI_{2012}	1.36	
$F_{CERT\ 6}$	5	

It can be seen from table, C_{FT}, the total cost of flight test program, is estimated \$2185. Again, this amount is accepted as underestimated and multiplied by ratio of 8.5 discussed in CER 1-Engineering Workhours

$$C_{FT} = 2185 * 8.5 = 18572 \ \$ \tag{6.11}$$

6.2.9 CER 7 – Total cost of tooling

The total cost of tooling is calculated by formula (2-15) of [7] given below. Calculation summary can be found Table following.

$$C_{\mathrm{TOOL}} = H_{\mathrm{TOOL}} \cdot R_{\mathrm{TOOL}} \cdot CPI_{2012} \tag{6.12}$$

R_{TOOL} = Rate of tooling labor in dollars per hour (e.g., \$61/h)

Table 6.9 : Total Cost of Tooling Calculation Summary

	Value	Unit
C_{TOOL}	**62716**	\$
H_{TOOL}	2562	h
R_{TOOL}	18	\$/h
CPI_{2012}	1.36	

6.2.10 CER 8 – Total cost of manufacturing

The total cost of manufacturing is calculated by formula (2-16) of [7] given below. Calculation summary can be found Table following.

$$C_{\mathrm{MFG}} = H_{\mathrm{MFG}} \cdot R_{\mathrm{MFG}} \cdot CPI_{2012} \tag{6.13}$$

R_{MFG} = Rate of manufacturing labor in dollars per hour (e.g., \$53/h)

Table 6.10 : Total Cost of Manufacturing Calculation Summary

	Value	Unit
C_{MFG}	**234915**	\$
H_{MFG}	11515	h
R_{MFG}	15	\$/h
CPI_{2012}	1.36	

6.2.11 CER 9 – Total cost of quality control

The total cost of quality control is calculated by formula (2-17) of [7] given below. Calculation summary can be found Table following.

$$C_{QC} = 0.13 \cdot C_{MFG} \cdot F_{CERT} \cdot F_{COMP} \quad (6.14)$$

where

F_{CERT}= 0.5 if certified as an LSA, F_CERT = 1 if certified as a 14 CFR Part 23 aircraft.

F_{COMP}= 1 + 0.5 * f_{comp}, a factor to account for the use of composites in the airframe.

Table 6.11 : Total Cost of Quality Control Calculation Summary

	Value	Unit
C_{QC}	**22904**	$
C_{MFG}	234915	$
$F_{CERT\ 9}$	0.5	
F_{COMP_9}	1.5	

6.2.12 CER 10 – Total cost of materials

The total cost of materials is calculated by formula (2-16) of [7] given below. Calculation summary can be found Table following.

$$C_{MAT} = 24.896 * W_{airframe}^{0.689} * V_H^{0.624} * N^{0.792} * CPI_{2012} * F_{CERT10} * F_{CF10} * F_{PRESS10} \quad (6.15)$$

F_{CERT10}= 0.75 if certified as LSA, =1 if certified as a 14 CFR Part 23 aircraft,

F_{CF10}= 1.02 for a complex flap system, =1 if a simple flap system,

$F_{PRESS10}$= 1.01 for a pressurized aircraft, =1 if unpressurized.

Table 6.12 : Total Cost of Materials Calculation Summary

	Value	Unit
C_{MAT}	**141242**	h
$W_{airframe}$	22.05	lb
V_H	75.8	knot
N	120	
CPI_{2012}	1.36	
$F_{CERT\ 10}$	0.75	
F_{CF_10}	1	
F_{PRESS_10}	1	

6.2.13 CER 11 – Fixed cost

The total cost is calculated by formula (2-19) of [7] given below. Calculation summary can be found Table following.

$$C_{fix} = C_{ENGR} + C_{DEV} + C_{FT} + C_{TOOL} \tag{6.16}$$

Table 6.13 Fixed Calculation Summary

	$
C_{fix}	**472833**
C_{ENGR}	338424
C_{DEV}	37813
C_{FT}	33880
C_{TOOL}	62716

6.2.14 CER 12 – Variable cost

The variable cost calculated by formula (2-20) of [7] given below.

$$C_{var} = \frac{C_{MFG} + C_{QC} + C_{MAT}}{N} + C_{VSC} + C_{INS} \tag{6.17}$$

where

C_{VSC}= Cost of all vendor supplied components that includes the appropriate QDF.

C_{INS}= Manufacturer's liability insurance per unit. Estimate as 12% to 17% of the selling price in lieu of better estimates.

Cost list for vendor supplied components, VSC, is provided following chapter.

6.2.15 VSC-Vendor supplied components

Cost of VSCs is listed Table 6.14. Avionics, engine propeller, are payload are selected to use for cost analysis considering general requirements of small UAVs. Main purpose is obtaining a rough estimation for project cost and unit selling price The aircraft planning to produce can has components different from which selected here.

Table 6.14 : Vendor Supplied Components

VSC	Name	Cost	Comment	Ref.
VSC_1	Avionics	$ 6,900	George G2 Integration Kit	[39]
VSC_2	Engine	$ 1,620	SP-28-cr	[11]
VSC_3	Propeller	$ 150	Propeller 18x8 CCW 2B	[40]
VSC_4	Payload	$ 15,649	Eagle Eye-30IE-U 2-Axis 30X EO/IR Dual Sensor Zoom Camera with Tracking and Geotagging	[41]
VSC_5	GCS	$ 35,200		
VSC_6	Catapult Launcher	$ 10,027		
VSC_7	Vertical Cable Recovery	$ 59,013	Cost divided into four	

6.2.15.1 GCS system cost

GCS system cost is estimated considering sub components of system which is

- Network hub
- Pilot mobile control system
- Payload operator mobile control system
- Communication equipment and antenna tracking unit
- Power generator

Price of pilot mobile control system and payload operator control system is found and listed in Table. For other subcomponents no information is found and total GCS cost is accepted as $ 35200 which 2 times of cost of known subsystem cost

Table 6.15 GCS System Cost Summary

	Name	Cost	Comment	Ref.
	GCS – (Total)	**$35200**		
1	Network hub			
2	Pilot mobile control system;	$ 8,800	Desert Rotor MIRA12X-Color Midnight Black	[42]
3	Payload operator mobile control system;	$ 8,800	Desert Rotor MIRA12X-Color Midnight Black	[42]
4	Communication equipment and antenna tracking	-		
5	Quadro pod	-		
6	Power generator	-		

6.2.15.2 Launcher cost

Launcher cost is determined using available price data on the internet. Table 6.16 shows specifications of launchers like price, launch capacity and launch speed. Regression analysis is applied considering price/launch energy chart. Launch energy calculated multiplying launch capacity with square of launch speed. Required capacity and launch velocity are taken as 25 kg, 25 m/s, respectively. Corresponding price value for it is $ 10027.

Table 6.16 : Required Engineering Hours Calculation Summary.

	Name of Launcher	Price of Launcher (USD)	Launch Capacity (kg)	Launch Speed (m/s)	Type	Ref.
1	UAV CT-60 Drone	153000	30	23	Pneumatic	[43]
2	Naja H-10	3400	10	14		[43]
3	Naja H-05 Mini	2500	6	134		[43]
4	Naja H-40	8900	40	20	Pneumatic	[43]
5	UAV Catapult 6-10M Pneumatic Version	35000	100	20	Pneumatic	[43]
6	UAV Catapult 7.7M QL-150 Pneumatic Complete	170000	120	35	Pneumatic	[43]
7	UAV Catapult 12M QL-750 Pneumatic	280000	750	35		[43]
8	UAV Catapult For X8 X5 Skycam	1417	4.5	14		[43]
9	UAV Catapult For Skywalker X8 X5	1315	4.5	14		[43]
10	Catapult Launcher Scorpion	6146	8	16	Elastic	[44]

6.2.15.3 Recovery cost

Vertical cable recovery system cost estimated using system acquisition cost provided by Erdman and Mitchum (2013) which is $ 236,050 considered for deck of coast guard cutters [45].

Assuming that one system will be used for every four airplanes, the cost of each system can be calculated as $59,013. This value can be arranged according to customer's demands.

6.2.16 Cost analysis summary

The entire estimation is tabulated in Figure 6.2. Followings can be observed from it.

- Total fixed cost of project is $ 472833, while cos per unit is $ 3940.
- Target price per unit for airframe without GCS, launch and recovery systems is $ 37000
- Target price per unit which consist of 4 air vehicles (AV) with 1GCS, 1 launch and recovery systems is $ 477000. Main cost comes from GCS, launch and recovery systems.
- Units to break-even for airframe without GCS, launch and recovery systems is 51, without QDF.
- Units to break-even for units of 4 air vehicles (AV) with 1GCS, 1 launch and recovery systems is 6, without QDF.
- Selling overall UAS is more profitable then selling only air vehicle.

FIXED COST		Workhours		Total Cost	Cost per Unit	Comments
Engineering ($27/hr)	H_{ENGR} =	9216	C_{ENGR} =	$ 338,424	$ 2,820	
Development support	------------------------>		C_{DEV} =	$ 37,813	$ 315	
Flight test operations	------------------------>		C_{FT} =	$ 33,880	$ 282	
Tooling ($18/hr)	H_{TOOL} =	2562	C_{TOOL} =	$ 62,716	$ 523	
Fixed Cost	------------------------>		C_{fix} =	$ 472,833	$ 3,940	
VARIABLE COST		**Workhours**		**Total Cost**	**Cost per Unit**	**Comments**
Manufacturing labor ($15/hr)	H_{MFG} =	11515	C_{MFG} =	$ 234,915	$ 1,958	
Quality control	------------------------>		C_{QC} =	$ 22,904	$ 191	
Materials/equipment	------------------------>		C_{MAT} =	$ 141,242	$ 1,177	
Units produced in 5 years	-->				120	
Quantity Discount Factor	-->				0.702	for 120 pieces
Without GCS, Launch and Recovery Systems				**Without QDF**	**With QDF**	
Avionics	+		VSC_1 =	$ 6,900	$ 4,842	
Engine(s)	+		VSC_2 =	$ 1,620	$ 1,137	
Propeller(s)	+		VSC_3 =	$ 150	$ 105	
Payload	+		VSC_4 =	$ 15,649	$ 10,981	
Variable Cost (per unit)	------------------------>		C_{var}	$ 27,645	$ 20,390	
Total Cost per Unit	------------------------>		C_{unit}	$ 31,585	$ 24,330	
Manufacturers liability insurance	-->			$ 5,369	$ 4,136	
MINIMUM SELLING PRICE	-->			**$ 36,954**	**$ 28,466**	1 AV
Target Price per Unit	------------------------>		P_{unit} =	**$**	**37,000**	
Units to Break-Even	------------------------>		N_{BE} =	**51**	**28**	
Quantity Discount Factor	-->				0.777	for 40 pieces
With GCS, Launch and Recovery Systems				**Without QDF**	**With QDF**	
Ground Control Station	+		VSC_5 =	$ 35,200	$ 27,350	1 for 4 AVs
Catapult Launcher	+		VSC_6 =	$ 10,027	$ 7,791	
Vertical Cable Recovery	+		VSC_7 =	$ 236,050	$ 183,411	
Variable Cost (per unit)	------------------------>		C_{var} =	$ 391,855	$ 300,111	
Total Cost per Unit	------------------------>		C_{unit} =	$ 407,616	$ 315,872	
Manufacturers liability insurance	-->			$ 69,295	$ 53,698	
MINIMUM SELLING PRICE	-->			**$ 476,911**	**$ 369,570**	4 AVs + 1 GCS+ 1 LRS
Target Price per Unit	------------------------>		P_{unit} =	**$**	**477,000**	
Units to Break-Even	------------------------>		N_{BE} =	**6**	**3**	

Figure 6.2 : Project Cost Analysis Summary

6.2.17 Comparison with similar aircrafts

HAVK can be compared with Insitu ScanEagle which system use vertical arresting system named "SkyHook". Each ScanEagle system costs $3.2 million (2006).[46] A complete system comprises four air vehicles or AVs, a ground control station, remote video terminal, the SuperWedge launch system and Skyhook recovery system. Considering inflation rate of January 2006 to January 2024 each ScanEagle system costs $4.98 million.

Considering each HAVK system unit cost which is $0.48 million, it can be seen that there is roughly 10 times difference between ScanEagle and HAVK in terms of cost. However, it must be taken into account that ScanEagle is fully equipped military aircraft which uses much more robust and advanced ground and air systems.

Figure 6.3 represents the cost of the system components of Small Unmanned Aerial Systems (sUASs) provided by the Office of Aviation Acquisition [45].

Procure Ops Test System		
Airframe Unit Cost - Baseline	$	133,671
Avionics - Baseline	$	149,047
Propulsion - HFE - Baseline	$	40,601
EO/IR - Baseline	$	268,268
Comms Relay	$	131,301
AIS	$	7,851
GCS - Ship	$	392,054
Launcher - Ship	$	236,050
Recovery - Ship	$	236,050
Peculiar Support Equipment (PSE) per System	$	69,624
EO/IR surface detect sys	$	75,000
Remove video terminal for boarding team (1)	$	10,000
One ship sys with 1 acft	$	1,749,517
One ship sys with 2 acft	$	2,515,067

Figure 6.3 : Cost of Equipment to Outfit One Cutter With sUAS, Not Including Spares[45]

Considering values given figure above project cost analysis summary is updated. This new output is named as "Military Version". Results can be seen from Figure 6.4. Assumptions used to prepare the table are given below;

- Fixed cost of project is estimated considering "Airframe Unit Cost – Baseline" which is $133,671 given figures above. From previous chapters it can be seen that Fixed Cost related with hourly rate of labor. From chapter 6.2.5 ratio between hourly rates of labor of the US and Turkey is 3.44. Thus, "cost per unit” is determined as $38.859 (see Figure 6.4). This value is multiplied by 120 to obtain total fixed cost which is $4,662,942.

- Manufacturing cost, quality control cost and material cost haven’t changed because of lack of information.
- Vendor supplied components are updated considering components cost given figure above.

Followings can be observed from Figure 6.4 for military version of the project;

- Total fixed cost of project is $ $4,662,942, while cos per unit is $38,858.
- Target price per unit which consist of 4 air vehicles (AV) with 1GCS, 1 launch and recovery systems is $3,588,000.

Target price of military version of the project ,$3.59 million comparable with cost of ScanEagle system unit, $4.98 million. According to this, it can be said that the assumptions made are consistent.

As a summary, it can be concluded that project fixed cost estimation, the cost should be considered before starting the project, varies between minimum $0.47 million and maximum $4.66 according to quality of subsystems, which subsystem will be purchased from supplier or designed, operational expectations, civil and military usage.

FIXED COST		Workhours		Total Cost	Cost per Unit	Comments
Engineering ($27/hr)	H_{ENGR} =	-	C_{ENGR} =	$ -	$ -	
Development support	------------------------>		C_{DEV} =	$ -	$ -	
Flight test operations	------------------------>		C_{FT} =	$ -	$ -	
Tooling ($18/hr)	H_{TOOL} =	-	C_{TOOL} =	$ -	$ -	
Fixed Cost	------------------------>		C_{fix} =	$ 4,662,942	$ 38,858	

VARIABLE COST		Workhours		Total Cost	Cost per Unit	Comments
Manufacturing labor ($15/hr)	H_{MFG} =	11515	C_{MFG} =	$ 234,915	$ 1,958	
Quality control	------------------------>		C_{QC} =	$ 22,904	$ 191	
Materials/equipment	------------------------>		C_{MAT} =	$ 141,242	$ 1,177	
Units produced in 5 years	--->				120	
Quantity Discount Factor	--->				0.702	for 120 pieces
Without GCS, Launch and Recovery Systems				**Without QDF**	**With QDF**	
Avionics		+	VSC_1 =	$ 149,047	$ 104,583	
Engine(s)		+	VSC_2 =	$ 40,601	$ 28,489	
Propeller(s)		+	VSC_3 =	$ 150	$ 105	
Payload		+	VSC_4 =	$ 268,268	$ 188,238	
Variable Cost (per unit)	------------------------>		C_{var}	$ 461,392	$ 324,741	
Total Cost per Unit	------------------------>		C_{unit}	$ 500,249	$ 363,599	
Manufacturers liability insurance	-->			$ 85,042	$ 61,812	
MINIMUM SELLING PRICE	-->			**$ 585,292**	**$ 425,411**	1 AV
Target Price per Unit	------------------------>		P_{unit} =	**$**	**586,000**	
Units to Break-Even	------------------------>		N_{BE} =	**37**	**18**	
Quantity Discount Factor	--->				0.777	for 40 pieces
With GCS, Launch and Recovery Systems				**Without QDF**	**With QDF**	
Ground Control Station		+	VSC_5 =	$ 592,979	$ 460,745	1 for 4 AVs
Catapult Launcher		+	VSC_6 =	$ 236,050	$ 183,411	
Vertical Cable Recovery		+	VSC_7 =	$ 236,050	$ 183,411	
Variable Cost (per unit)	------------------------>		C_{var} =	$ 2,910,645	$ 2,126,531	
Total Cost per Unit	------------------------>		C_{unit} =	$ 3,066,076	$ 2,281,962	
Manufacturers liability insurance	-->			$ 521,233	$ 387,934	
MINIMUM SELLING PRICE	-->			**$ 3,587,309**	**$ 2,669,896**	4 AVs + 1 GCS+ 1 LRS
Target Price per Unit	------------------------>		P_{unit} =	**$**	**3,588,000**	
Units to Break-Even	------------------------>		N_{BE} =	**7**	**4**	

Figure 6.4 : Project Cost Analysis Summary (Version 2)

7. CONCLUSIONS AND RECOMMENDATIONS

7.1 Conclusions

The design and development of the "HavaKaşifi" UAV, specifically designed for long-endurance ISR missions, has successfully demonstrated that integrating the catapult-assisted take-off system and vertical arrest cable-based recovery system significantly increases the operational flexibility and efficiency of the UAV. Following the conceptual design, detailed preliminary design steps including weight estimation, aerodynamic analysis and structural load assessments predicted a maximum takeoff weight of 16 kg, well below 20 kg, in addition to verifying the feasibility of achieving the targeted 20-hour flight endurance with a payload capacity of 3.5 kg.

Due to current technological limitations in battery capacity, the use of a piston engine instead of electric propulsion provided the necessary endurance while maintaining payload capacity and operational efficiency. The high aspect ratio wing design, together with the selected MH-114 airfoil, contributed to the long endurance capabilities of the UAV by providing optimum aerodynamic cruise performance.

The cost analysis, which included development and variable costs, provided a comprehensive financial overview, which is crucial for potential investors and institutions interested in the project.

7.2 Recommendations

Recommendations can be listed as given below:

Autonomous Systems: Development of more advanced autonomous navigation and recovery systems, including machine learning algorithms for real-time decision-making and obstacle avoidance.

Advanced Aerodynamics: Exploration of innovative aerodynamic designs and morphing wing technologies to improve lift-to-drag ratios and overall flight efficiency.

Sensor Integration: Integration of advanced sensor payloads, such as LiDAR, hyperspectral cameras, and communication relays, to expand the UAV's capabilities in various mission scenarios.

1. Motion Analysis of Recovery Phase: In this study, no analysis was made for the recovery phase, and the studies that were carried out were scaled and interpreted. A detailed motion analysis of the rescue phase needs to be performed using both aircraft and rescue system parameters. Thus, this will help understand the dynamics and forces involved during the vertical arrest process and increase the reliability and safety of the recovery system.
2. Vertical Rope Arresting Recovery System Design: Design and refine the vertical rope arresting recovery system, focusing on improving its efficiency and reliability. This includes analyzing the material properties, load capacities, and mechanical design to ensure safe and effective UAV recovery.
3. Computational Fluid Dynamics (CFD) Analysis: Use CFD analysis to calculate the UAV's flight loads and optimize its aerodynamic performance. This involves simulating the airflow over the surfaces of the UAV to minimize drag and maximize lift, improving overall flight efficiency.
4. Stability and Control Analysis: Carry out in-depth stability and control analysis to ensure the UAV maintains stable flight under various conditions. This includes analyzing the effects of control surface deflections and external disturbances on the UAV's stability.
5. Structural Design and Analysis Studies: Performing extensive structural design and analysis to ensure the UAV can withstand the various loads encountered during flight, take-off and recovery. This includes finite element analysis (FEA) to simulate stress and strain on different components.
6. Enhanced Cost Analysis: The cost analyses are based on the methods used for heavy aircraft. Methods compatible with UAV systems should be researched/developed.

7.3 Practical Application of This Study

Practical applications of this study can be listed as given below;

1. Military ISR Missions: Enhancing surveillance capabilities for military operations, providing real-time data for strategic decision-making.
2. Environmental Monitoring: Continuous monitoring of environmental parameters such as forest health, wildlife tracking, and pollution levels.
3. Disaster Response: Rapid aerial assessments in disaster-stricken areas, aiding efficient resource allocation and rescue operations.
4. Agricultural Surveillance: Supporting precision farming through detailed crop health monitoring, irrigation management, and pest control, increasing agricultural productivity.
5. Maritime Operations: Enhancing maritime security and monitoring, including anti-piracy operations, fisheries management, and coastal surveillance.

REFERENCES

[1] UAV Power Plant Selection Committee. (2023). *Analysis of Power Plant Options for UAVs*. Journal of UAV Systems, 45(3), 123-130.

[2] Energy Research Institute. (2023). *The Energy Density of Aviation Fuels*. International Journal of Energy Research, 29(2), 201-210.

[3] Advanced Battery Technology Lab. (2023). *Current Limitations of Battery Technology in UAVs*. International Journal of Battery Research, 7(4), 234-245.

[4] UAV Systems Engineering Group. (2023). *Battery Capacity and UAV Endurance: A Critical Analysis*. Journal of UAV Development, 22(5), 410-422.

[5] Url-1 <*http://www.janes.com*>, date retrieved 10.2.2023.

[6] Sadraey, M. H. (2012). *Aircraft design: A systems engineering approach*. John Wiley & Sons.

[7] Gudmundsson, S. (2021). *General aviation aircraft design: Applied methods and procedures* (2nd ed.). Butterworth-Heinemann.

[8] Yuzgec, C. N. (2023). *Yüksek seyir süresine sahip küçük bir iha'nın kavramsal tasarımı*. (Bitirme Ödevi). ISTANBUL Teknik Üniversitesi, Uçak ve Uzay Bilimleri Fakültesi, ISTANBUL.

[9] Roskam, J. (1997). *Airplane design part II: Preliminary configuration design and integration of the propulsion system.* DARcorporation.

[10] Url-2 < *https://www.engineeringtoolbox.com/fuels-densities-specific-volumes-d_166.html*>, date retrieved 17.5.2023.

[11] Url-3 < *https://skypower.online/produkt/sp-28-cr/*>, date retrieved 17.5.2023.

[12] Url-4 < *https://www.defenseadvancement.com/suppliers/electro-optical-infrared-eoir-systems//*>, date retrieved 17.5.2023.

[13] Url-5 < *https://ukrspecsystems.com/drone-gimbals/usg-405/*>, date retrieved 17.5.2023.

[14] Roskam, J. (1997). *Airplane design part V: Component weight estimation.* DARcorporation.

[15] Url-6 < *https://hitecrcd.com/products/servos/analog/sport-2/hs-322hd/product*>, date retrieved 17.5.2023.

[16] Url-7 < *https://www.cubepilot.com/#/herepro/features* >, date retrieved 17.5.2023.

[17] Url-8 < *https://www.cubepilot.com/#/herelink/specs* >, date retrieved 17.5.2023.

[18] Url-9 < *https://genstattu.com/tattu-5200mah-14-8v-35c-4s1p-lipo-battery-pack-with-xt60-plug.html* >, date retrieved 17.5.2023.

[19] Url-10 < *https://www.cubepilot.com/#/cube/specs*>, date retrieved 17.5.2023.

[20] Url-11 < *https://rfdesign.com.au/modems/#RFD900x*>, date retrieved 17.5.2023.

[21] Roskam, J. (1997). *Airplane design part VI: Preliminary calculation of aerodynamic thrust and power characteristics.* DARcorporation.

[22] Roskam, J. (1997). *Airplane design part I: Preliminary sizing of airplanes.* DARcorporation.

[23] Silkov, V., & Zirka, A. (2014). *Calculation of the characteristics of a UAV launch from a ramp*. Aviation, 18(4), 178-184. https://doi.org/10.3846/16487788.2014.985476

[24] Sanghi., D., Sharma, D., & Raghava, N.S. (2015). *Design, Fabrication and Testing of an Unmanned Aerial Vehicle Catapult Launcher*.

[25] Url-19 < *https://www.uav.ee/products/uav-pneumatic-catapult-pl-40/*>, date retrieved 23.04.2024.

[26] Reed, W. H., III. (1952, November 5). *An analysis of the effect of a curved ramp on the take-off performance of catapult-launched airplanes* (Research Memorandum No. RM L52I05). National Advisory Committee for Aeronautics.

[27] Url-20 < *https://www.insitu.com/*>, date retrieved 23.04.2024.

[28] Ma, C., Liu, X., & Zhang, C. (2018). *Parameter research of UAV vertical rope-type recovery system*. MATEC Web of Conferences, 179, 03001. https://doi.org/10.1051/matecconf/201817903001

[29] Federal Aviation Administration. (1964). Sec. 23.337 - Limit maneuvering load factors. Federal Aviation Regulations. Retrieved from https://www.risingup.com/fars/info/part23-337-FAR.shtml

[30] Bahumanyam, P. K. (2014). *Evaluation of novel wing design for UAV*. In Proceedings of the 2014 COMSOL Conference in Boston. University of Alabama in Huntsville.

[31] Majka, A. (2013). *Flight loads of mini-UAV*. Solid State Phenomena, 198(1), 194-199.

[32] Landolfo, G. (2008). Aerodynamic and structural design of a small nonplanar wing UAV (Master's thesis). University of Dayton, Dayton, Ohio.

[33] Besson, Z. S., & Barcelos Júnior, M. N. D. (2012). *Structural design of mini-UAVs with conventional and alternative materials.* In Proceedings of the 14th Brazilian Congress of Thermal Sciences and Engineering, November 18-22, Rio de Janeiro, RJ, Brazil.

[34] Sadraey, M. H. (2020). *Design of Unmanned Aerial Systems*. https://doi.org/10.1002/9781119508618. John Wiley & Sons.

[35] Malone, P., Apgar, H., Stukes, S., & Sterk, S. (2013). (*Unmanned aerial vehicles unique cost estimating requirements*. In 2013 IEEE Aerospace Conference (pp. 1-8). Big Sky, MT, USA. https://doi.org/10.1109/AERO.2013.6496852

[36] Valerdi, R. (2005). Cost metrics for unmanned aerial vehicles. In Proceedings of the Infotech@Aerospace 2005 Conference, September 26-29, Arlington, Virginia. AIAA 2005-7102.

[37] Ortiz-Ospina, E., & Molteni, M. (2017). *What are PPP adjustments and why do we need them?* Our World in Data. Retrieved from https://ourworldindata.org/what-are-ppps

[38] Url-12 <*https://www.imf.org/en/Publications/WEO/weo-database/2024/April/*>, date retrieved 23.04.2024.

[39] Url-13 <*https://uavionix.com/product/george-g2i-skystation2-evaluation-kit/*>, date retrieved 23.04.2024.

[40] Url-14 <*https://shop.mejzlik.eu/propeller-18x8-ccw-2b/*>, date retrieved 23.04.2024.

[41] Url-15 <*https://www.yangdaonline.com/eagle-eye-30ie-u-2-axis-30x-eo-ir-dual-sensor-zoom-camera-with-tracking-and-geotagging/*>, date retrieved 23.04.2024.

[42] Url-16 <*https://ozrobotics.com/shop/portable-drone-ground-control-station-gcs-intel-i3-embedded-pc-combo-with-control-links-color-midnight-black/*>, date retrieved 23.04.2024.

[43] Url-17 < *https://www.austars-model.com/*>, date retrieved 23.04.2024.

[44] Url-18 < *https://ozrobotics.com/shop/catapult-launcher-scorpion/*>, date retrieved 23.04.2024.

[45] Erdman, T. J., & Mitchum, C. (2013). *Life-cycle cost analysis for small unmanned aircraft systems deployed aboard coast guard cutters* (Master's thesis, Naval Postgraduate School). Graduate School of Business & Public Policy, Naval Postgraduate School.

[46] Url-21 < https://en.wikipedia.org/wiki/Boeing_Insitu_ScanEagle#cite_note-AF_factsh-3/>, date retrieved 23.05.2024.

APPENDICES

APPENDIX A: Chord calculation for given distance from root.
APPENDIX B: Equations of Motion after take-off.
APPENDIX C: Aircraft parameters for take-off calculations.

APPENDIX A: Chord calculation for given distance from root.

Considering Figure A.1 :. Chord length at any y loaction is calculated using triangle similarity as below [3]:

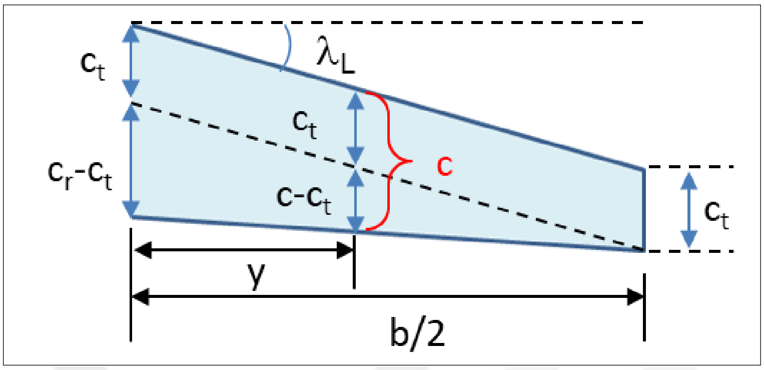

Figure A.1 : Wing geometry

From similarity

$$\frac{c_r - c_t}{\frac{b}{2}} = \frac{c - c_t}{\frac{b}{2} - y}$$

$$c - c_t = (c_r - c_t) * \frac{\frac{b}{2} - y}{\frac{b}{2}}$$

$$\lambda = \frac{c_t}{c_r} \rightarrow c_t = \lambda c_r$$

$$c - \lambda c_r = (c_r - \lambda c_r) * \left(1 - \frac{2y}{b}\right)$$

$$c = \lambda c_r + c_r(1 - \lambda) * \left(1 - \frac{2y}{b}\right)$$

$$c = c_r\left(\lambda + (1 - \lambda) * \left(1 - \frac{2y}{b}\right)\right)$$

$$c = c_r\left(\lambda + 1 - \frac{2y}{b} - \lambda + \lambda\frac{2y}{b}\right)$$

$$\boldsymbol{c = c_r\left[1 - (1 - \lambda)\frac{2y}{b}\right]}$$

APPENDIX B: Equations of Motion after take-off.

Equation of motion for after take-off can be written as given below [26].

$$m\dot{V} = T\cos\ \alpha - D - W\sin\ \gamma \tag{A.1}$$

$$mV\dot{\gamma} = L + T\sin\ \alpha - W\cos\ \gamma \tag{A.2}$$

$$mk_y^2\ddot{\theta} = \mathrm{M} \tag{A.3}$$

While lift, drag and pitching moment;

$$L = qSC_L \tag{A.4}$$

$$D = qSC_D \tag{A.5}$$

$$M = qS\bar{c}C_m \tag{A.6}$$

Where;

$$C_L = C_{L_O} + C_{L_\alpha}\alpha + C_{L_{\delta e}}\delta_e \tag{A.7}$$

$$C_D = C_{D_0} + \frac{C_L^2}{\pi Ae} = C_{D_0} + KC_L^2 \tag{A.8}$$

$$C_M = C_{M_O} + C_{M_\alpha}\alpha + C_{M_{\delta e}}\delta_e + C_{M_q}\frac{c}{2V}q + C_{M_{\dot{\alpha}}}\frac{c}{2V}\dot{\alpha} \tag{A.9}$$

APPENDIX C: Aircraft parameters for take-off calculations.

Aircraft parameters for take-off given below:

Table C.1 : The aircraft and environmental specifications

Symbol	Value	Unit
W	156	N
m	15.89	kg
k_y	0.3542	m
T	30	N
S	0.8083	m2
AR	14	
c	0.2414	m
δ_e	5	deg
ρ	1.225	kg/m^3
g	9.81	m/s^2

Table C.2 : The aerodynamic coefficients.

Symbol	Value	Unit
C_{L0}	0.82	
$C_{L\alpha}$	6.125	1/rad
$C_{L\delta e}$	0.37	1/rad
C_{D0}	0.035	
e	0.94	
C_{M0}	-0.023	
C_{ML}	-0.1	
$C_{M\alpha}$	-0.613	1/rad
$C_{M\delta e}$	0.56	1/rad
C_{Mq}	-25.57	
$C_{MD\alpha}$	-5.19	

Table C.3 : Initial value of variables.

Symbol	Value	Unit
V_i	13.9	m/s
α_i	0	deg
γ_i	11	deg
θ_i	11	deg
$d\theta_i/ds$	0	rad/m

CURRICULUM VITAE

Name Surname : **Şems İkbal Yüzgeç**

EDUCATION :

- **B.Sc.** : 2021, Istanbul Technical University, Faculty of Aeronautics and Astronautics, Department of Astronautical Engineering

PROFESSIONAL EXPERIENCE AND REWARDS:

- 2021-Now : Structural Analysis Engineer at Turkish Aerospace

PUBLICATIONS, PRESENTATIONS AND PATENTS ON THE THESIS:

OTHER PUBLICATIONS, PRESENTATIONS AND PATENTS: